MATHEMATICAL MODELING OF GLUCOSE AND INSULIN DYNAMICS IN ADOLESCENT GIRLS TO QUANTIFY MEASURES OF INSULIN SENSITIVITY

by

Kai Bartlette

A thesis submitted to the Faculty and the Board of Trustees of the Colorado School of Mines in partial fulfillment of the requirements for the degree of Doctorate of Philosophy of Science (Applied Mathematics).

Golden, Colorado

Date _____

Signed: _____
Kai Bartlette

Signed: _____
Dr. Cecilia Diniz Behn
Thesis Advisor

Golden, Colorado

Date _____

Signed: _____
Dr. Gregory Fasshauer
Professor and Head
Department of Applied Mathematics and Statistics

ABSTRACT

The regulation of plasma glucose is a key component of human metabolism and is largely regulated by insulin that facilitates glucose uptake by tissues. When tissues become more resistant to insulin, glucose concentrations remain elevated longer and more insulin is required to elicit the same physiologic response. Insulin resistance (IR) is a crucial element of the pathology of the metabolic syndrome, which includes increased risk of stroke, heart disease, type 2 diabetes mellitus, and nonalcoholic fatty liver disease (NAFLD). Decreased insulin sensitivity (S_I) is associated with pubertal changes, is more prevalent in teenage girls, and obesity is known to further decrease S_I. The Oral Minimal Model (OMM) is a differential-equations based model that describes glucose-insulin dynamics during an oral glucose tolerance test (OGTT) to quantify S_I. However, the OMM framework was developed for adult data and practical identifiability issues create challenges with applying the models to diverse metabolic phenotypes. This research focuses on extending the OMM framework to describe OGTT data from a group of adolescent girls with obesity. Initial application of OMM in this cohort established OGTT protocol duration dependence of estimates of S_I. To better understand which features of the data facilitate robust model parameter identification, we conducted a local sensitivity analysis of the OMM. We found that the model was least sensitive to changes in a subset of parameters and, therefore, these parameters could be difficult to estimate reliably. This finding was confirmed in an uncertainty quantification of OMM whereby we used a Markov Chain Monte Carlo approach to obtain the precision on key parameter estimates. The addition of glucose tracers in the OGTT enables estimation of the rate of appearance of exogenous glucose (Ra_{exo}), a key input of OMM-type models developed for separately assessing total and hepatic S_I. Published methods for approximating Ra_{exo} had a significant impact on estimates of both total and hepatic S_I. To overcome this limitation, we developed an Ra_{exo} model-independent method to estimate hepatic S_I in this

population. These methodologies may inform the analysis and adaptation of physiological models for other applications.

TABLE OF CONTENTS

ABSTRACT iii

LIST OF FIGURES vii

LIST OF TABLES xii

LIST OF ABBREVIATIONS xiv

ACKNOWLEDGMENTS xvi

DEDICATION xvii

CHAPTER 1 INTRODUCTION 1

CHAPTER 2 BACKGROUND 5

CHAPTER 3 DATA AND PROTOCOL 19

CHAPTER 4 DURATION DEPENDENCE OF OMM 23

4.1 Introduction 23

4.2 Methods and Materials 25

4.3 Results 29

4.4 Discussion 41

CHAPTER 5 ANALYSIS OF OMM 44

5.1 Introduction 44

5.2 Materials 48

5.3 Local Sensitivity Analysis 49

5.3.1 Results 51

5.4 Uncertainty Quantification 59

5.4.1 Results 62
5.5 Discussion 68
CHAPTER 6 RATE OF APPEARANCE OF EXOGENOUS GLUCOSE 72
6.1 Introduction 72
6.2 Materials 73
6.3 Methods 74
6.3.1 Steele's Non-Steady State Ra 74
6.3.2 Exogenous Ra 76
6.3.3 Implementation into OMM/OMM* 82
6.4 Results: Ra_{exo} Methods 85
6.5 Discussion: Ra_{exo} Methods 92
6.6 Methods: Strategies to Alleviate the Method Dependence of S_I Estimates . . . 99
6.7 Results: Strategies to Alleviate the Method Dependence of S_I Estimates . . 101
6.8 Discussion: Strategies to Alleviate the Method Dependence of S_I Estimates . 107
CHAPTER 7 QUANTIFYING HEPATIC S_I IN OBESE ADOLESCENT GIRLS . . 111
7.1 Introduction 111
7.2 Materials and Methods 113
7.3 Results 117
7.4 Discussion 119
CHAPTER 8 CONCLUSIONS 120
REFERENCES CITED 125
APPENDIX A RESCALED OMM 137
APPENDIX B OMM^{PD} SENSITIVITY INDICES DERIVATION 140

LIST OF FIGURES

Figure 2.1 Schematic of the Minimal Model of Glucose Disappearance 7

Figure 3.1 OGTT protocol with two stable isotope tracers showing blood sample times and protocol duration 20

Figure 4.1 OGTT protocol showing blood sampling times and duration 25

Figure 4.2 Glucose and insulin concentrations. Glucose (A) and insulin (B) concentration ranges for all study participants (n = 68) for a six hour OGTT. Mean glucose and insulin concentrations (blue line), ± max/min values (light blue shading) indicate range of variability across the cohort. 30

Figure 4.3 Simulated glucose dynamics based on different OMM time models. Glucose and insulin (A, B, C, D) profiles for representative participants with high (A, B) or low (C, D) insulin sensitivity as assessed by 6-hour OMM S_I. The simulated glucose dynamics obtained using the 2h Ex, 3h Ex, 4h Tr, 4h Ex, and 6h implementations of OMM are plotted with the glucose data for four participants. For truncated models (4h Tr and 6h), there are no assumptions of glucose dynamics beyond the specified time breakpoints. For the exponential models (2h Ex, 3h Ex and 4h Ex), exponential decay of the rate of appearance of glucose is assumed after 120 min., 180 min., and 240 min., respectively. 31

Figure 4.4 Estimate rate of appearance of drink glucose by OMM model duration. The rate of appearance of exogenous glucose ($Ra_{exo}(\boldsymbol{\alpha}, t)$) estimated for each model for the 4 representative participants reported in Figure 4.3. Onset of exponential decay of 2h Ex, 3h Ex and 4h Ex OMM models is initiated after 120, 180, and 240 min, respectively. 32

Figure 4.5 Comparing Bayesian Estimated T versus T Fixed to 60 min. Comparing the results of when T is estimated versus when T is fixed to 60 min. The histograms of the estimated T values from the 3h Ex (A) and the 4h Ex models. Below (C, D) the scatter plots of the S_I estimates calculated with an estimated T versus T fixed to 60 min show that the estimates are virtually equivalent. Shown is the line of equality. . 33

Figure 4.6 Correlations between S_I estimated with the 6-hour OMM as a reference and OMM implemented with shorter durations (n = 68). Scatter plots showing the correlations of the 2-hour exponential (A), the 3-hour exponential (B), the 4-hour truncated (C), and the 4-hour exponential (D) OMM S_I estimates with the 6-hour OMM S_I estimates. The blue line is the least squares fit to the data, and the black line indicates equality of estimates obtained using different models. 35

Figure 4.7 Bland-Altman plots showing the bias of the S_I estimates computed with the 6-hour OMM and with shorter OMM implementations (n = 68). The bias (solid line), the confidence interval of the bias (shaded region), and the 95% limits of agreement (dashed line) are reported. The 2-hour exponential model (A), 3-hour exponential model (B), and 4-hour exponential model (C), all showed a small positive bias indicating that these models underestimate S_I. The 4-hour truncated model (D) had a small negative bias indicating this model overestimated S_I. 37

Figure 4.8 Bland-Altman plot showing bias and limits of agreement for percent differences of S_I estimates computed with the 6-hour OMM and with shorter model implementations (n = 68). The bias (solid line), the confidence interval of the bias (shaded region) and the 95% limits of agreement (dashed line) are reported. (A) 2-hour exponential model, (B) 3-hour exponential model, (C) 4-hour exponential model, (D) 4-hour truncated model. 38

Figure 4.9 S_I correlations divided into subgroups by 4-hour glucose levels. Strength of correlation of S_I estimates using 4- and 6-hour OMM protocols varies for subgroups specified by participants' 4-hour glucose concentrations relative to their baseline glucose concentrations. S_I estimates calculated with the 4-hour exponential OMM were strongly correlated with 6-hour OMM S_I estimates for participants who were 10 mg/dL within (n = 24, all female, $p < 0.001$) and below (n = 37, all female, $p < 0.001$) their baseline glucose concentrations after the first 4 hours of the OGTT protocol but not for participants who were 10 mg/dl above (n = 7, all female, p = 0.06) (A). S_I estimates calculated with the 4-hour truncated OMM were correlated with 6-hour OMM S_I estimates for participants who were 10 mg/dl above (n = 7, all female, p = 0.03), within (n = 24, all female, $p < 0.001$), and below (n = 37, all female, $p < 0.001$) their baseline glucose concentrations after the first 4 hours of the OGTT protocol (B). 40

Figure 5.1 Local sensitivities of OMM glucose output for Subject 20. 52

Figure 5.2 The perturbations of the OMM simulated glucose profile for Subject 20 when the partial derivatives in the sensitivity measures s_{f_i/θ_j} were approximated with a large $\Delta\theta_j$ to highlight the changes to the glucose model output. 53

Figure 5.3 Local sensitivities of Rescaled OMM glucose output for Subject 20. 54

Figure 5.4 Local sensitivities of the OMM and the Rescaled OMM insulin action output for Subject 20. 55

Figure 5.5 The perturbations of the Rescaled OMM simulated glucose profile for Subject 20 when the partial derivatives in the sensitivity measures s_{f_i/θ_j} were approximated with a large $\Delta\theta_j$ to highlight the changes to the glucose model output. 56

Figure 5.6 Local sensitivities of $\boldsymbol{\alpha}$ without the constraint on $Ra_{exo}(\boldsymbol{\alpha}, t)$ for Subject 20. 56

Figure 5.7 Bar plot of the median overall sensitivity of the glucose outputs for the OMM and the Rescaled OMM to each parameter for all participants (n = 68). The errorbars represent the 75^{th} and 25^{th} percentiles. 59

Figure 5.8 The sequence of MCMC chains S_G, p_2, and S_I for the fabricated dataset. . 62

Figure 5.9 The MCMC simulated glucose and the data for the Simulated Subject. . 63

Figure 5.10 The posterior densities of S_I, S_G, and p_2 for the simulated individual. . . 64

Figure 5.11 The sequence of MCMC chains S_G, p_2, and S_I for Subject 60. 65

Figure 5.12 The posterior densities of S_I, S_G, and p_2 for Subject 60. 66

Figure 5.13 The MCMC simulated glucose and data for Subject 60 and Subject 20. . 67

Figure 5.14 The sequence of MCMC chains S_G, p_2, and S_I for Subject 20. 67

Figure 5.15 The posterior densities of S_I, S_G, and p_2 for Subject 20. 68

Figure 6.1 OGTT protocol with two stable isotope tracers showing blood sample times and protocol duration 73

Figure 6.2 Schematic of glucose kinetics where Ra is the total rate of appearance of glucose, F is the infusion rate of glucose tracer, Rd is the rate of disappearance of glucose, $A(t)$ is the amount of tracer II and $B(t)$ is the amount of tracee. 74

Figure 6.3 Schematic showing change in tracers in one compartment where Ra_{13C} is the rate of appearance of tracer I, F_{2H} is the infusion rate of tracer II and G is the accessible compartment of each tracer. 77

Figure 6.4 Schematic showing change in tracers in two compartments where Ra_{13C} is the rate of appearance of tracer I, F_{2H} is the infusion rate of tracer II, k_{12}, k_{21} and k_{01} are rate parameters, G and Q are the accessible and remote compartments, respectively, of each tracer. 80

Figure 6.5 Glucose concentration, insulin concentration and Steele's total Ra for Subject 10. 85

Figure 6.6 Glucose concentration, insulin concentration and Steele's total Ra for Subject 12. 86

Figure 6.7 Glucose concentration, insulin concentration and Steele's total Ra for Subject 15. 86

Figure 6.8 The calculated Ra_{exo} and the corresponding Ra_{endo} for each method for Subject 10. 86

Figure 6.9 The calculated Ra_{exo} and the corresponding Ra_{endo} for each method for Subject 12. 87

Figure 6.10 The calculated Ra_{exo} and the corresponding Ra_{endo} for each method for Subject 15. 87

Figure 6.11 OMM/OMM* glucose simulations for total and meal glucose with the Ra_{exo} constraint on a select α_i for Subject 12. 88

Figure 6.12 OMM/OMM* glucose simulations for total and meal glucose with the Ra_{exo} constraint on a select α_i for Subject 15. 89

Figure 6.13 The simulated total and meal glucose for each of the 4 Ra_{exo} methods for Subject 10. 89

Figure 6.14 The simulated total and meal glucose for each of the 4 Ra_{exo} methods for Subject 12. 90

Figure 6.15 The simulated total and meal glucose for each of the 4 Ra_{exo} methods for Subject 15. 90

Figure 6.16 The OMM estimated Ra_{exo} resulting from the initialization with different Ra_{exo} methods for the representative participants. 91

Figure 6.17 Steele's total, exogenous, and endogenous Ra for Subject 10 computed using regularization method. 102

Figure 6.18 Steele's total, exogenous, and endogenous Ra for Subject 12 computed using regularization method. 102

Figure 6.19 The total, exogenous, and endogenous Ra for Subject 10 computed using interpolating polynomials. 103

Figure 6.20 The total, exogenous, and endogenous Ra for Subject 12 computed using interpolating polynomials. 103

Figure 6.21 The estimated OMM/OMM* $Ra_{exo}(\boldsymbol{\alpha}, t)$ initialized with each Ra_{exo} method after 200 iterations for Subject 10. 106

Figure 6.22 The estimates of the OMM and OMM* parameters at each iteration for Subject 10. 106

Figure 6.23 The estimates of S_I , S_I^* and S_I^{Dyn} initialized with each Ra_{exo} method after 200 iterations for Subject 10. 107

Figure 7.1 OGTT protocol with two stable isotope tracers showing blood sampling times and duration 113

Figure 7.2 Total, exogenous and endogenous glucose with OMM^{PD} simulations, insulin concentrations, OMM^{PD} estimated $Ra_{exo}(\boldsymbol{\alpha}, t)$ and endogenous glucose production profile for Subject 10. 118

LIST OF TABLES

Table 4.1 Participant Characteristics 30

Table 4.2 Average S_I estimates, Precision and MSE 34

Table 4.3 Linear regression results of S_I estimates from shorter OMM implementations compared to 6-hour model 36

Table 4.4 Bland-Altman Bias, CI and Limits of Agreement 38

Table 4.5 Bland-Altman Percent Difference Bias, CI and Limits of Agreement 39

Table 5.1 List of the parameters considered in the local sensitivity analysis of the OMM and the Rescaled OMM. 49

Table 5.2 The overall sensitivity of the OMM glucose output to each parameter as measured by sensitivity metric r_{f_i/θ_j} for all participants (n = 68). 57

Table 5.3 The overall sensitivity of the Rescaled OMM glucose output to each parameter as measured by sensitivity metric r_{f_i/θ_j} for all participants (n = 68). 58

Table 5.4 List of the parameters considered in the uncertainty quantification of the rescaled OMM. 59

Table 6.1 Estimates of S_I^{ref}, 10^{-4} and S_I, 10^{-4} for the 4 Ra_{exo} methods. 91

Table 6.2 Estimates of S_I^{*ref}, 10^{-4} and S_I^*, 10^{-4} for the 4 Ra_{exo} methods. 92

Table 6.3 The mean and standard deviation of S_I, S_I^{ref}, S_I^* and S_I^{*ref} (10^{-4}) for each participant (n = 9). 92

Table 6.4 Estimates of S_I^{Dyn}, 10^{-5} for the 4 Ra_{exo} methods for each participant (n = 9). 93

Table 6.5 The correlations of S_I estimates across Ra_{exo} methods. 93

Table 6.6 The correlations of S_I^* estimates across Ra_{exo} methods. 93

Table 6.7 The correlations of S_I^{Dyn} estimates for the Ra_{exo} methods. 93

Table 6.8 Estimates of S_G, 10^{-2} for the 4 Ra_{exo} methods for all participants (n = 9). 94

Table 6.9 Estimates of S_G^*, 10^{-2} for the 4 Ra_{exo} methods for all participants (n = 9). 94

Table 6.10 Estimates of V (dl/kg) for the 4 Ra_{exo} methods for all participants (n = 9). 94

Table 6.11 Estimates of V^* (dl/kg) for the 4 Ra_{exo} methods for all participants (n = 9). 95

Table 6.12 The estimates of S_I, 10^{-4} for each Ra_{exo} method computed with interpolating polynomials for all participants (n = 9). 104

Table 6.13 The estimates of S_I^*, 10^{-4} for each Ra_{exo} method computed with interpolating polynomials for all participants (n = 9). 104

Table 6.14 The estimates of S_I^{Dyn}, 10^{-5} for each Ra_{exo} method computed with interpolating polynomials for all participants(n = 9). 105

Table 6.15 The correlations of S_I^{Dyn} estimates across Ra_{exo} methods that were computed using interpolating polynomials. 105

Table 6.16 Final iterative scheme estimates of S_G, S_G^*, V and V^* for each Ra_{exo} method for Subject 10. 108

Table 6.17 Final iterative scheme estimates of S_I, S_I^*, and S_I^{Dyn} for each Ra_{exo} method for Subject 10. 108

LIST OF ABBREVIATIONS

Rate of appearance of glucose	Ra
Rate of appearance of exogenous glucose	Ra_{exo}
Rate of appearance of endogenous glucose	Ra_{endo}
Oral Glucose Tolerance Test	OGTT
Intravenous Glucose Tolerance Test	IVGTT
Mixed Meal Tolerance Test	MMT
Meal Glucose Tolerance Test	MGTT
Insulin Resistance/Resistant	IR
Impaired Glucose Tolerance	IGT
Insulin Sensitivity	S_I
Peripheral Insulin Sensitivity	S_I^*/S_I^D
Hepatic Insulin Sensitivity	S_I^P
Dynamic Insulin Sensitivity	S_I^{Dyn}
Minimal Model	MM
Oral Minimal Model	OMM
Labeled Oral Minimal Model	OMM*
Production and Disposal Oral Minimal Model	OMM^{PD}
Reference Model	RM
Reference-Labeled Model	RM*
Tracer-to-Tracee Ratio	TTR

Hyperinsulinemic euglycemic . . . . . HE

Glucose infusion rate . . . . . GIR

Nonalcoholic Fatty Liver Disease . . . . . NAFLD

Polycystic ovary syndrome . . . . . PCOS

Hepatic Steatosis . . . . . HS

Reactive hypoglycemia . . . . . RHG

Sensitivity Analysis . . . . . SA

Uncertainty Quantification . . . . . UQ

Total glucose . . . . . G

Exogenous glucose from the test drink . . . . . G_{exo}

Endogenous glucose from the liver . . . . . G_{end}

Volume of distribution for glucose V

Rate constant governing decay of insulin action . . . . . p_2

Rate constant governing growth of insulin action for insulin concentrations above baseline . . . . . p_3

Glucose effectiveness per unit distribution volume to promote glucose disposal and inhibit hepatic glucose production . . . . . S_G

ACKNOWLEDGMENTS

There are numerous people that I would like to thank for supporting me professionally and personally throughout my doctoral studies. First, I would like to thank my advisor Dr. Cecilia Diniz Behn, who consistently pushed me to think deeper and hone my skills as an applied mathematician. Not only did Dr. Diniz Behn help me deliver a strong thesis, she also helped me develop as a researcher and independent thinker.

I would also like to thank our lead collaborator at Children's Hospital Colorado Anschutz Medical Campus, Dr. Melanie-Cree Green, without whom none of this analysis would have been possible.

I would like to acknowledge my colleagues Nora Stack, Caitlyn Hannum, Rebecca Conrad, Nick Fisher, Zach Grey, Paul Diaz, Andrew Glaws, Alicia Colclasure, Ada Palmisano, Brett Powers, and Michael Kelley. Their insights and subsequent friendships have greatly shaped my research and my life in graduate school.

I would like to thank my grandmother, mother, father, aunts and uncles for their prayers and cultivating my curiosity from a young age. Finally, I would like to thank my sisters and friends for their constant words of encouragement and optimism that helped me to cross the final finish line.

To my mother.

CHAPTER 1

INTRODUCTION

Glucose is the main source of energy for the brain and everyday bodily functions. The body, specifically the liver and pancreas, works to maintain a healthy range of blood glucose throughout the day to ensure a constant supply of fuel for the brain. During the fasted state, endogenous glucose is released from the liver into the bloodstream. After a meal, blood glucose concentrations increase and the pancreas releases insulin in response to the elevated glucose. This hormone signals the liver to switch from releasing glucose to storing glucose and allows the other peripheral tissues such as muscle and adipose to take in glucose. The introduction of exogenous glucose and increased insulin concentrations suppress endogenous glucose production [1]. The regulation of blood glucose is an important and complex metabolic process that, when disrupted, can lead to various health issues such as metabolic syndrome. If an individual is less sensitive to the insulin they produce, their glucose concentrations remain elevated for an extended period of time which, left untreated, can lead to comorbidities such as chronic hyperglycemia and type 2 diabetes. An improved understanding of this intricate process will lead to the support of new therapeutic approaches.

From models of glucose-insulin dynamics, investigators are able to gather a wealth of knowledge from an individual and or a specific population. The research in this thesis focuses on glucose and insulin dynamics in obese adolescent girls with and without polycystic ovary syndrome (PCOS). Most models and analysis of glucose-insulin dynamics have been performed in adults with fewer studies performed in adolescents [2–5]. This research seeks to validate existing models of glucose-insulin dynamics in youth and ascertain metabolic characteristics of this specific population. To do so in a physiological setting, participants underwent an oral glucose tolerance test (OGTT) with two stable isotope glucose tracers

as an oral test will capture all the physiological changes undergone by the body after meal ingestion. Blood samples were collected at regular intervals during the protocol and gas chromatography mass spectrometry was used to measure the relative abundance of glucose tracers and tracee. The presence of the tracers enables us to track exogenous glucose coming from the test drink and endogenous glucose coming from the liver.

The main model framework chosen here to represent glucose dynamics is the Oral Minimal Model (OMM), developed to model glucose-insulin dynamics during an oral glucose excursion. The parameters governing this model enable measurement of the effectiveness of glucose to promote glucose disposal, capture an individual's insulin response to exogenous glucose and quantify an insulin sensitivity index, S_I. S_I quantifies an individual's sensitivity to insulin for regulating blood glucose. The quantification of S_I during an OGTT has been a very important development in assessing an individual's sensitivity to the insulin produced under physiological conditions. A brief timeline of computing S_I indices measured from glucose tolerance tests is included in the next chapter.

In an application of OMM presented here we seek to understand the OGTT protocol duration dependence of estimates of S_I in adolescent girls with obesity. Identifying model dependence of S_I estimates on protocol duration will aid in establishing methodologies to reliably estimate S_I in this population from shorter OGTT protocols. Previous validation of OMM in youth was based on a 7 hour OGTT and concluded that a reduced 3 hour model produced similar estimates of S_I compared to the 7-hour S_I estimates [2]. In our cohort of obese adolescent girls, estimates of S_I from reduced protocol durations were compared to estimates from a full 6 hour OMM implementation. For this particular population, we concluded that the duration of the protocol does affect estimates of S_I, specifically through the assumptions made on the rate of appearance of exogenous glucose (Ra_{exo}).

The development of OMM has contributed a great deal to the study of metabolism and endocrinology. However, this model is a simple description of glucose-insulin dynamics built in adult populations. Therefore, a sensitivity analysis was performed to assess which features of the data in adolescent girls with obesity are needed to estimate the model parameters. By determining which aspects of the glucose and insulin curves contribute to reliable parameter estimation, we can obtain a better understanding of how to apply this model framework to populations with diverse physiology. With a better understanding of the model structure and assumptions, we can determine how uncertainties in these model inputs affect estimates of insulin sensitivity indices. This quantification of the uncertainty in model inputs enables the determination of the precision of parameter estimates.

The stable isotope glucose tracer information gathered during the OGTT protocol was used to compute the total rate of appearance of glucose (Ra), the rate of appearance of exogenous glucose (Ra_{exo}) and the rate of appearance of endogenous glucose (Ra_{endo}). Researchers have developed multiple methods for computing Ra_{exo}. Since total Ra describes the contributions of both exogenous and endogenous glucose appearance, Ra_{endo} is typically defined to be the difference of computed total Ra and Ra_{exo}. This thesis compares the implementation and results of four published methods for computing Ra_{exo}. These methods will be individually motivated, derived and the method-dependence of these implementations on estimates of insulin sensitivity measures will be investigated.

Decreased S_I is common during adolescence, is lower for girls and is highly prevalent in obese adolescents [3, 4, 6, 7]. This reduced S_I means the body requires more insulin to regulate blood glucose but this reduction of S_I could differ depending on the tissues. The current gold standard for evaluating tissue specific S_I is the multistage hyperinsulinemic euglycemic (HE) clamp [8]. The HE clamp protocol involves artificially raising insulin concentrations well above baseline while simultaneously intravenously infusing glucose into the blood at a

variable rate chosen to maintain constant basal glucose levels. The glucose infusion rate (GIR) when steady state is achieved measures glucose disposal into the tissues and is a measure of S_I [8]. To quantify tissue specific S_I under physiological conditions, the addition of the stable isotope glucose tracers with the OGTT give the needed information to track the various glucose sources. The tracer data was used to calculate the exogenous and endogenous glucose. This data combined with the Production and Disposal Oral Minimal Model (OMM^{PD}) enables quantification of both peripheral and hepatic insulin sensitivity indices simultaneously. Improved understanding of hepatic S_I in obese adolescent girls will help in characterization of this population group and may support the development of targeted therapeutic interventions. A descriptive summary of blood glucose maintenance and a brief history of glucose-insulin models follows in the upcoming chapter.

CHAPTER 2

BACKGROUND

Glucose homeostasis is a complex metabolic process where plasma glucose is maintained within a narrow range. Blood glucose concentrations range primarily from 63 to 108 mg/dl and rarely exceed 198 mg/dl in arterial blood or 180 mg/dl in venous blood in healthy adults [1]. During the postprandial state, exogenous glucose enters the blood stream through gut absorption. This results in a surplus of glucose in the blood that signals the release of insulin and the suppression of glucagon production by the β-cells and α-cells of the pancreas, respectively. Increased insulin levels enable the uptake and utilization of glucose into insulin-sensitive peripheral tissues such as muscle, skin and adipose tissue. In combination with decreased glucagon and increased insulin, the liver is prompted to switch from releasing glucose to storing it in its polymeric form, glycogen. In the fasted state, insulin concentrations are low and no longer suppress the production of glucagon. This hormone, glucagon, signals the liver to break down stored glycogen to be released as glucose back into the blood. The kidneys also release a small amount of glucose into the bloodstream. This process keeps blood glucose concentrations from going dangerously low while fasted [1].

Insulin is the key hormone capable of reducing glucose concentrations by enabling glucose uptake and inhibiting endogenous glucose production [1]. When the response to insulin is diminished, peripheral tissues are not as insulin sensitive. They then require more insulin than before to absorb glucose and suppress endogenous glucose production [7]. This decrease in insulin sensitivity and increased insulin resistance (IR) leads to increased risk for many metabolic diseases and syndromes such as type 2 diabetes, polycystic ovary syndrome (PCOS) and cardiovascular disease. Increased IR impacts roughly 10 - 25 % of the population and the risk increases with obesity [7]. This thesis focuses on quantifying and assessing

IR and measures of S_I in obese adolescent girls with and without PCOS. Previous work has shown that adolescents have a 50% reduction in insulin sensitivity [3, 4] due to pubertal changes and this is even more pronounced in adolescent girls [6].

As previously described in the Introduction, the hyperinsulinemic euglycemic (HE) clamp has been the gold standard for estimating S_I in the clinical setting. This protocol involves achieving steady-state where the dynamics of the system are not influx and are simpler to interpret. Thus, the glucose infusion rate (GIR) at steady-state is a natural marker of S_I [8]. This is an invasive, labor intensive procedure, therefore, many methods have been developed to quantify insulin sensitivity, or, inversely, IR, that require simpler protocols such as an intravenous glucose tolerance test (IVGTT), a Mixed Meal Test/Meal Glucose Tolerance Test (MMT/MGTT), and or an oral glucose tolerance test (OGTT). Recent methods that utilize these less invasive tests are the Homeostasis Model Assessment (HOMA) [9] or the Mastuda-De Fronzo index (ISI) that uses area under the curve (AUC) of glucose and insulin during a glucose tolerance test [10]. Additionally, insulin sensitivity has been computed utilizing fasting glucose and insulin values such as 1/(fasting insulin) and (fasting glucose/ fasting insulin) [3, 5].

There have been a variety of mathematical models, ranging in complexity, developed to describe glucose-insulin dynamics in humans over the last several decades. Some analyze whole body glucose homeostasis by incorporating components that represent glucose absorption in the gastrointestinal tract, the role of incretin production on pancreatic insulin production all connected to sub-models of glucose, insulin and glucagon [11]. In an alternate direction, models were developed that explicitly consider β-cell mass and function to account for varying insulin secretion rates and possible β-cell decay [12]. These models were able to incorporate a large amount of the physiology to predict responses to a glucose challenge [11] and learn about the pathogenesis of type 2 diabetes [12]. A deeper understanding of the me-

chanics of glucose homeostasis will lead to more targeted therapies and earlier identification of risk factors that enable robust interventions.

One of the earliest models of glucose-insulin dynamics was the widely used Minimal Model (MM), developed to describe glucose-insulin dynamics and compute an insulin sensitivity index, S_I from an IVGTT [13,14]. The dynamics are represented by a system of two ordinary

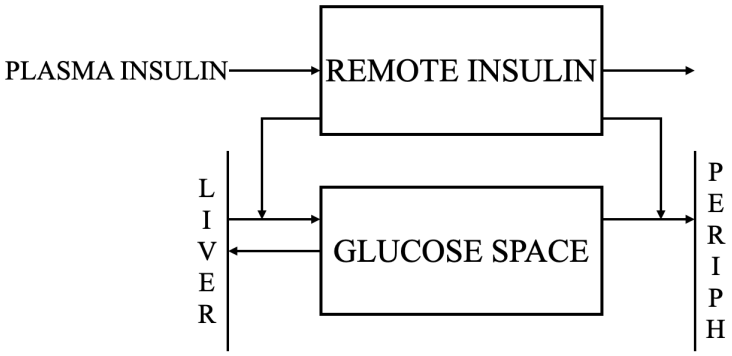

Figure 2.1: Schematic of the Minimal Model of Glucose Disappearance [14].

differential equations:

$$\begin{cases} \frac{dG}{dt} = [p_1 - X(t)] \cdot G(t) + p_4, & G(0) = G_0 \\ \frac{dX}{dt} = p_2 \cdot X(t) + p_3 \cdot I(t), & X(0) = 0 \end{cases} \tag{2.1}$$

where G is glucose concentration, G_0 is the intravenous glucose dose injected at time 0, $I(t)$ is measure insulin concentration above baseline, X is insulin action, p_4 is the net glucose balance expected when plasma glucose concentration is extrapolated to 0, p_1 is glucose effectiveness to promote glucose uptake and inhibit glucose production at constant basal insulin concentrations, p_2 governs the rate of change of insulin action and p_3 governs the amplitude of insulin entering the system. The parameters to be estimated are p_1, p_2, p_3 and p_4. This model assumes a single-compartment for glucose with insulin acting from a remote compartment that circumvents the need to model insulin separately by using the insulin concentrations as a forcing function within the model (Figure 2.1). The remote insulin

compartment expressed an insulin dependent change in glucose explicitly which is simple to model and physiological. The model dependent quantification of an insulin sensitivity index was derived to be

$$S_I = -\frac{p_3}{p_2} \tag{2.2}$$

where this index measures both the ability of insulin to uptake glucose and suppress glucose production. This was the first instance of an insulin sensitivity index, S_I, computed using a single glucose excursion test and has units of fractional glucose disappearance rate per unit insulin concentration [13].

In the following years, the more frequently used set of equations for the MM are

$$\begin{cases} \dot{G}(t) = -[p_1 + X(t)] \cdot G(t) + p_1 \cdot G_b, & G(0) = G_0 \\ \dot{X}(t) = -p_2 \cdot X(t) + p_3 \cdot [I(t) - I_b], & X(0) = 0 \end{cases} \tag{2.3}$$

where p_1 is glucose effectiveness, and G_b and I_b are baseline values of glucose and insulin concentrations, respectively [14–16]. The other notable difference in this set of equations compared to 2.1 is that p_2 has changed signs and is now strictly positive. This effect remains the same and it is explicit that p_2 governs the rate of decay of insulin action [17]. This final formulation of the MM utilizes glucose and insulin concentrations collected during an IVGTT to model the body's response to a glucose load and estimates S_I as

$$S_I = \frac{p_3}{p_2} \tag{2.4}$$

where the units are fractional glucose disappearance rate per unit insulin (for example, 1/min per μU/ml). The inclusion of p_1 allowed for estimation of glucose effectiveness, a key factor in understanding an individual's return to baseline glucose concentrations following glucose perturbations [15]. This parameter remains to be an important component in the following models and in assessing glucose metabolism.

A method to quantify S_I from an oral load was introduced decades later when the need to perform simpler glucose challenge protocols in large groups presented itself. The OGTT and meal tests are easier to perform and more physiological than an IVGTT that bypasses the gut. The first instance of modeling glucose-insulin dynamics during an oral load involved coupling the MM with a simple description of the post-hepatic appearance of newly absorbed glucose, $Ra_{ABS}(t)$ [18].

$$\begin{cases} \dot{G}(t) = -[p_1 + X(t)] \cdot G(t) + p_1 \cdot G_b + \frac{Ra_{ABS}(t)}{V} & G(0) = G_b \\ \dot{X}(t) = -p_2 \cdot X(t) + p_3 \cdot [I(t) - I_b] & X(0) = 0 \end{cases} \tag{2.5}$$

where V is the volume of distribution, and G_b and I_b are the basal glucose and insulin concentrations, respectively. The $Ra_{ABS}(t)$ has the following relationship to glucose above baseline:

$$\Delta\dot{G}(t) = -a\Delta G(t) + bRa_{ABS}(t) \tag{2.6}$$

where $\Delta G(t) = G(t) - G_b$.

Then the model becomes

$$\begin{cases} \dot{G}(t) = -[p_1 + X(t)] \cdot G(t) + p_1 \cdot G_b + \frac{[a\Delta G(t) + \Delta\dot{G}(t)]}{bV} & G(0) = G_b \\ \dot{X}(t) = -p_2 \cdot X(t) + p_3 \cdot [I(t) - I_b] & X(0) = 0 \end{cases} \tag{2.7}$$

The parameters to be estimated are p_1, p_2, p_3, V, a, and b. After integrating the insulin action differential equation, the oral S_I estimate is calculated as

$$S_I = \frac{p_3}{p_2} V = \frac{\int_0^\infty X(t)\, dt}{\int_0^\infty [I(t) - I_b]\, dt} V \tag{2.8}$$

$$= \frac{f \cdot D \frac{AUC[\Delta G(t)/G(t)]}{AUC[\Delta G(t)]} - GE \cdot AUC[\Delta G(t)/G(t)]}{AUC[\Delta I(t)]} \tag{2.9}$$

where D is the oral dose, f is the fraction of absorbed glucose, $GE = p1 \cdot V$ is glucose effectiveness and AUC denotes area under the curve and was computed using the trapezoidal rule. This integral approach requires glucose and insulin concentrations to return to baseline

during the protocol [18]. This model is then difficult to implement for glucose tolerance impaired populations as they may not return to their baseline glucose and insulin concentrations by the end of the protocol.

To overcome this constraint, researchers decided upon a piecewise linear representation of $Ra_{exo}(t)$. Then the Oral Minimal Model (OMM) describes glucose-insulin dynamics from glucose and insulin concentrations from a meal test [19].

$$\begin{cases} \dot{G}(t) = -[S_G + X(t)] \cdot G(t) + S_G \cdot G_b + \frac{Ra_{exo}(\boldsymbol{\alpha},t)}{V} & G(0) = G_b \\ \dot{X}(t) = -p_2 \cdot X(t) + p_3 \cdot [I(t) - I_b] & X(0) = 0 \end{cases} \tag{2.10}$$

where

$$Ra_{exo}(\boldsymbol{\alpha}, t) = \begin{cases} \alpha_{i-1} + \frac{\alpha_i - \alpha_{i-1}}{t_i - t_{i-1}}(t - t_{i-1}) & \text{per } t_{i-1} \leq t \leq t_i \quad i = 1, \cdots, n \\ 0 & \text{otherwise} \end{cases} \tag{2.11}$$

where $S_G = p_1$ and the $\boldsymbol{\alpha} = [\alpha_1, \cdots, \alpha_n]^T$ are unknown amplitudes and the time breakpoints t_i are known and chosen. Then insulin sensitivity is computed as

$$S_I = \frac{p_3}{p_2} V \tag{2.12}$$

and has units dl/kg/min per μU/ml. The parameters to estimate in OMM are S_G, p_2, p_3, V and $\boldsymbol{\alpha}$. However, the OMM is not structurally identifiable, specifically, S_G is not uniquely identifiable and $\boldsymbol{\alpha}$ and V are not separately identifiable. Thus, the developers of OMM first calculated a reference estimate of Ra_{exo} by using data from a triple-tracer OGTT protocol with an appropriate model of non-steady state glucose kinetics. This reference Ra_{exo} fixes the $\boldsymbol{\alpha}$ in $Ra_{exo}(\boldsymbol{\alpha}, t)$ (Eq. 2.11) so that the remaining parameters can be estimated. Then, these reference parameter estimates are used to identify the OMM. To make OMM identifiable, S_G and V are fixed to either the reference population mean or median S_G and V values then p_2, p_3 and the $\boldsymbol{\alpha}$ can be estimated.

To reduce the oral glucose load protocol duration, the investigators initially assumed exponential decay of Ra_{exo} after 2 hours in their population of healthy adults. The initial formulation of the exponential decay Ra_{exo} is below:

$$Ra_{exo}(\boldsymbol{\alpha}, t) = \begin{cases} \alpha_{i-1} + \frac{\alpha_i - \alpha_{i-1}}{t_i - t_{i-1}}(t - t_{i-1}) & \text{per } t_{i-1} \leq t \leq t_i \quad i = 1, \cdots, 4 \\ \alpha_4 \exp(-k \cdot t) & \text{per } t > t_4 \end{cases} \tag{2.13}$$

where k = 0.017 min^{-1} is the decay constant and there are 5 time break points. Then a slight modification was made to

$$Ra_{exo}(\boldsymbol{\alpha}, t) = \begin{cases} \alpha_{i-1} + \frac{\alpha_i - \alpha_{i-1}}{t_i - t_{i-1}}(t - t_{i-1}) & \text{per } t_{i-1} \leq t \leq t_i, i = 1, .., n \\ \alpha_n e^{-(\frac{t - t_n}{T})} & \text{for } t > T_{final} \text{ min} \end{cases} \tag{2.14}$$

where T = 60 minutes governs the decay and T_{final} is the end of the protocol, usually 2 hours in adults and 3 hours in youth. They validated 2-hour OMM S_I estimates on 200 adults without type 2 diabetes [20] and a 3-hour OMM implementation in a small cohort of adolescents [2].

The addition of glucose tracers to an OGTT protocol allows tracking of exogenous glucose from the meal separate from endogenous glucose. Thus, it is possible to model solely meal glucose and compute an insulin sensitivity index that measures the disposal of exogenous glucose. The Labeled Oral Minimal model (OMM*) was developed to simulate meal glucose by using such data.

$$\begin{cases} \dot{G}_{meal}(t) = -[S_G^* + X^*(t)] \cdot G_{meal}(t) + \frac{Ra_{exo}(\boldsymbol{\alpha}, t)}{V^*}, & G_{meal}(0) = 0 \\ \dot{X}^*(t) = -p_2^* \cdot X^*(t) + p_3^* \cdot [I(t) - I_b] & X(0) = 0 \end{cases} \tag{2.15}$$

where S_G^*, p_3^*, and p_2^* are meal glucose parameters, X^* is insulin action on meal glucose and $Ra_{exo}(\boldsymbol{\alpha}, t)$ is the same description introduced earlier in the OMM (Eq. 2.11). Then S_I^* computed as

$$S_I^* = \frac{p_3^*}{p_2^*} V^* \tag{2.16}$$

with units dl/kg/min per μU/ml measures the ability of insulin to promote glucose disposal only. OMM* is similarly not structurally identifiable, therefore, a reference scheme similar to that used on OMM was used to identify this model.

Since S_I^* measures the ability of insulin to promote glucose uptake into the peripheral tissues, it is a measure of peripheral insulin sensitivity. To make up total S_I, the liver's sensitivity to insulin or hepatic insulin sensitivity needs to be taken into account. A measure of hepatic S_I would then be computed as $S_I - S_I^*$. However, OMM* (Eq. 2.15) produced estimates of S_I^* that were higher than total S_I in 19% of the study's cohort which produces non-physiological negative hepatic S_I estimates [21].

A separate endogenous glucose production (EGP) model was developed to directly estimate hepatic S_I [22].

$$EGP(t) = EGP_b - k_G \cdot [G(t) - G_b] - X^L(t) - X^{Der}(t), \quad EGP(0) = EGP_b \tag{2.17}$$

$$\begin{cases} \dot{X^L}(t) = -k_1 \cdot X^L(t) + k_1 \cdot X_1(t) \quad X^L(0) = 0 \\ \dot{X_1}(t) = -k_1 \cdot [X_1(t) - k_2 \cdot (I(t) - I_b)] \quad X_1(0) = 0 \end{cases} \tag{2.18}$$

$$X^{Der}(t) = \begin{cases} k_{GR} \cdot \frac{dG(t)}{dt} & if \quad \frac{dG(t)}{dt} \geq 0 \\ 0 & if \quad \frac{dG(t)}{dt} < 0 \end{cases} \tag{2.19}$$

where EGP_b is basal endogenous glucose production, X^L is the delayed liver insulin action, X_1 causes the delay in liver insulin action, k_1 and k_2 are rate parameters and X^{Der} is a surrogate for portal insulin that depends on the rate of change of glucose concentration. Then hepatic S_I (S_I^L, dl/kg/min per μU/ml) is derived from the model equations at steady-

state and computed as

$$S_I^L = \frac{k_2}{G_b} \tag{2.20}$$

and measures the ability of insulin to inhibit glucose production by the liver [22]. This index was combined with the insulin disposal index from OMM* to compute total S_I as:

$$S_I = S_I^L + S_I^*. \tag{2.21}$$

This model was later validated against a clamp protocol in adults [23].

The next model developed allowed for simultaneous identification of production and disposal insulin sensitivity indices. The Production and Disposal Oral Minimal Model (OMM^{PD}) was developed as a combination of the previously described EGP model and the OMM [24].

$$\begin{cases} \dot{G}(t) = \frac{\mathrm{EGP}(t)+F+Ra_{exo}(t)-R_d(t)}{V}, & G(0) = G_b \\ \dot{G}_{exo}(t) = \frac{Ra_{exo}-R_{d\,exo}(t)}{V}, & G_{exo}(0) = 0 \\ \dot{G}_{end}(t) = \frac{\mathrm{EGP}(t)-R_{d\,end}(t)}{V}, & G_{end}(0) = G_{end\,b} \end{cases} \tag{2.22}$$

where G, G_{exo} and G_{end} is total, exogenous and endogenous glucose, respectively, and F is the intravenous infusion rate of labeled glucose. Ra_{exo} is the same piecewise linear description from the OMM (Eq. 2.11), R_d, $R_{d\,exo}$, and $R_{d\,end}$ are the rates of disappearance of total, exogenous and endogenous glucose, respectively. The full set of model equations is provided in Ch 7. This model is identified on total, exogenous and endogenous glucose data from an OGTT or a MMT/MGTT protocol with glucose tracers. The production (hepatic) and disposal (peripheral) insulin sensitivity indices, S_I^P and S_I^D, are derived from the model equations and total S_I can be computed from this model as

$$S_I = S_I^P + S_I^D \tag{2.23}$$

The researchers illustrated that OMM^{PD} appeared to be a reliable method of estimating both peripheral and liver insulin sensitivity when an OGTT protocol is coupled with glucose

tracers enabling exogenous and endogenous glucose contributions to be specified.

Coinciding with this work to develop estimates of total and tissue-specific insulin sensitivity indices from a meal test, the Cobelli group derived a new dynamic insulin sensitivity index, S_I^{Dyn}, that incorporated the dynamics of insulin action for a more robust measure of insulin's ability to control glucose [25]. They derived this index from the MM (Eq. 2.3). S_I^{Dyn} is defined as

$$S_I^{Dyn} = S_I \left[1 - \frac{1 - e^{-p_2 T}}{p_2 T}\right] \tag{2.24}$$

where T = 60 min is a fixed value . The value in the brackets, η, ranges from [0,1] and is described as the efficiency of S_I to regulate glucose. It is defined as follows:

$$\eta(p_2, T) = \frac{S_I^{Dyn}}{S_I} = \left[1 - \frac{1 - e^{-p_2 T}}{p_2 T}\right] \tag{2.25}$$

Additionally, they developed an analogous dynamic insulin sensitivity index derived from a HE clamp protocol, $S_{I\,clamp}^{D}$. Since S_I is a measure of the maximal capacity of the effect of insulin action on glucose metabolism, the developers concluded that S_I^{Dyn} is able to account for the speed and capacity of the insulin response. Thus, they show S_I^{Dyn} is better equipped to rank individuals based on the strength of their insulin action response than S_I. Additionally, they argue that S_I^{Dyn} may be more appropriate in individuals with impaired glucose tolerance (IGT) and type 2 diabetes as insulin action is typically slower compared to healthy subjects since their insulin response is not as robust.

A follow up application of S_I^{Dyn} was done in patients with type 2 diabetes where they utilized data from an IVGTT, a MGTT and a HE clamp [26]. The S_I^{Dyn} index computed from the MGTT used the formulation that accounts for the volume of distribution (Eq. 2.12). This paper showed that S_I^{Dyn} was a better marker for control of glucose metabolism than S_I, especially in adults with IGT and type 2 diabetes. Specifically, S_I^{Dyn} was estimated with much greater precision, less affected by assumptions of prior distributions, OGTT-based S_I^{Dyn}

correlated with the clamp S_I^{Dyn}, and correlated very strongly with clamp S_I estimates in the IGT group. Note that the validation against the clamp was done using the OGTT-S_I^{Dyn} [26].

Markov Chain Monte-Carlo for Uncertainty Quantification

The aforementioned mathematical models enable quantification of estimates of total whole body and tissue-specific S_I. Therefore, for successful application of the OMM framework in adolescents, we need to determine how certain we are in these estimates of S_I and of the remaining model parameters. An uncertainty quantification (UQ) characterizes the uncertainties of model outputs, other quantifies of interest [27–29] and how these uncertainties may propagate through to model simulations [30].

Uncertainty is measured using probability [31, 32] and, therefore, asks questions such as: what is the probability parameter θ takes on a certain value or what is the probability the simunlation falls within a certain range. This probability yields the precision of parameter estimates. When a parameter's probability distribution is unknown, Markov chain Monte Carlo (MCMC) methods can be used to build the empirical distributions necessary for inference. With these distributions, we can determine the uncertainty of model simulations as well as compute the precision of parameter estimates.

MCMC is a Bayesian statistical inference method that allows for the characterization of a distribution without knowing all of its mathematical aspects by randomly sampling values from the posterior densities [33–36]. It is the combination of two properties, Markov chain and Monte Carlo. A Markov chain is a sequential process that generates random samples where each new sample depends only on the previous one [30, 33–36]. The Monte Carlo approach is the principle of estimating properties of the distribution by examining random samples from the posterior distribution [33, 35, 36]. We construct these distributions using Bayes' formula

$$p(\theta|y) \propto p(y|\theta)p(\theta) \tag{2.26}$$

where $p(\theta|y)$ is the posterior density or the probability of the parameters θ given the data y and is proportional to $p(y|\theta)$ the probability or the likelihood, $l(y|\theta)$, of the data given the parameters and $p(\theta)$ the prior of the *a priori* probability of the parameters. MCMC is useful in Bayesian inference as it can create posterior distributions which may be difficult to express analytically or those that have no analytic expression. This enables approximation of properties of the distribution such as the mean, variance, range, etc [34, 36].

Consider, in general, the model

$$\boldsymbol{y} = f(\boldsymbol{x}, \theta) + \epsilon \tag{2.27}$$

where $\boldsymbol{y}$ is the observed data modeled by function, f, with states $\boldsymbol{x}$ and parameter set θ. The error, $\epsilon \sim N(0, \sigma^2 \boldsymbol{I})$, is assumed to be Gaussian independent and identically distributed with known variance σ^2. Then $\epsilon = y - f(\boldsymbol{x}, \theta)$ yields the likelihood function of the form

$$l(\boldsymbol{y}, \theta) \propto \prod_{i=1}^{n} l(y_i|\theta) \propto \exp\left(-\frac{1}{2\sigma^2}\sum_{i=1}^{n}[y_i - f(x_i, \theta)]^2\right) \tag{2.28}$$

where n is the number of observations. To avoid underflow and make computations simpler, we observe instead the log of the likelihood function $L(\boldsymbol{y}, \theta)$ that is expressed as

$$L(\boldsymbol{y}, \theta) \propto -\frac{1}{2\sigma^2}\sum_{i=1}^{n}[y_i - f(x_i, \theta)]^2. \tag{2.29}$$

This log of the likelihood function is used to compare the likelihood of the proposed parameter set θ when the error is assumed Gaussian [33, 35]. A similar process is taken for modeling data from other distributions where the density function is known. Maximizing $L(\boldsymbol{y}, \theta)$ is analogous to minimizing the least squares estimate defined as finding the θ that minimizes

$\sum_{i=1}^{n}[y_i - f(x_i, \theta)]^2$ [35].

There are numerous MCMC algorithms used but a general algorithm follows [36]:

1. Begin with an initial guess $\hat{\theta}^k$.
2. Randomly generate a new proposal, $\hat{\theta}^*$. This can be done either by sampling from a known distribution or by taking the last sample and adding random noise from a proposal distribution. Generally, this proposal distribution is symmetric.
3. Compare the probability of $\hat{\theta}^*$ and $\hat{\theta}^k$ given the data using a likelihood function.
4. If the new proposal $\hat{\theta}^*$ has a higher probability than the recent sample, accept the new proposal with some probability.
5. If the new proposal has a lower probability, then randomly choose to accept or reject the new proposal. There are multiple ways to make this decision and they depend on the chosen algorithm.
6. If the new proposal $\hat{\theta}^*$ is accepted, it is added to the chain as $\hat{\theta}^{k+1} = \hat{\theta}^*$. Alternatively, the next sample in the chain is a copy of the previously accepted proposal, $\hat{\theta}^{k+1} = \hat{\theta}^k$.
7. This completes one iteration and the algorithm repeats from step 2.
8. Stop when there are enough iterations. There are many methods to decide when there are enough iterations.

This approach [36] will be used to obtain distributions of the parameters of OMM. With these distributions, we can obtain the uncertainty and, therefore, the precision of the parameter estimates.

MCMC has become popular in the last couple decades as a method for both optimization and uncertainty quantification of model parameters [30,34]. The application of MCMC here

on models of glucose-insulin dynamics focuses on uncertainty quantification of parameters of interest, mainly estimates of insulin sensitivity indices. More details about the chosen MCMC algorithm and assumptions will be discussed in Section 5.4.

CHAPTER 3

DATA AND PROTOCOL

Participants were recruited from pediatric clinics at the Children's Hospital Colorado to complete an OGTT with stable isotope tracers. They included obese girls (BMI $\geq$ 90th percentile for age) without diagnosis of type 2 diabetes. All were sedentary (less than 3 hours per week of exercise, verified by standardized 3-day activity recall, and 7-day accelerometer recording, Actigraph, Pensacola, FL) and had achieved Tanner Stage 5 in puberty [1] (as assessed by physical exam by a pediatric endocrinologist, Kristen J. Nadeau or Melanie Cree-Green). Participants with and without polycystic ovary syndrome (PCOS) were included in this analysis. Participants with PCOS were defined according to the NIH criteria: 1) an irregular menstrual cycle, 2) 18 months post-menarche and, 3) clinical and biochemical evidence of hyperandrogenism. Prior to the study, pregnancy, anemia, liver diseases other than nonalcoholic fatty liver disease (NAFLD), and an alanine transferase (ALT) level greater than 125 (IU/L) were ruled out in all subjects. This study was approved by the University of Colorado Anschutz Medical Campus Institutional Review Board and the Children's Hospital of Colorado Scientific Advisory Review Committee. Parental informed consent and participant assent was obtained from all participants less than 18 years old and participant consent from those aged 18 years and above.

Three days before the overnight stay, participants consumed 3 days of an isocaloric diet (55 % carbohydrate, 15% protein, 30% fat) and refrained from physical activity. The tracer infusion protocol began with baseline blood samples (for background enrichment of glucose and concentrations of glucose and insulin) taken at approximately 6 AM then a constant infusion of glucose stable isotope began. A bolus of 4.5 mg/kg $[6,6\text{-}^2H_2]$ glucose (tracer II,

[1] The Tanner Scale is a scale of pubertal development in children and adolescents based on external primary and secondary sex characteristics. Tanner Stage 5 is the final stage.

Isotex, Miamisville, IA) was given. Then [6, 6-$^2H_2$] glucose was intravenously infused at a constant rate of 0.04 mg/kg/min continually throughout the study. Starting at 7:30 AM, blood was sampled 4 times, each 10 minutes apart, for glucose and insulin concentrations and to assure basal glucose tracer enrichment values [37] then the subjects received a sugary drink (Glucola) containing a standard 75 grams of glucose with an additional 40 mg/kg of [1-^{13}C] glucose (tracer I). Blood samples were collected initially every 10 minutes for 30 minutes then every 15 minutes for 2 hours then every 30 minutes for 2 hours then every hour until the end of the study (Figure 3.1). Previous knowledge of plasma glucose rate of appearance following ingestion suggests that glucose changes rapidly following drink ingestion and then changes more slowly as it recovers baseline values. To more accurately capture the initial appearance of exogenous Ra, measurements were sampled more frequently in the beginning of the protocol and less frequently towards the end.

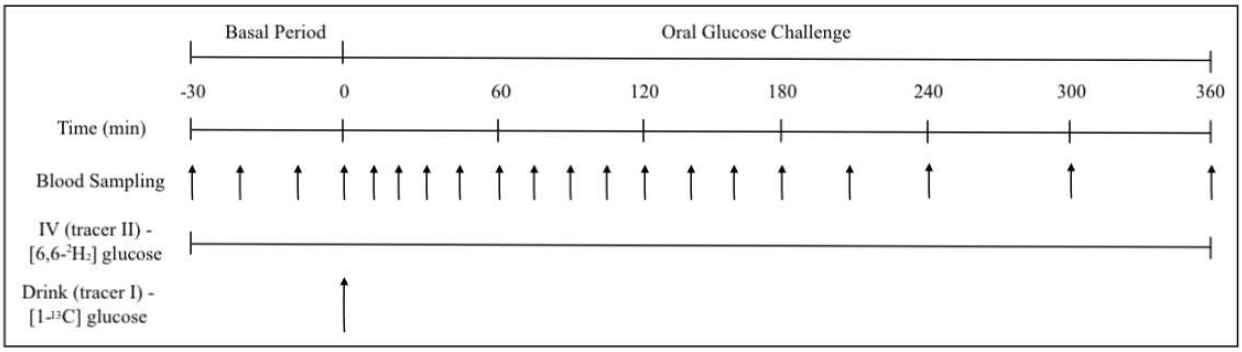

Figure 3.1: OGTT protocol with two stable isotope tracers showing blood sample times and protocol duration

Samples for plasma glucose were analyzed using a modification of the negative ion chemical ionization gas chromatography mass spectrometry [37–39]. The 331, 332 and 333 fragments produced by chemical ionization were measured [40]. Fragment 331 corresponds to glucose tracee, 332 to glucose tracer I and 333 to glucose tracer II. Blood glucose concentrations were found using modified glucose oxidase-based method on a StatStrip®hospital glucose monitoring system (Nova Biomedical, Waltham, MA), which has been previously

demonstrated to be equivalent with with a YSI 2300 STAT Plus™(YSI, Inc, Yellow Springs, OH) glucose analyzer [41]. Serum insulin concentration was determined with radioimmunoassay (Millipore, Billerica, MA).

The ratios of tracer I and tracer II to tracee were used to track changes in relative enrichment. Relative abundance of each tracer is reported as tracer-to-tracee ratio (TTR). The raw tracer data was corrected to account for the patients' background enrichments and glucose isotopes coming from other sources. The corrections for [1-^{13}C] glucose tracer I were computed as follows:

- Compute TTR of tracer I to tracee using raw counts.
- Correct for patient's background enrichment by subtracting 6 am value.
- Subtract average of 6 am to 8 am TTR to correct for [1-^{13}C] glucose coming from the IV.
- Correct for naturally occurring [1-^{13}C] glucose by multipyling by (1-0.011) called the skew correction.
- Compute amount of tracer 1 being recycled by the liver by scaling the skew corrected tracer I TTR by the ratio of tracer II TTR in the plasma at the current time by the tracer II TTR at time 0 min.
- Correct for liver recycling by subtracting the previously computed quantity from the skew corrected tracer I amounts immediately after minimum tracer II TTR in the blood indicating max liver suppression of glucose production.

For [6, 6-$^{2}H_2$] glucose tracer II, the corrections were computed as follows:

- Compute TTR of tracer II to tracee using raw counts.
- Subtract 6 am value to correct for patient's background.

- Multiply the skew corrected measurement of tracer I by the proportion of tracer II to tracer I in the test drink to compute the amount of $[6,6\text{-}^2H_2]$ glucose tracer II coming from the drink.

- Subtract $[6,6\text{-}^2H_2]$ glucose tracer II coming from the drink.

The corrected glucose tracer data was used to compute glucose fluxes in Ch 6 and exogenous and endogenous glucose contributions in Ch 6 and Ch 7.

CHAPTER 4

DURATION DEPENDENCE OF OMM

4.1 Introduction

Insulin sensitivity (S_I) indices quantify the ability of insulin to both promote glucose disposal and inhibit endogenous glucose suppression during a glucose challenge. The decrease of S_I leads to increased risk for metabolic syndrome and is a principle component of diseases such as type 2 diabetes mellitus, type 1 diabetes, and polycystic ovary syndrome (PCOS) [42–45]. Adolescents with obesity are at higher risk for decreased S_I [46, 47]; teenagers experience a puberty related reduction in S_I; have greater insulin secretion rates compared to adults [3, 4, 48]; and S_I is significantly lower in adolescent girls compared to boys [6, 49, 50].

Evaluation of therapies to improve S_I in youth requires reliable quantification of S_I with a method validated in the target population. The hyperinsulinemic euglycemic (HE) clamp remains the gold standard for measuring S_I in adults and youth, but it is invasive, labor intensive, non-physiological, and cost prohibitive for large-scale research [8, 51, 52]. The intravenous glucose test (IVGTT) is another method to quantify S_I but it is similarly non-physiological since the IV injection of glucose circumvents the gut [13, 17]. Several simple methods such as HOMA [53], QUICKI [54], and the Matsuda index [10], have been developed to quickly quantify S_I in the clinical setting [5, 9, 10, 54–56]. Alternatively, the Oral Minimal Model (OMM), a differential-equations based model of glucose-insulin dynamics [19, 21, 57] may be used to estimate S_I in the physiological setting of an oral glucose tolerance test (OGTT). The OMM describes glucose and insulin action dynamics, and it is fit to glucose data and forced by time-varying insulin data. Therefore, an individual's insulin response and insulin sensitivity are both represented in the model, and model parameters are used to

derive a measure of S_I. The identification of differences in S_I between groups and changes in S_I post-treatment is essential for characterizing metabolic phenotypes in different populations and assessing the efficacy of interventions. Previous work has demonstrated that the OMM can robustly estimate S_I and is more sensitive to changes in S_I than other fasting and OGTT-based indices of S_I [42, 58–61].

The OMM was developed in adults with some implementations in youth [2, 19, 20, 62–65]. Initial quantification of OMM-based measures of S_I used data from 7 hour meal glucose tolerance test (MGTT) and OGTT, and these S_I estimates we validated against the HE clamp in healthy adults [62] and adults with type 2 diabetes [66]. Shorter OGTT protocol durations are preferable to reduced demands on participants and resources, and assumptions on the rate of appearance of exogenous glucose after the last measured time point have enabled the implementation of shorter protocols as validated in adults without type 2 diabetes [19, 20], lean to obese adolescents [2], and adolescent girls [64, 65]. However, insulin resistance (IR) changes the glucose-insulin dynamics typically described by OMM, and the protocol duration dependence of OMM S_I estimates is not well understood in populations expressing diverse metabolic phenotypes.

To address this gap, we compared S_I estimates computed using a 6-hour protocol to S_I estimates computed with data from shorter protocols in a highly IR cohort of adolescent girls with obesity. In this cohort and other IR populations, glucose concentrations tend to remain elevated for longer periods indicating disrupted glucose-insulin dynamics [67]. For populations experiencing IR, data collected for a longer time period after peak glucose may allow for more reliable OMM-based estimation of S_I [63]. This constraint required extending the OGTT protocol to 6 hours in our participants with significantly decreased S_I [19]. Given the extended period of elevated glucose in this population, we hypothesized that estimates of S_I would depend on protocol duration in this population with at least 4 hours of data re-

quired to accurately estimate S_I using OMM. This work has been submitted for publication in the Metabolism Open journal.

4.2 Methods and Materials

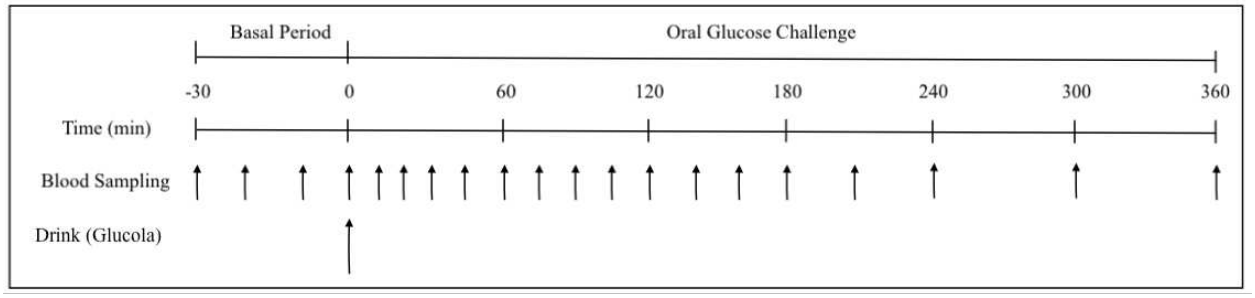

Figure 4.1: OGTT protocol showing blood sampling times and duration

Participants and Protocol

This is a secondary analysis of data collected during a frequently sampled OGTT with stable isotope glucose tracers. A detailed description of this dual tracer OGTT protocol can be found in Chapter 3. In brief, sixty-eight (18 with normal menses and 50 with PCOS), medication naïve, sedentary overweight and obese (BMI $\geq$ 90th percentile for age and sex) adolescent (Tanner Stage 5) girls underwent a frequently sampled 6-hour OGTT. Blood was sampled at -30,-20,-10, 0, 10, 20, 30, 45, 60, 75, 90, 105, 120, 135, 150, 180, 210, 240, 300 and 360 minutes following ingestion of 75 g plus an additional 40 mg/kg of glucose (Figure 4.1) for glucose and insulin concentrations.

The Oral Minimal Model

The OMM was used to model glucose-insulin dynamics and estimate S_I [19]. Recall

$$\begin{cases} \dot{G}(t) = -[S_G + X(t)] \cdot G(t) + S_G \cdot G_b + \frac{Ra_{exo}(\boldsymbol{\alpha},t)}{V} & G(0) = G_b \\ \dot{X}(t) = -p_2 \cdot X(t) + p_3 \cdot [I(t) - I_b] & X(0) = 0 \end{cases} \tag{4.1}$$

where

$$Ra_{exo}(\boldsymbol{\alpha}, t) = \begin{cases} \alpha_{i-1} + \frac{\alpha_i - \alpha_{i-1}}{t_i - t_{i-1}}(t - t_{i-1}) & \text{per } t_{i-1} \leq t \leq t_i \quad i = 1, \cdots, n \\ 0 & \text{otherwise} \end{cases} \tag{4.2}$$

where G is total glucose, X is insulin action, I is insulin concentration, G_b and I_b are basal glucose and insulin concentrations, respectively, S_G, p_2, and p_3 are rate constants and $\boldsymbol{\alpha}$ denotes $[\alpha_0, \alpha_1, \cdots, \alpha_n]^T$ [19,57,62]. The time breakpoints t_i were specified by the sampling schedule and protocol duration. Specific breakpoints were chosen as follows: 2 hour protocol: 0, 10, 30, 60, 90, 120 min; 3 hour protocol: 0, 10, 30, 60, 90, 120, 150, 180 min; 4 hour protocol: 0, 10, 30, 60, 90, 120, 150, 180, 210, 240 min; 6 hour protocol: 0, 10, 30, 60, 90, 120, 150, 180, 210, 240, 300, 360 min. The time breakpoints for the 6-hour protocol represent the full glucose profile, and the breakpoints for the shorter protocols represent the truncation of the 6-hour breakpoints based on protocol duration [20].

There were both "truncated" and "exponential" versions of OMM. For sufficiently long protocols that allowed glucose and insulin concentrations to return to baseline (4 and 6 hours), OMM was directly applied to compute S_I ("truncated models"). To model data from shorter OGTT protocols, it has been recommended to assume exponential decay of $Ra_{exo}(\boldsymbol{\alpha}, t)$ after the last time breakpoint [68]. We implemented this approach for 2-, 3-, and 4-hour OGTT protocols using both fixed and estimated decay time constants ("exponential models"). In the exponential models, S_I was estimated directly, and in the truncated models S_I was defined to as

$$S_I = \frac{p_3}{p_2} \cdot V \tag{4.3}$$

with units dl/kg/min per μU/ml [19,57].

The 2-, 3- and 4-hour exponential models describe $Ra_{exo}(\boldsymbol{\alpha}, t)$ as follows:

$$Ra_{exo}(\boldsymbol{\alpha}, t) = \begin{cases} \alpha_{i-1} + \frac{\alpha_i - \alpha_{i-1}}{t_i - t_{i-1}}(t - t_{i-1}) & \text{per } t_{i-1} \leq t \leq t_i \quad i = 1, \cdots, n \\ \alpha_n \cdot e^{\frac{-(t-t_n)}{T}} & \text{for } t \geq T_{final} min \end{cases} \tag{4.4}$$

where $Ra_{exo}(\boldsymbol{\alpha}, t)$ is assumed to decay exponentially for $T_{final} > 120$ min, $T_{final} > 180$ min, $T_{final} > 240$ min, respectively [19]. For the 2-hour exponential OMM implementation, the decay constant $T = 60$ minutes [19]. For exponential OMM implementations with more than two hours of data, T may be estimated as a Bayesian parameter rather than fixed to 60 minutes [68]. Both approaches were implemented in the 3- and 4-hour exponential models.

To improve the numerical identifiability of OMM, two constraints were applied. Initially, $Ra_{exo}(\boldsymbol{\alpha}, t)$ was constrained by the total amount of glucose ingested and absorbed using the equation below:

$$\int_0^T Ra_{exo}(\boldsymbol{\alpha}, t)\, dt = \frac{D \cdot f}{BW} \tag{4.5}$$

where $T = 240$ minutes for the 4-hour truncated model, $T = 360$ minutes for the 6-hour model, $T = \infty$ for the exponential models, D is the glucose dose, f is the fraction of glucose absorbed and is set to 0.9, and BW is the body weight (kg) of the participant [19, 57]. To further improve numerical identifiability of the model, we constrained S_G as

$$S_G = \frac{GEZI + S_I \cdot I_b}{V} \tag{4.6}$$

where $GEZI$, glucose effectiveness at zero insulin, was fixed to 0.025 dl/kg/min [68]. I_b was measured for each participant; V was fixed to 1.45 dl/kg; and S_I (dl/kg/min per μU/ml) was estimated.

The OMM was implemented for all participants using 2, 3, 4 and 6 hours of data. All model equations were implemented in SAAM II (SAAM II software v 2.2, The Epsilon Group, Charlottesville, VA, USA).

Statistical Analysis and Model Comparison

All model comparisons were performed in MATLAB (Mathworks, Natick, MA). The estimated S_I values obtained from each method were compared using ANOVA. Data are reported as the mean ± SD. The 6-hour OMM S_I estimates were taken to be the reference estimates since they utilized data the full duration of the OGTT protocol and glucose concentrations returned to baseline for all participants within 6 hours [19, 20]. These estimates were compared to the S_I estimates from shorter OMM protocol durations using Pearson's correlation coefficients, linear regressions, and Bland-Altman plots [69] to quantify the differences between estimates obtained using different methods. The Williams correlation test was used for pairwise comparison of the strengths of the correlations [70]. We computed the mean squared error (MSE) between 6-hour OMM S_I estimates and S_I estimates from protocols of shorter duration, and we compared these errors using paired t-tests. For Bland-Altman plots we report the bias, the 95% confidence intervals of the bias, and the 95% limits of agreement between the S_I estimates obtained using the 2 methods are reported.

To investigate the differences in S_I values estimated using the 4-hour truncated model and the 4-hour exponential model, participants were divided into subgroups based on glucose concentrations at four hours being above, below or within 10 mg/dl of their baseline glucose levels. For each subgroup, the MSE between 4-hour S_I estimates associated with the exponential and truncated models and the 6-hour estimates were computed. These errors were compared using paired t-tests. Correlations between S_I estimates from the 6-hour OMM and the S_I estimates from both 4-hour exponential and truncated models were computed and compared for each subgroup using **corr_rtest** [70].

The error between the 6-hour glucose concentrations and the simulated glucose for each of the models was computed as the l^2 norm of the difference between the data and the model

output. To illustrate how the exponential assumption for $Ra_{exo}(\boldsymbol{\alpha}, t)$ translates to glucose dynamics during the OGTT, the 2-, 3-, and 4-hour exponential models were simulated for 6 hours. Predicted glucose concentrations associated with each model were plotted with the glucose concentration data and the 6-hour model simulations. Model simulations were performed using the MATLAB built-in ode solver **ode45**. P-values < 0.05 were considered significant; we report p-values greater than 0.001 and otherwise report p-values as < 0.001.

4.3 Results

Participants

Participant demographics are summarized in Table 4.1. Mean 2-hour glucose is close to the pre-diabetes cut off of > 140 mg/dl demonstrating that dysglycemia was common in this group. The average glucose and insulin concentrations during the OGTT protocol illustrate the moderate variability in glucose concentrations and large variability of insulin concentrations for this participant group (Figure 4.2).

OMM Implementations

For four representative participants ordered from more to less insulin sensitive, glucose and insulin data are presented with simulated glucose time traces for each model (Figure 4.3). The measured insulin concentrations describe each individual's response to the OGTT and are used to force the insulin action dynamics in OMM.

All models accurately described glucose concentrations over the duration of specified data. By contrast with the 6-hour and 4-hour truncated models, the exponential models predicted glucose beyond the duration of specified data using the assumption of the exponentially decaying $Ra_{exo}(\boldsymbol{\alpha}, t)$. However, in general, the exponential models did not accurately reproduce glucose profiles. Error decreased monotonically with increased model duration with errors 60.73 ± 36 (mean $\pm$ SD), 40.80 ± 23, 29.61 ± 17 and 19.43 ± 6 mg/dl for the 2-, 3-,

Table 4.1: Participant Characteristics

Age	15.8 ± 1.2
Race/Ethnicity (N)	
Non-Hispanic White	23
Hispanic White	35
Black	8
Asian	2
Family history of T2D (%)	76
Weight (kg)	94 ± 16.5
Height (cm)	164 ± 7
BMI (kg/m^2)	35.4 ± 5.6
BMI percentile	97.6 ± 2
Fasting glucose (mg/dL)	90 ± 9
2 hour glucose (mg/dL)	136 ± 24
Fasting Insulin (mIU/L)	28 ± 16
2 hour insulin (mIU/L)	276 ± 200

Data shown are mean ± standard deviation of the mean unless otherwise noted.

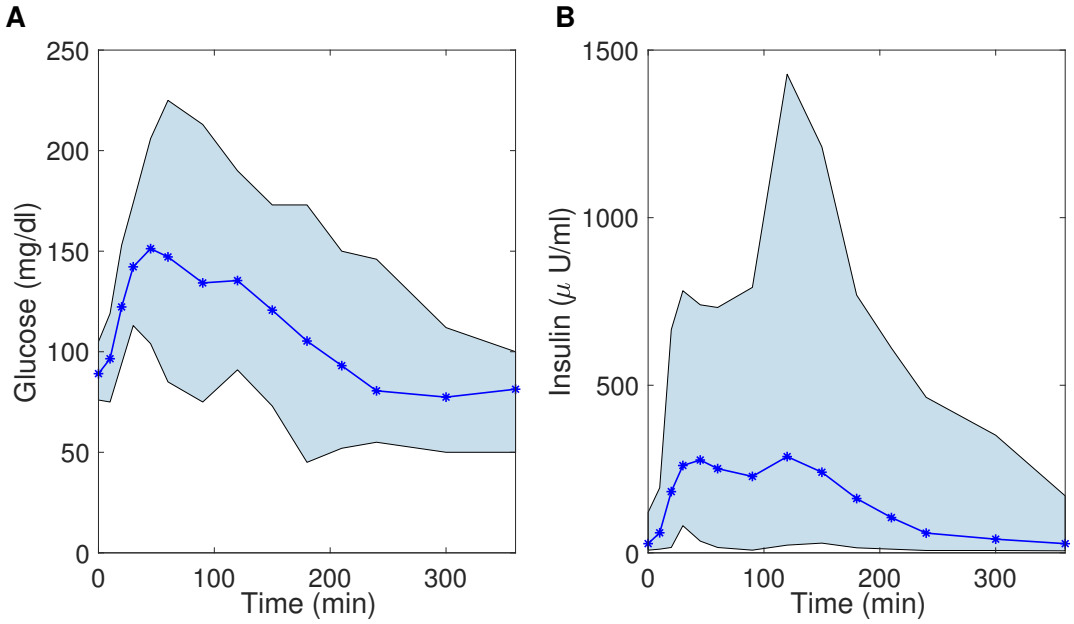

Figure 4.2: **Glucose and insulin concentrations.** Glucose (**A**) and insulin (**B**) concentration ranges for all study participants (n = 68) for a six hour OGTT. Mean glucose and insulin concentrations (blue line), ± max/min values (light blue shading) indicate range of variability across the cohort.

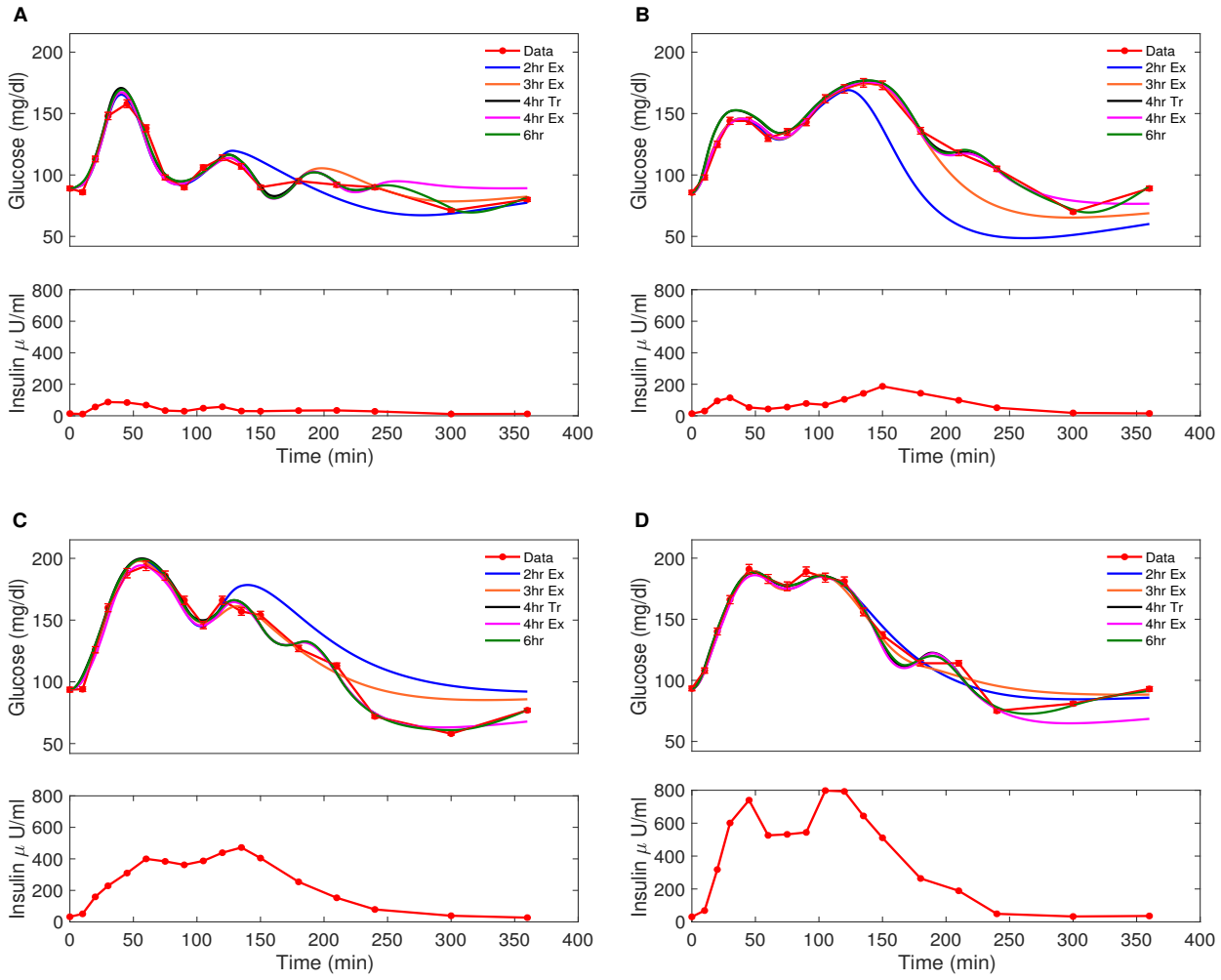

Figure 4.3: **Simulated glucose dynamics based on different OMM time models.** Glucose and insulin (**A**, **B**, **C**, **D**) profiles for representative participants with high (**A**, **B**) or low (**C**, **D**) insulin sensitivity as assessed by 6-hour OMM S_I. The simulated glucose dynamics obtained using the 2h Ex, 3h Ex, 4h Tr, 4h Ex, and 6h implementations of OMM are plotted with the glucose data for four participants. For truncated models (4h Tr and 6h), there are no assumptions of glucose dynamics beyond the specified time breakpoints. For the exponential models (2h Ex, 3h Ex and 4h Ex), exponential decay of the rate of appearance of glucose is assumed after 120 min., 180 min., and 240 min., respectively.

4-hour exponential models and the 6-hour model, respectively.

The estimated profiles of $Ra_{exo}(\boldsymbol{\alpha}, t)$ also varied with model duration as seen for the four representative participants (Figure 4.4). In general, the assumption of exponential decay in

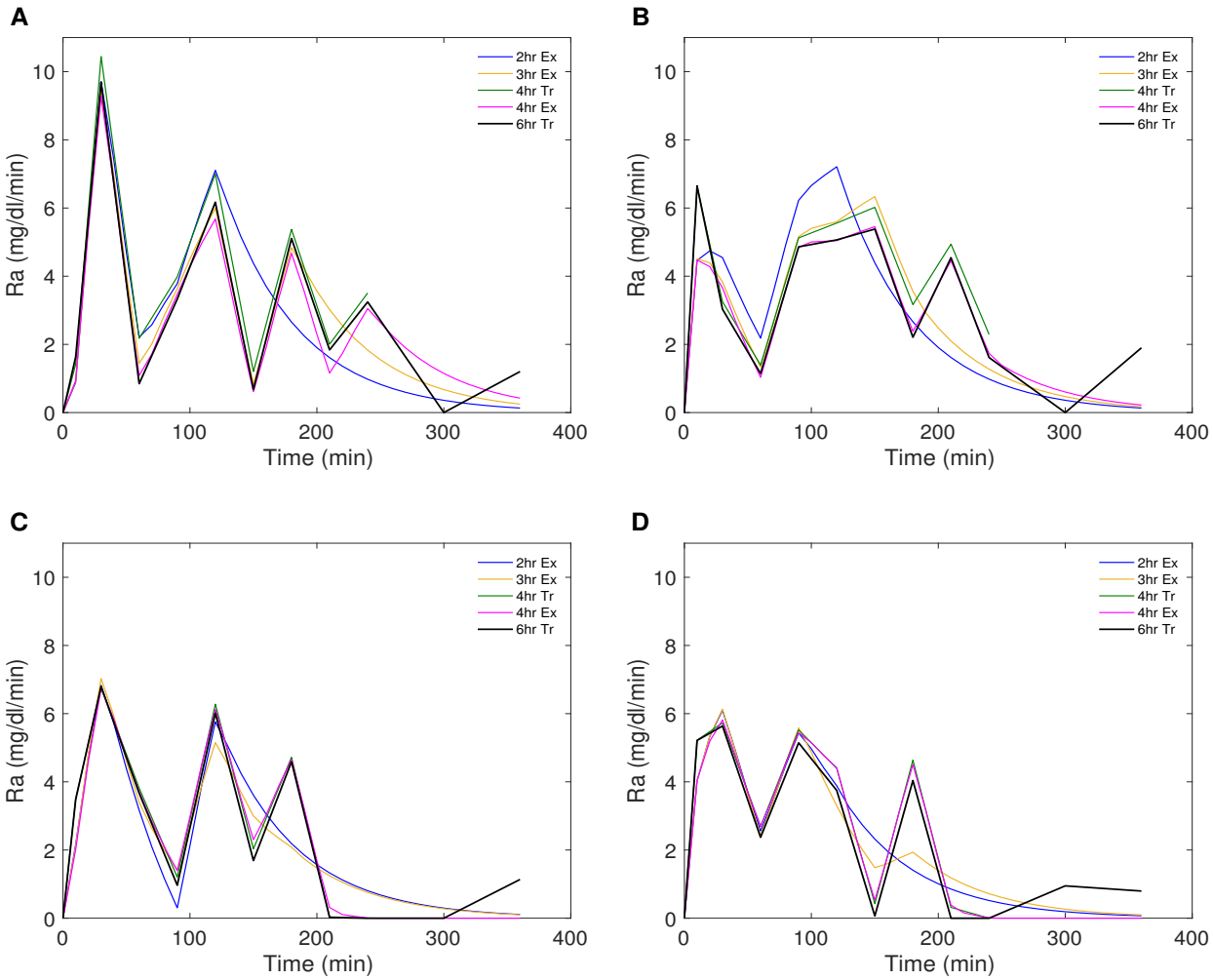

Figure 4.4: **Estimate rate of appearance of drink glucose by OMM model duration.** The rate of appearance of exogenous glucose ($Ra_{exo}(\boldsymbol{\alpha}, t)$) estimated for each model for the 4 representative participants reported in Figure 4.3. Onset of exponential decay of 2h Ex, 3h Ex and 4h Ex OMM models is initiated after 120, 180, and 240 min, respectively.

the 2-, 3- and 4-hour exponential methods resulted in less variability in $Ra_{exo}(\boldsymbol{\alpha}, t)$ compared to the rates predicted in the 6-hour OMM implementation. Both the 3- and 4- hour exponential models were implemented with the time constant of decay, T, fixed to 60 min and estimated as a Bayesian parameter. Estimated T values were close to the fixed T value of 60 min for all participants (3-hour exponential: median T = 59.92; minimum T = 54.66; maximum T = 60.51; 4-hour exponential: median T = 59.99; minimum T = 55.31; maximum T = 60.03). Individualized estimates for T did not affect S_I estimates nor improve the

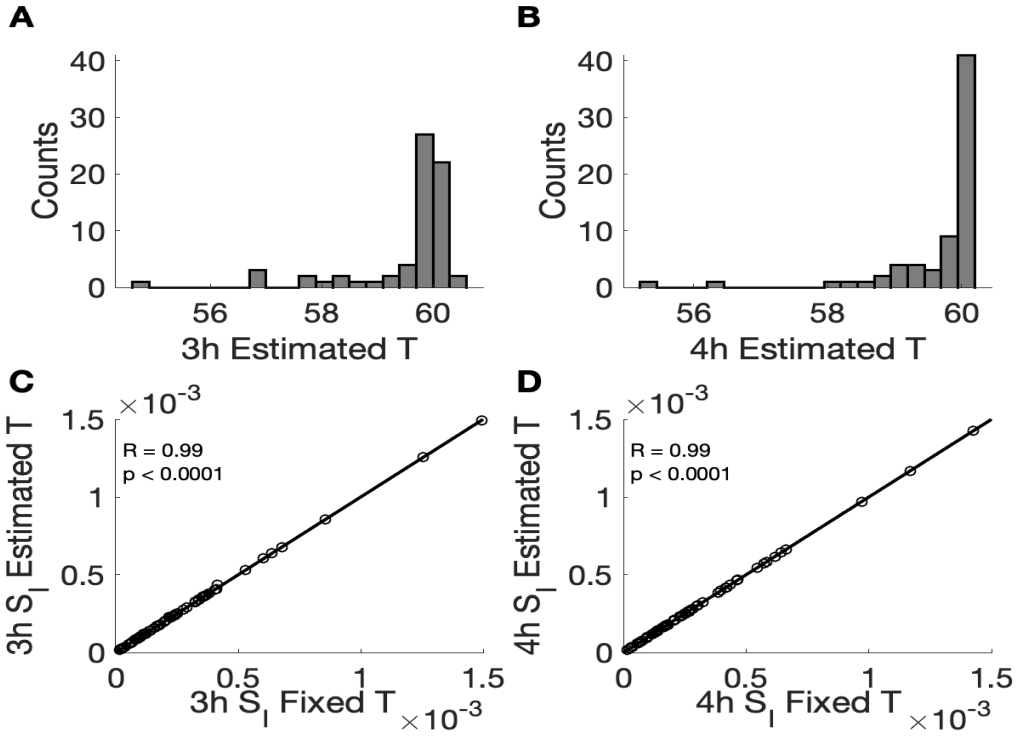

Figure 4.5: **Comparing Bayesian Estimated T versus T Fixed to 60 min.** Comparing the results of when T is estimated versus when T is fixed to 60 min. The histograms of the estimated T values from the 3h Ex (**A**) and the 4h Ex models. Below (**C**, **D**) the scatter plots of the S_I estimates calculated with an estimated T versus T fixed to 60 min show that the estimates are virtually equivalent. Shown is the line of equality.

ability of the exponentially decaying $Ra_{exo}(\boldsymbol{\alpha}, t)$ to predict glucose concentrations following the last time point of data (Figure 4.5). Therefore, we focused the results on exponential OMM implementations with T fixed to 60 minutes to facilitate comparison of exponential models.

Model Comparisons

To investigate the effect of model duration on estimated S_I, we compared S_I values calculated using the 6-hour OMM to S_I values calculated from OMMs with shorter durations over all participants. For each model, average S_I estimates and average precision of S_I estimates given as the coefficient of variation (CV) were determined (Table 4.2). Mean S_I

values for all participants were not significantly different across methods (ANOVA, p = 0.79). However, the MSE between the 6-hour S_I estimates and S_I estimates from shorter OMM implementations decreased with protocol duration with lowest errors associated with the 4-hour truncated model. Specifically, the errors for S_I estimates from the 4-hour truncated model were significantly lower compared to the errors for the S_I estimates from other models with the exception of the 2-hour exponential model (4-hour exponential: $p < 0.001$; 3-hour exponential: p = 0.01; 2-hour exponential: p = 0.07). Similarly, the errors for S_I estimates from the 4-hour exponential model were lower compared to the errors for S_I estimates from the 3-hour exponential model (p = 0.01) and not significantly different from the errors for S_I estimates from the 2-hour exponential model (p = 0.78).

Table 4.2: Average S_I estimates, Precision and MSE

OMM Implementation	S_I, 10^{-4} dl/kg/min per μU/ml	Precision, CV %	MSE, 10^{-9}
2-hour Ex	2.86 ± 3.31	24.27 ± 5	16.1
3-hour Ex	2.55 ± 2.62	19.35 ± 7	10.3
4-hour Ex	2.81 ± 2.59	16.25 ± 6	6.79
4-hour Tr	3.13 ± 3.14	18.60 ± 6	5.97
6-hour	3.06 ± 2.85	12.77 ± 6	-

Values are mean ± SD. Reported is the average precision of S_I estimates given as the coefficient of variation (CV %) and the mean squared error (MSE) of S_I estimates from shorter OMM implementations to estimates of S_I from the 6-hour.

The correlations between the S_I estimates from OMMs with shorter durations and the S_I estimates from the 6-hour OMM were high and increased monotonically with protocol duration from the 2-hour exponential model (R = 0.93) to the 4-hour truncated model (R = 0.97) (Figure 4.6). Comparisons of correlations showed that the correlations between the 6-hour OMM S_I estimates and the 2-hour and 3-hour exponential S_I estimates, respectively, were generally weaker than the correlations between the 6-hour OMM S_I estimates and the 4-hour exponential or 4-truncated S_I estimates (2-hour exponential v. 4-hour exponential,

p = 0.008; 2-hour exponential v. 4-hour truncated, p < 0.001; 3-hour exponential v. 4-hour truncated, p = 0.02). However, in general, correlations between the 6-hour OMM S_I estimates and OMM S_I estimates from OMM exponential implementations were not significantly different (2-hour exponential v. 3-hour exponential, p = 0.07; 3-hour exponential v. 4-hour exponential, p = 0.29). Moreover, the correlation between the 4-hour truncated S_I estimates and the 6-hour OMM S_I estimates was not significantly different from the correlation of the 4-hour exponential S_I estimates and the 6-hour OMM S_I estimates (p = 0.09).

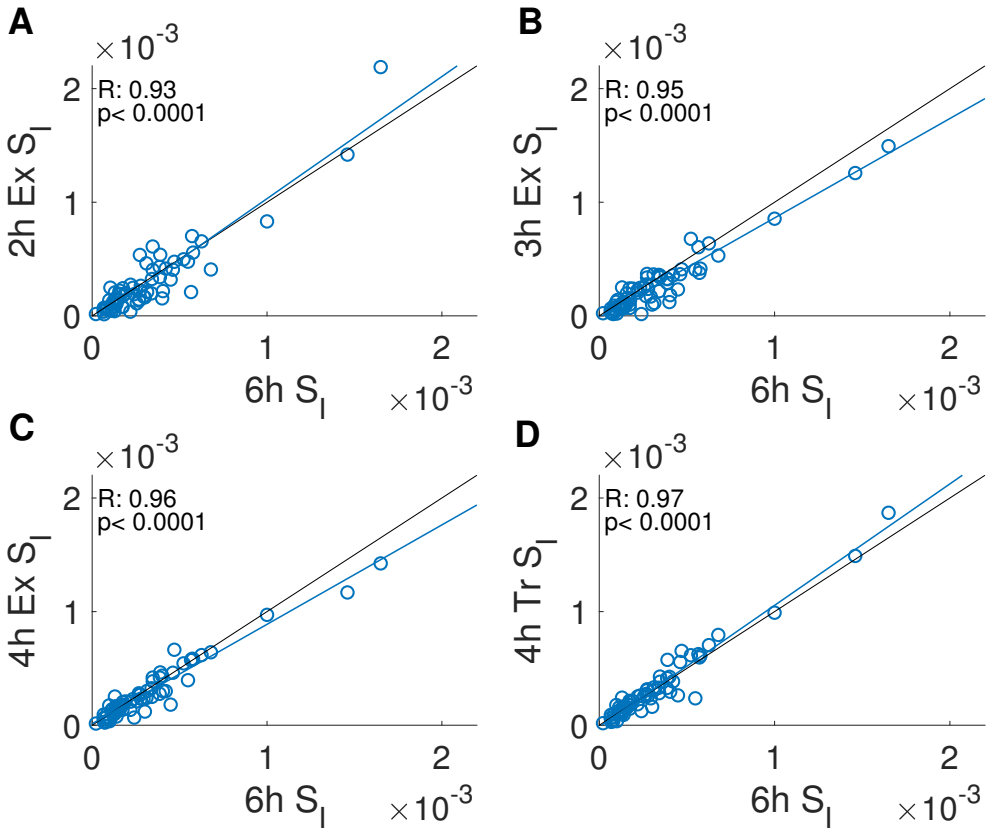

Figure 4.6: **Correlations between S_I estimated with the 6-hour OMM as a reference and OMM implemented with shorter durations (n = 68).** Scatter plots showing the correlations of the 2-hour exponential (**A**), the 3-hour exponential (**B**), the 4-hour truncated (**C**), and the 4-hour exponential (**D**) OMM S_I estimates with the 6-hour OMM S_I estimates. The blue line is the least squares fit to the data, and the black line indicates equality of estimates obtained using different models.

To further characterize the correlations between S_I estimates obtained using different OMM implementations, we compared the regression lines associated with S_I estimates from different methods to the identity line. The regression line for the 4-hour exponential model S_I estimates was not significantly different from the identity line ($p < 0.001$) as the 95% confidence intervals for both the slope and intercept contained 1 and 0, respectively (Table 4.3). The slope for the 3-hour exponential was also not significantly different from 1 but had an intercept significantly different from 0 ($p < 0.001$). The regression lines of the 2-hour exponential and 4-hour truncated were significantly different from the identity but the 4-hour truncated had the smallest intercept compared to the 2- and 3-hour exponential ($p < 0.001$).

Table 4.3: Linear regression results of S_I estimates from shorter OMM implementations compared to 6-hour model

OMM Implementation	Slope (CI)	Intercept (CI), 10^{-5}
2-hour Ex	0.79 (0.72, 0.88)	7.77 (4.29, 11.24)
3-hour Ex	1.03 (0.95, 1.12)	4.24 (1.25, 7.22)
4-hour Ex	1.05 (0.98, 1.13)	0.87 (-1.94, 3.68)
4-hour Tr	0.88 (0.83, 0.94)	3.03 (0.68, 5.39)

The slope and intercept with their 95% confidence intervals (CI) for regression lines comparing S_I estimates from shorter OMM implementations to 6-hour S_I estimates. All $p < 0.001$.

Bland-Altman plots demonstrated the differences between the S_I estimates from shorter protocols compared to the 6-hour S_I estimates (Figure 4.7). The differences in S_I estimates obtained using different models do not show systemic change with average S_I values, demonstrates that the variability in the differences is not related to the size of the measurement. The biases for the S_I estimates from the 2-, 3-, and 4-hour exponential models were order 10^{-5}, positive and, for the 3- and 4-hour exponential models, significantly different from zero (Table 4.4), indicating that these models underestimate S_I compared to the estimates from the 6-hour model. In contrast, the bias for the 4-hour truncated model was an order

of magnitude smaller, negative and the CI of the bias contained zero. The Bland-Altman plots for the percent differences gave similar results where the smallest bias in the percent differences occurred for the 4-hour truncated model (Table 4.5, Figure 4.8).

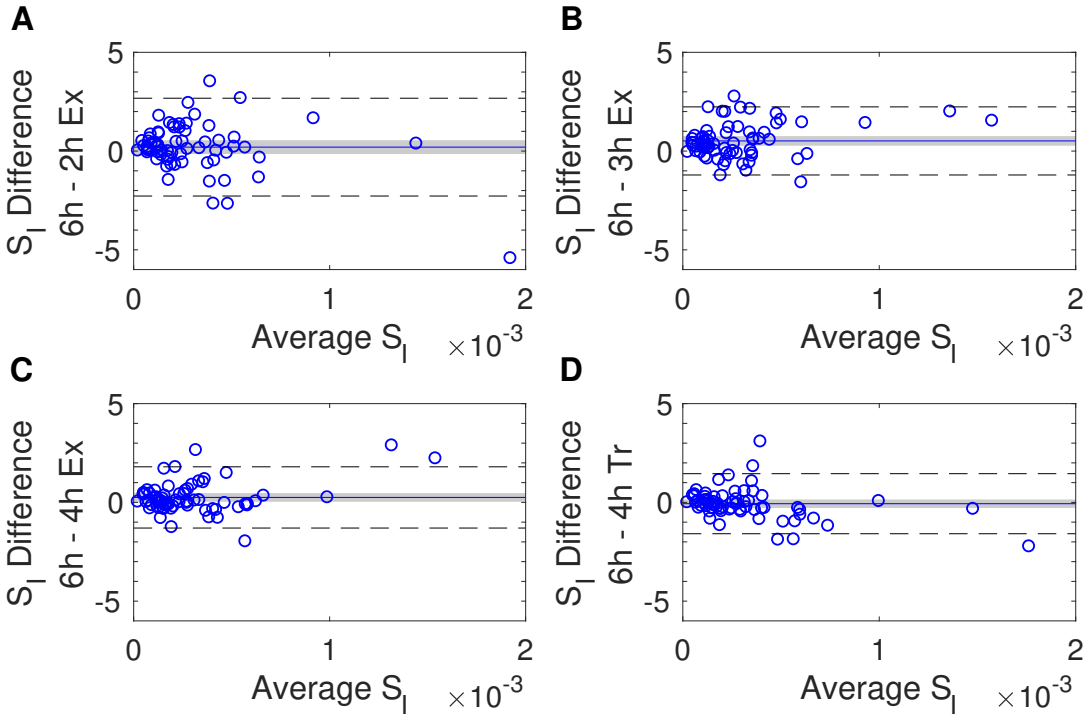

Figure 4.7: **Bland-Altman plots showing the bias of the S_I estimates computed with the 6-hour OMM and with shorter OMM implementations (n = 68).** The bias (solid line), the confidence interval of the bias (shaded region), and the 95% limits of agreement (dashed line) are reported. The 2-hour exponential model (**A**), 3-hour exponential model (**B**), and 4-hour exponential model (**C**), all showed a small positive bias indicating that these models underestimate S_I. The 4-hour truncated model (**D**) had a small negative bias indicating this model overestimated S_I.

Baseline glucose affects variability in S_I estimates

To better understand the effects of delayed return to baseline glucose levels and reactive hypoglycemia (RHG) on the 4-hour OMM S_I estimates, we considered glucose concentrations 4 hours after drink ingestion relative to baseline glucose for each participant. Participants were divided into subgroups based on whether they were above, below or within 10 mg/dl of

Table 4.4: Bland-Altman Bias, CI and Limits of Agreement

OMM Implementation	Bias (CI), 10^{-5}	Limits of Agreement, 10^{-4}
2-hour Ex	2.00 (-1.50, 5.50)	-2.28, 2.68
3-hour Ex	5.14 (2.70, 7.57)	-1.21, 2.24
4-hour Ex	2.51 (0.318, 4.70)	-1.30, 1.80
4-hour Tr	-0.672 (-2.82, 1.47)	-1.59, 1.45

Reported is the bias, confidence interval of the bias (CI) and the 95% limits of agreement of S_I estimates from shorter OMM implementations compared to the 6-hour S_I estimates.

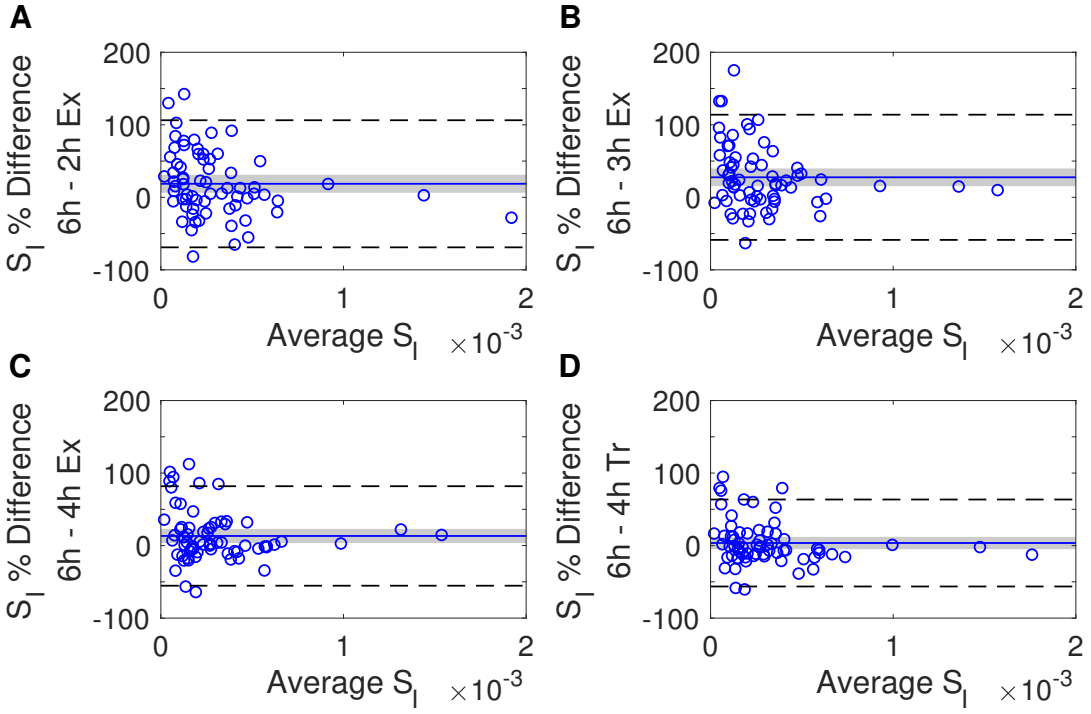

Figure 4.8: **Bland-Altman plot showing bias and limits of agreement for percent differences of S_I estimates computed with the 6-hour OMM and with shorter model implementations (n = 68).** The bias (solid line), the confidence interval of the bias (shaded region) and the 95% limits of agreement (dashed line) are reported. (**A**) 2-hour exponential model, (**B**) 3-hour exponential model, (**C**) 4-hour exponential model, (**D**) 4-hour truncated model.

their baseline glucose concentrations after 4 hours of the OGTT protocol. Then we compared the S_I estimates obtained from both the 4-hour exponential and truncated models for each subgroup. Approximately 54% (n = 37) of participants had 4-hour glucose concentrations

Table 4.5: Bland-Altman Percent Difference Bias, CI and Limits of Agreement

OMM Implementation	Bias (CI), %	Limits of Agreement, %
2-hour Ex	18.67 (6.29, 31.04)	-68.97, 106.30
3-hour Ex	27.62 (15.42, 39.81)	-58.71, 113.94
4-hour Ex	13.28 (3.59, 22.97)	-55.33, 81.88
4-hour Tr	3.57 (-4.90, 12.04)	-56.39, 63.54

Reported is the bias, confidence interval of the bias (CI) and the 95% limits of agreement of S_I estimates from shorter OMM implementations compared to the 6-hour S_I estimates.

at least 10 mg/dl below their baseline glucose levels; 10% (n = 7) of participants had 4-hour glucose at least 10 mg/dl above their baseline glucose levels; and the remaining participants (n = 24) had 4-hour glucose concentrations within 10 mg/dl of their baseline glucose levels.

The differences in S_I estimates between the 4-hour models and the 6-hour S_I estimates were evaluated using MSE. The MSE of the 4-hour exponential S_I estimates was 1.07 x 10^{-8}, 1.27 x 10^{-8}, and 2.21 x 10^{-9} for subgroups with 4-hour glucose concentrations that were 10 mg/dL above, within, or below baseline glucose concentrations, respectively. The MSE of the 4-hour truncated S_I estimates was 3.50 x 10^{-9}, 9.98 x 10^{-9}, and 3.50 x 10^{-9} for the above, within, and below 10 mg/dL subgroups, respectively. For each subgroup, the errors in S_I estimates from the 4-hour exponential and 4-hour truncated models were significantly different. The errors in S_I estimates associated with the 4-hour exponential model were lower for the 10 mg/dl below baseline subgroup (p = 0.003), and errors in S_I estimates from the 4-hour truncated model were lower for the 10 mg/dl above (p = 0.002) and within (p = 0.03) subgroups.

The comparison of correlations of S_I estimates from both 4-hour models to 6-hour S_I estimates by subgroup revealed differences in correlation by subgroup but did not detect differences in S_I estimates based on the 4-hour model used. For the 4-hour exponential model, the correlation in S_I estimates for the 10 mg/dl above baseline subgroup (R = 0.74) was

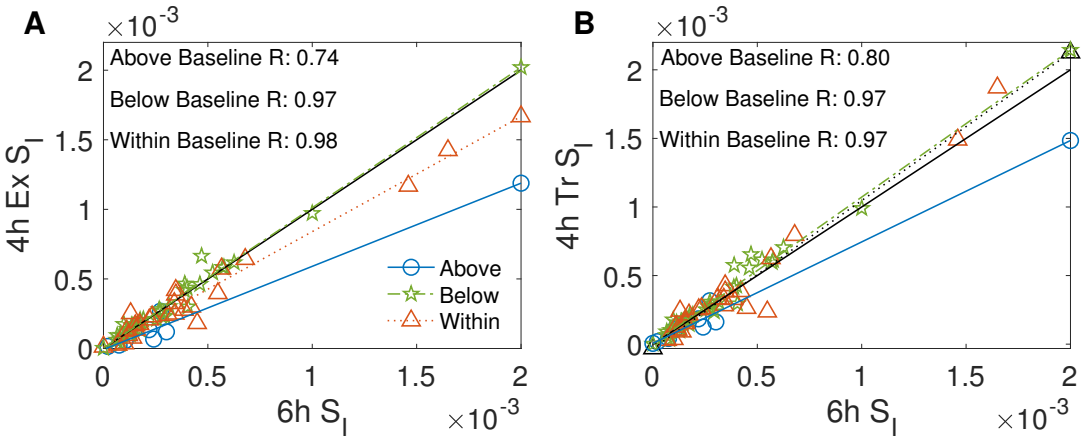

Figure 4.9: S_I **correlations divided into subgroups by 4-hour glucose levels.** Strength of correlation of S_I estimates using 4- and 6-hour OMM protocols varies for subgroups specified by participants' 4-hour glucose concentrations relative to their baseline glucose concentrations. S_I estimates calculated with the 4-hour exponential OMM were strongly correlated with 6-hour OMM S_I estimates for participants who were 10 mg/dL within (n = 24, all female, $p < 0.001$) and below (n = 37, all female, $p < 0.001$) their baseline glucose concentrations after the first 4 hours of the OGTT protocol but not for participants who were 10 mg/dl above (n = 7, all female, $p = 0.06$) (**A**). S_I estimates calculated with the 4-hour truncated OMM were correlated with 6-hour OMM S_I estimates for participants who were 10 mg/dl above (n = 7, all female, $p = 0.03$), within (n = 24, all female, $p < 0.001$), and below (n = 37, all female, $p < 0.001$) their baseline glucose concentrations after the first 4 hours of the OGTT protocol (**B**).

weaker compared to the correlations for the other subgroups (all $R \geq 0.97$: within: $p = 0.02$; below: 0.02) (Figure 4.9). Similarly for the 4-hour truncated model, the correlation in S_I estimates for the 10 mg/dl above baseline subgroup ($R = 0.80$) was weaker compared to the correlation for the 10 mg/dl within baseline subgroup ($R = 0.97$; $p = 0.05$) and marginally weaker compared to the correlation for the 10 mg/dl below baseline subgroup ($R = 0.97$; $p = 0.06$). There were no significant differences in the correlations of S_I estimates from either 4-hour model for the 10 mg/dl below or within subgroups (4-hour exponential: $p = 0.92$, 4-hour truncated: $p = 0.73$). These results show that the S_I values computed using either 4-hour model were less reliable for the 10 mg/dl above baseline subgroup compared to the other subgroups.

4.4 Discussion

We investigated differences in S_I estimates obtained from 2-, 3- and 4-hour implementations of OMM as compared to a 6-hour OMM implementation to describe OGTT glucose concentration data in adolescent girls with obesity. Insulin sensitivity is decreased in adolescents compared to adults [3, 4, 71], and the estimates of S_I in this group of adolescent girls with obesity are consistent with reduced insulin sensitivity reported in published studies [72]. However, our results establish that in this IR population, OMM-based S_I estimates depend on the duration of the data considered and generally improve with the addition of more data up to 6 hours. S_I estimated using OMM utilize the full dynamics of glucose and insulin during the course of an OGTT to describe S_I [73]. In this analysis, S_I estimates from a 6-hour OMM implementation represented the reference estimate against which other S_I estimates are compared as the 6-hour protocol was sufficiently long to allow glucose condentrations to return to baseline for all participants, a featured associated with optimal numerical identifiability of OMM. Moreover, longer protocol durations enabled the inclusion of the entire glucose profile, so more features of the data were represented in these estimates of S_I.

Of the shorter implementations, the 4-hour truncated OMM provided the most reliable estimates of S_I compared to S_I estimates from other OMM implementations. The glucose concentrations returned to baseline after 4 hours for a majority of participants, and, therefore, the 4- and 6-hour S_I estimates reflected similar features of the data. Estimates of S_I using OMM implementations for shorter durations of data were highly correlated with the 6-hour OMM S_I estimates consistent with results in healthy adult populations [20] and in a small cohort of adolescents [2]. However, in our IR cohort, 2-, 3-, and 4-hour exponential OMM implementations showed significant bias indicating that these methods may underestimate S_I compared to a 6-hour OMM S_I estimates, thereby potentially misrepresenting the degree of metabolic disorder experience by a particular individual or patient population. These results suggest that, in a cohort of adolescent girls with obesity, reliable estimates of

S_I using OMM require OMM implementations based on OGTT data of at least 4 hours. These findings are consistent with results indicating that glucose and insulin concentrations at the 4 hour time point may help estimate S_I in adults with severe type 2 diabetes [63].

In contrast with our results, previous studies that explored the effect of protocol duration on OMM-based estimates of S_I did not find that S_I was sensitive to protocol duration [20]. However, these studies focused on adult populations or small populations of adolescents [2, 20]. The protocol duration-dependence observed here may arise from assumptions regarding the rate of appearance of exogenous glucose that are inappropriate for our IR cohort of adolescent girls with obesity. We observed more variability in the rate of appearance of glucose ($Ra_{exo}(\boldsymbol{\alpha}, t)$)) in our cohort compared to published estimates in adults [57]. This difference reflect the increased variability in glucose profiles following drink ingestion, longer periods of elevated glucose, and frequent incidence of RHG in our cohort compared to the glucose profiles of healthy adults [4]. To account for the different features of the glucose profiles in our participants, we included more time breakpoints in our linear approximation of $Ra_{exo}(\boldsymbol{\alpha}, t))$. This approach robustly estimated the glucose profiles, however, it may have contributed to overfitting of $Ra_{exo}(\boldsymbol{\alpha}, t))$ in our cohort. More work is needed to establish a suitable set of breakpoints for the representation of $Ra_{exo}(\boldsymbol{\alpha}, t))$ in populations, such as obese adolescent girls, with atypical glucose trajectories following drink ingestion.

We found the glucose-insulin dynamics in our IR population were not well described by implementations of OMM that assumed exponential decay of $Ra_{exo}(\boldsymbol{\alpha}, t)$ after 2, 3, or 4 hours in contrast to results for other populations [57]. Specifically, OMM implemented using 2 or 3 hours of OGTT data imposed an exponential decay in $Ra_{exo}(\boldsymbol{\alpha}, t)$ to account for the time course of glucose absorption in protocols when glucose concentrations have not returned to baseline by the end of a 2 or 3 hour protocol, respectively. This method was developed in relatively healthy adults and successfully described glucose dynamics in these

participants [19]. However, this assumption did not model the glucose dynamics observed in most of the participants in this study even when the time constants of decay were estimated as a parameter in the model. The discrepancy was most pronounced in glucose profiles of participants with the lowest S_I values whose glucose concentrations tended to remain high beyond 2 hours. Additionally, the exponential decay assumption in the 4-hour exponential model adversely affected S_I estimates. This effect was minimized for participants whose 4-hour glucose concentrations were below or near baseline glucose levels where the assumption had minimal affect on glucose dynamics. These results highlight the challenges of applying OMM in populations with diverse metabolic phenotypes such as youth with high insulin secretion rates, women and girls with PCOS, and individuals with other metabolic diseases.

Our results demonstrate that estimates of S_I may depend on protocol duration and suggest that preliminary assessment of the typical features of the glucose-insulin dynamics of the study population is necessary to select an optimal protocol duration sufficiently long to enable reliable estimation og S_I. Specifically, shorter OGTT protocols may be suffient for OMM-based estimates of S_I when the return to baseline following peak glucose is rapid but may not be sufficient for populations with atypical glucose-insulin dynamics. Hence, the requirements for the precision of S_I estimates should be considered when designing OGTT protocols for OMM-based measures of S_I in IR populations. Furthermore, are should be taken when comparing S_I estimates computed using OMM implementations of different durations. Future work using data assimilation techniques may allow for more robust identification of optimal protocol durations for computing S_I in patient populations with diverse metabolic phenotypes.

CHAPTER 5

ANALYSIS OF OMM

5.1 Introduction

The utilization of data from an oral glucose tolerance test (OGTT) or a mixed meal test (MTT) together with the Oral Minimal Model (OMM) has enabled quantification of S_I in a more physiological context compared to the hyperinsulinemic euglycemic (HE) clamp [18, 19, 21, 57, 62]. The Minimal Model (MM) and OMM have proven in multiple instances to provide a robust measure of S_I, capable of detecting differences in S_I when comparing groups [58, 59, 74]. As explained in Ch 2, the OMM framework allows for quantification of the metabolic health of an individual and therefore, is helpful in understanding the mechanistic impact of different disease states on the metabolism. The comparison of OMM applied to varying durations of OGTT data in adolescent girls with obesity in Ch 4 identified the need to qualitatively understand how different features of this adolescent data may affect the identification of OMM. This will not only lead to a better understanding of how to apply OMM for use in adolescents with obesity but to other populations with diverse metabolic physiology.

Glucose and insulin dynamics adolescents differ greatly compared to their adult counterparts [3, 4]. Typically in an OGTT performed in adults, glucose concentrations return to baseline within 2 to 3 hours post drink administration. This group of insulin resistant adolescent girls returned to basal glucose and insulin concentrations closer to 3.5 - 4 hours and 6 hours, respectively, post drink (see Ch 4). Also, reactive hypoglycemia (RHG), where glucose concentrations fall well below baseline levels during the recovery from the glucose challenge, was a common occurrence among these participants. Additionally, 73.5% of study participants had poly cystic ovary syndrome (PCOS) that is known to affect metabolic dy-

namics in women [7] but less is known of the affects during adolescence when PCOS initially presents itself. We seek to determine how these specific dynamics play a role in OMM parameter estimation and to identify potential parameters that may be difficult to estimate in this population.

The challenges of model identifiability are a known aspect of model development, especially in nonlinear dynamic models of physiological systems [75]. In general, identifiability of a model determines whether all the model parameters can be uniquely identified given the model structure and the data [75–78]. However, there are 2 categories, global or structural and practical or numerical identifiability. The first observes whether parameters can be found when the noise free data are known at every time point and the latter concerns the practical estimation of parameters given the noise and bias associated with real-world data [77]. Structural identifiability is a prerequisite to practical identifiability and both are needed for optimal parameter estimation [77, 78].

Determining structural identifiability of nonlinear models is usually performed using analytic differential algebra or Taylor series expansion methods [75–77, 79] and, unfortunately, does not guarantee practical identifiability of the model parameters. Models may be practically unidentifiable for a large number of reasons. The model may be extremely sensitive to measurement errors in the data; model output could be insensitive to a certain parameter making reliable estimation difficult; the practical identifiability properties may differ depending on where the true parameters are within the parameter space [76]; or interactions between parameters may make individual parameter estimation difficult [78].

The OMM and models within this framework have a minimal description of the physiology with known structural and numerical identifiability issues [19, 21, 24, 57, 79, 80]. Specifically, OMM is not *a priori* globally identifiable as all the model parameters cannot be simul-

taneously estimated given the data [19]. To help with OMM identification, initially the developers of OMM had to fix a subset of parameters to published population values for application in their adult study group [19]. Later on, the developers of OMM established a reference model approach to estimate the necessary parameters as a perquisite step to OMM identification [21, 57]. We want to better understand how both the structural and practical unidentifiability of the OMM qualitatively relates to parameter estimation in adolescent girls with obesity.

In order to determine the importance of the various aspects of the data for estimation of parameters, we can perform a sensitivity analysis (SA) by examining how perturbations of the model inputs impact the model output. Primarily, SA is a set of mathematical approaches used to attribute uncertainties in model outputs to uncertainties in model inputs [27, 28, 81]. Additionally, these approaches can be used to qualitatively understand the processes within a model by examining how perturbations in the parameters affect model output. Therefore, these analyses can identify unforeseen dependence of the output on an input, highlighting a potentially unexpected feature of the system [27, 28, 81, 82].

The local approach to SA is a common method modelers implement to quantify model sensitivity to the inputs. There a couple ways a local SA can be done. Frequently, sensitivity measures are found by finding the derivative of the model output with respect to the input. These derivatives are typically approximated and are computed at a fixed nominal value in the parameter space. Another variation observes the ratio of the difference between the maximum and minimum in model output to the difference between the maximum and minimum input value. These methods are deemed 'local' because they perturb one parameter at a time [27, 83, 84]. This contrasts with global SA methods that are able to explore the full parameter space. Global methods determine the global impact of a parameter as well as influential parameter combinations [27, 28, 81]. Local methods are best

suited for linear systems but may still be informative [28] and useful in the OMM framework.

There have been a couple of sensitivity analyses performed within the MM and the OMM framework. Both local and global sensitivity analyses of the MM were performed using data from a simulated intravenous glucose tolerance test (IVGTT) which concluded that measurements past 62 min did not give additional information needed for parameter estimation [83]. For SA of the OMM, there is a built-in-feature in the software developed to solve OMM, SAAM II (SAAM II software v 2.2, The Epsilon Group, Charlottesville, VA, USA), that performs a local SA. The user can supply a range for a particular parameter to vary. Then the glucose model outputs are plotted at each value within the range while the remaining parameters are fixed at their optimal values. To our knowledge, a qualitative approach to the SA of the OMM has not been done.

The complement of SA is uncertainty quantification (UQ) [28, 84] and obtaining parameter distributions are key to performing an UQ of a model [31, 32]. SA identifies which parameters contribute the most to model uncertainty or determine parameters that have minimal effect on model uncertainty and thus can potentially be fixed to a specific value [27]. In the broad sense, UQ is "the science of identifying, quantifying and reducing uncertainties associated with models, numerical algorithms, experiments, and predicted outcomes or quantities of interests" [30]. It is the systematic quantification of uncertainties and errors in models, simulations and experiments and the analysis of how they propagate through complex models to affect predicted outcomes as well as the "quantification of measurement uncertainties and numerical errors" [30]. UQ combines the knowledge and techniques from applied mathematics, statistics and engineering to assist in the evaluation of models and the system they simulate [29].

In general, the scheme for UQ begins with a set of assumptions about the distributions of the inputs, such as parameter independence. For each input, we sample from their respective distributions until we have N samples. Then we run the model using the N parameter combinations to produce N corresponding model outputs. From here, we can summarize the sample of model outputs by computing the average, variance, and quantiles of both the model inputs and outputs. This process manifests an UQ of a given model [27, 32, 81].

Markov chain Monte Carlo (MCMC) is a popular set of Bayesian statistical techniques that can build the necessary parameter distributions needed to perform UQ (see Bayes' theorem Eq. 2.26 in Ch 2). After selecting an appropriate algorithm and model assumptions, MCMC can build the target parameter distributions where empirical estimates of quantities of interest can be found such as confidence bounds of the model output [34, 81]. To take advantage of this statistical technique, an MCMC approach was applied to OMM to quantify the uncertainty in key subset of parameters. In an effort to directly estimate the posterior distribution of S_I, OMM was rescaled such that S_I was explicitly represented in the model equations for these analyses.

5.2 Materials

Participants

This is a secondary analysis of data collected during a frequently sampled OGTT with stable isotope glucose tracers. A detailed description of this OGTT protocol can be found in Chapter 3. In brief, sixty-eight overweight and obese (BMI $\geq$ 90th percentile for age and sex) adolescent (Tanner Stage 5) girls underwent a frequently sampled 6-hour OGTT. Blood was sampled at -30,-20,-10, 0, 10, 20, 30, 45, 60, 75, 90, 105, 120, 135, 150, 180, 210, 240, 300 and 360 minutes following ingestion of 75 g plus an additional 40 mg/kg of glucose (Figure 4.1) for glucose and insulin concentrations.

OMM Optimization

The OMM was implemented using data from the full 6-hour OGTT protocol for all the participants in SAAM II (SAAM II software v 2.2, The Epsilon Group, Charlottesville, VA, USA) following the methods described in Ch 4. The SA and UQ was performed in MATLAB (Mathworks, Natick, MA).

5.3 Local Sensitivity Analysis

The local sensitivity performed here is a partial derivative approach to perform the analysis and the formulation for the sensitivity measures follows.

Table 5.1: List of the parameters considered in the local sensitivity analysis of the OMM and the Rescaled OMM.

Parameter (units)	Description
$\boldsymbol{\alpha} = [\alpha_1, \cdots, \alpha_n]$(mg/kg/min)	amplitudes of the piecewise linear description of the rate of appearance of exogenous glucose
$S_G\,(1/min)$	glucose effectiveness (per unit distribution volume) to promote glucose disposal and inhibit endogenous glucose production
$S_I\,(dl/kg/min$ per $\mu U/ml)$	insulin sensitivity index measuring insulin's ability to promote glucose disposal and inhibit endogenous glucose production
$p_2\,(1/min)$	rate constant governing decay of insulin action
$p_3\,(1/min^2 \cdot ml/\mu U)$	rate constant governing growth of insulin action for insulin concentrations above baseline
$V\,(dl/kg)$	volume of distribution for glucose
$G_b\,(mg/dl)$	baseline glucose concentration
$I_b\,(\mu U/ml)$	baseline insulin concentration

Consider a system of differential equations

$$f(t,\vec{\theta}) = col(f_1(t,\vec{\theta}), \cdots, f_M(t,\vec{\theta})), \qquad 0 \le t \le T,\ \vec{\theta} \in \mathscr{K} \tag{5.1}$$

where $T > 0$, $f_i(t,\vec{\theta})$, $i = 1, \cdots, M$ is the individual model output for M number of outputs of the system, $\vec{\theta} \in \mathscr{K} \subset \mathbb{R}^p$ for open subset $\mathscr{K}$ and for p parameters. The sensitivity of a model output $f_i(t,\theta)$ with respect to a parameter θ_j is measured as

$$s_{f_i/\theta_j}(t) = \lim_{\Delta\theta_j \to 0} \frac{\Delta f_i(t,\theta)/f_i(t,\theta)}{\Delta\theta_j/\theta_j}, \quad j = 1, ..., p, \ i = 1, ..., M$$

which simplifies to a partial derivative of the model output f_i with respect to the parameter θ_j times the parameter divided by the model output:

$$s_{f_i/\theta_j}(t) = \frac{\partial f_i(t,\theta)}{\partial\theta_j} \cdot \frac{\theta_j}{f_i(t,\theta)}, \quad j = 1, ..., p, \ i = 1, ..., M \tag{5.2}$$

These sensitivity functions $s_{f_i/\theta_j}(t)$ quantify the changes of the parameters on the model outputs by describing the parameters to which the model is most or least sensitive [83].

This method requires computing the partial derivatives with respect to θ_j of each model output, $\frac{\partial f_i(t,\theta)}{\partial\theta_j}$, which are unknown analytically. To overcome this, the partial derivatives were approximated using a first order forward finite difference scheme

$$\frac{\partial}{\partial\theta_j} f_i(t;\vec{\theta}) \approx \frac{f_i(t;\vec{\theta} + \Delta\theta_j) - f_i(t;\vec{\theta})}{\Delta\theta_j} \tag{5.3}$$

This method is first order so we choose $\Delta\theta_j \approxeq \frac{\theta_j}{100}$ sufficiently small to minimize the error.

To observe the overall sensitivity of the model output f_i to parameter θ_j we can compute a sensitivity metric r_{f_i/θ_j} as

$$r_{f_i/\theta_j} = \int_0^T |s_{f_i/\theta_j}(t)|\, dt \tag{5.4}$$

where $|\cdot|$ is the absolute value.

Recall the equations of the OMM from Ch 2

$$\begin{cases} \dot{G}(t) = -[S_G + X(t)] \cdot G(t) + S_G \cdot G_b + \frac{Ra_{exo}(\boldsymbol{\alpha},t)}{V} & G(0) = G_b \\ \dot{X}(t) = -p_2 \cdot X(t) + p_3 \cdot [I(t) - I_b] & X(0) = 0 \end{cases} \tag{5.5}$$

where

$$Ra_{exo}(t) = \begin{cases} \alpha_{i-1} + \frac{\alpha_i - \alpha_{i-1}}{t_i - t_{i-1}}(t - t_{i-1}) & \text{for } t_{i-1} \leq t \leq t_i \quad i = 1, \cdots, n \\ 0 & \text{otherwise} \end{cases} \tag{5.6}$$

and

$$\int_0^T Ra_{exo}(\boldsymbol{\alpha}, t)\, dt = \frac{D \cdot f}{BW} \tag{5.7}$$

where $T = 360$ minutes is the length of the OGTT protocol. The main quantity of interest is the measure of total insulin sensitivity, $S_I = \frac{p_3}{p_2} V$. Therefore, I also considered a rescaled version of the OMM such that S_I was an explicit parameter in the model. The Rescaled OMM equations follow

$$\begin{cases} \dot{G} &= -[S_G + \frac{p_2}{V} Y] \cdot G + S_G \cdot G_b + \frac{Ra_{exo}(\boldsymbol{\alpha}, t)}{V} \\ \dot{Y} &= -p_2 \cdot Y + S_I[I(t) - I_b] \end{cases} \tag{5.8}$$

where Y is the rescaled insulin action and $Ra_{exo}(t)$ has the same piecewise linear description as in OMM (5.6). The details of the rescaling can be found in Appendix A. The sensitivity measures $s_{f_i/\theta_j}(t)$ were computed for all the parameters of the OMM and the Rescaled OMM. The parameters and their range of values were $S_G\,(1 \times 10^{-4}, 1 \times 10^{-1})$, $p_2\,(1 \times 10^{-4}, 3 \times 10^{-2}$, $p_3\,(1 \times 10^{-7}, 1 \times 10^{-4})$, V (1.45, fixed), $G_b\,(75, 105)$, $I_b\,(8, 121)$ and $\boldsymbol{\alpha}\,(0, 10)$ for OMM and the same set with p_3 replaced by $S_I\,(1 \times 10^{-5}, 2 \times 10^3)$ for Rescaled OMM.

5.3.1 Results

Presented here are the sensitivity measures $s_{f_i/\theta_j}(t)$ computed for the α_i, G_b, I_b, S_G, p_2, p_3 and V in one representative subject and the overall sensitivity metric r_{f_i/θ_j} for all participants. The local sensitivity analysis of OMM and the Rescaled OMM to changes in these parameters is shown below. Negative sensitivity measures indicate negative change or a decrease in the model output and positive sensitivities indicate a positive change or increase in the model output. The sensitivity analysis for the Rescaled OMM directly shows

the sensitivity of model outputs to changes in S_I.

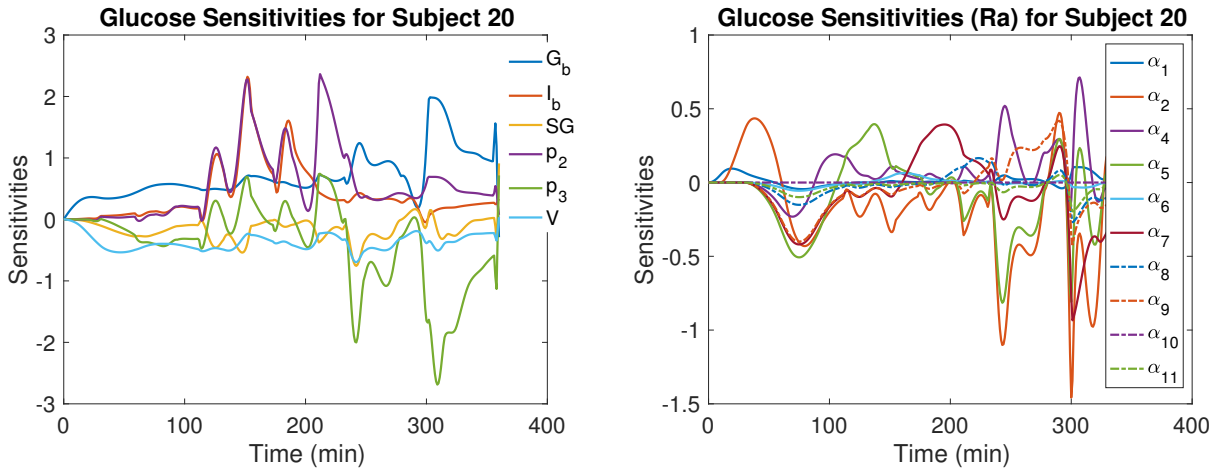

(a) Sensitivities to G_b, I_b, S_G, p_2, p_3 and V

(b) Sensitivities to α_i

Figure 5.1: Local sensitivities of OMM glucose output for Subject 20.

Since G_b and I_b are also key parameters in the model equations, they were considered in this sensitivity analysis on OMM and the Rescaled OMM. Figure 5.1 shows the glucose model sensitivity measures $s_{f_i/\theta_j}(t)$ for G_b, I_b, p_2, p_3 and V separate from the sensitivity measures for the α_i. Note that the scales of $s_{f_i/\theta_j}(t)$ are different for the α_i compared to the other parameters. In Figure 5.1(a), the magnitude of the sensitivities are relatively similar and ranged between -1 and 1 for approximately the first 2 hours; we begin to see relatively large sensitivities towards the end of the protocol. Particularly, the glucose model sensitivity to G_b was initially relatively unimportant for the fist 230 min, but the model increased in sensitivity towards G_b in the end of the protocol. Similarly, the sensitivity of the model to p_3 increased in magnitude in the last half of the protocol. This suggests that the parameters G_b and p_3 are important for model identification during the return to baseline phase of the OGTT protocol. The parameters p_2 and I_b seem to have a similar effect on the glucose output since their curves largely overlap until approximately 200 min where the sensitivity to I_b decreases to near 0 and the sensitivity to p_2 increases again before also decreasing to near 0. The sensitivity measures for S_G and V remained the smallest and least variable

in comparison to the other parameters with the model output being the least sensitive to changes in S_G (Table 5.2).

The sensitivity measures for the α_i in $Ra_{exo}(\boldsymbol{\alpha}, t)$ are shown in Figure 5.1(b) where we see that α_i with larger values such as α_2, α_4, α_5 and α_7, had more impact on glucose model output. The piecewise linear description of $Ra_{exo}(\boldsymbol{\alpha}, t)$ 5.6) pairs each amplitude α_i with a corresponding time point t_i. For example, α_3 corresponds to $t_3 = 60$ minutes. Based off of the Ra formulation, we would expect the model to be sensitive to changes in α_3 mainly between time points $t_2 = 30$ to $t_4 = 90$ minutes. The $\boldsymbol{\alpha}$ sensitivity measures show how the imposed constraint (see Eq. 5.7) affects model output by making the glucose model output sensitive to each α_i for most of the protocol. This phenomenon illustrates the forced dependence of each α_i on the remaining α_i.

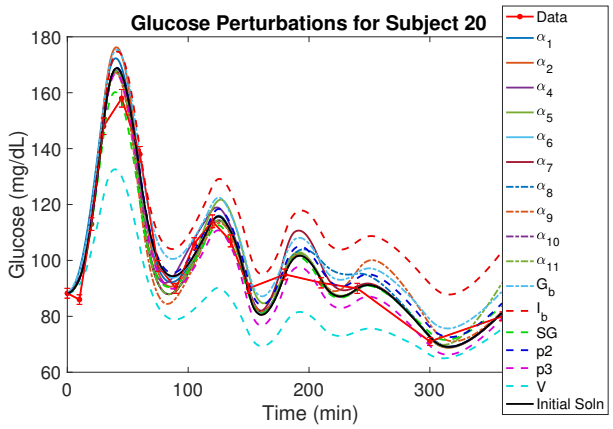

Figure 5.2: The perturbations of the OMM simulated glucose profile for Subject 20 when the partial derivatives in the sensitivity measures s_{f_i/θ_j} were approximated with a large $\Delta\theta_j$ to highlight the changes to the glucose model output.

Figure 5.2 illustrates how changes of the same magnitude in each parameter affect the glucose model output. The original solution $G(t, \vec{\theta})$ is shown in the black line and the perturbed solutions $G(t; \vec{\theta} + \Delta\theta_j)$ for each θ_j are in color. $\Delta\theta_j$ was chosen to be the same order of magnitude as θ_j, i.e. $\Delta\theta_j \approxeq \theta_j$, which is considerable large than initial $\Delta\theta_j$ values (see Eq. 5.3). For example, for $\theta_j = V = 1.45$, $\Delta\theta_j = 1$ so $G(t; \vec{\theta} + \Delta_j)$ is solved with

$V = 2.45$. The largest changes in glucose output were mainly due to V and I_b and to a lesser extent some of the α_i values. These highlight how large errors in the parameters can affect model output, the fit to the data and, therefore, estimates of S_I.

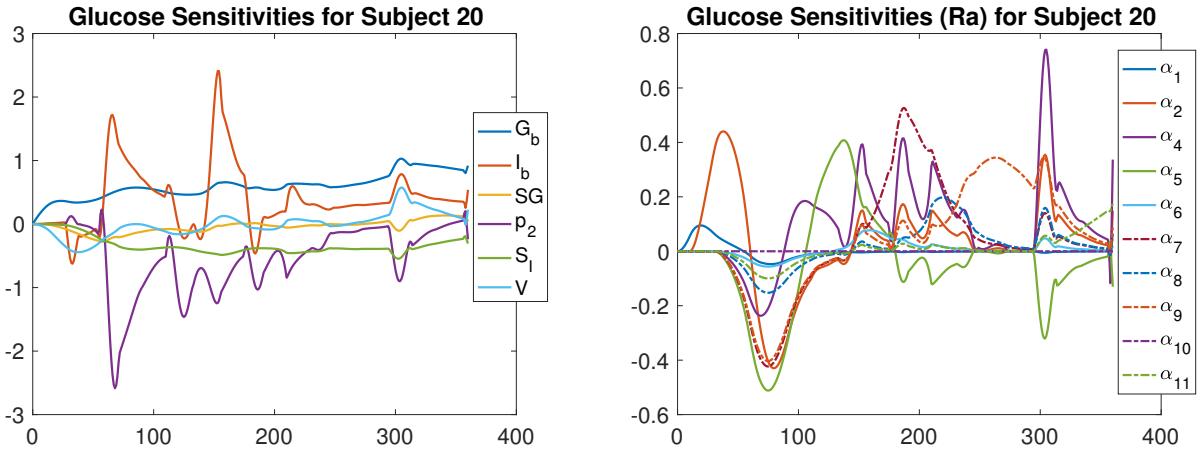

(a) Sensitivities to G_b, I_b, S_G, p_2, p_3 and V

(b) Sensitivities to α_i

Figure 5.3: Local sensitivities of Rescaled OMM glucose output for Subject 20.

The sensitivity measures of the α_i computed for the Rescaled OMM (Figure 5.3(a)) showed a similar relation to those computed for the standard OMM (see Figure 5.1(b)) whereby the sensitivity of the model output to each α_i depended on the full length of the OGTT protocol. A notable difference is that the magnitudes of the α_i sensitivity measures are smaller for the Rescaled OMM. The sensitivity to G_b increases to 1 then stays relatively constant for most of the protocol with a small increase in the last hour which is in contrast to the behavior observed for this parameter in OMM. I_b exhibited a similar effect here compared to the effect of I_b in OMM. A large difference captured here is the impact of p_2. Perturbations in p_2 in the Rescaled OMM produced a negative change in the glucose model output in contrast to the positive change produced in the OMM. Sensitivity to S_I was small for approximately 60 minutes then increased in magnitude to -0.5 and was constant for the remainder of the protocol. Similar to the sensitivity measures computed in the OMM, sensitivity to changes S_G and V remained minor with the model being the least sensitive to

changes in S_G.

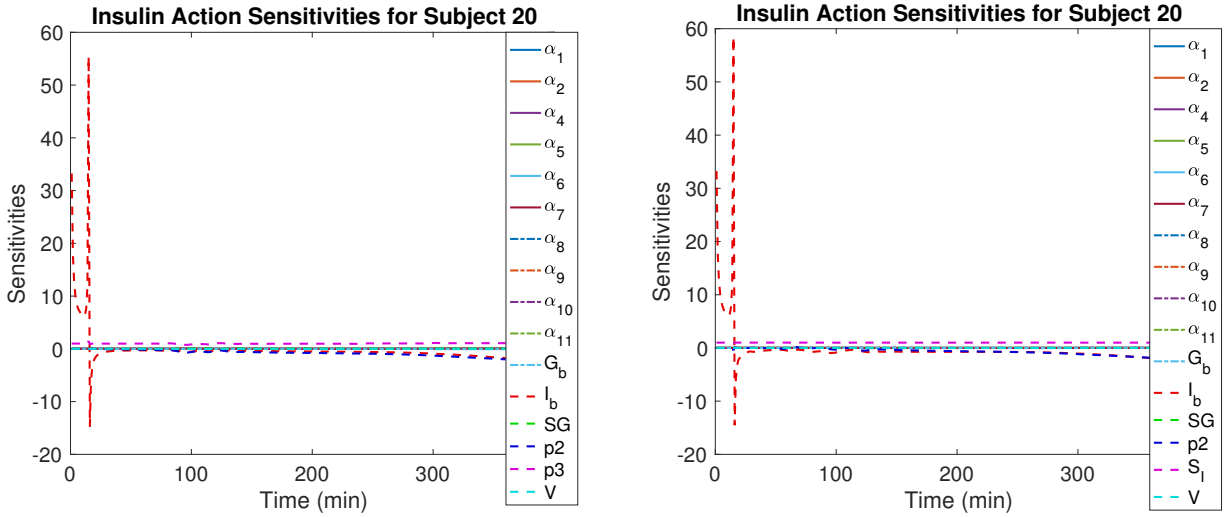

(a) The OMM (b) The Rescaled OMM

Figure 5.4: Local sensitivities of the OMM and the Rescaled OMM insulin action output for Subject 20.

The sensitivity measures for insulin action were virtually the same for the OMM and the Rescaled OMM. OMM Insulin action was most sensitive to changes in I_b, then to a lesser extent p_2 and p_3. Similarly, the Rescaled OMM insulin action was largely sensitive to I_b in the first 20 minutes then decreased to near -0.6 for the remainder of the protocol. The sensitivity measure for S_I remained constant and the sensitivity to p_2 gradually increased in magnitude from 0 near 2 hours to -1.85 by the end of the protocol.

In Figure 5.5, plotted are the results of $G(t;\vec{\theta}+\Delta\theta_j)$ compared to $G(t;\vec{\theta})$ for the Rescaled OMM where $\Delta_j\theta_j$ was the same order of magnitude of θ_j. Changes in the parameters of the Rescaled OMM created a similar effect on the glucose output compared to the perturbed glucose output of the OMM. However, we can explicitly see how change in S_I most affected glucose model output after 90 minutes coinciding with this individual's return to baseline. Also in constrast, we see that perturbed glucose output due to V only affected the simulated glucose output in the first 90 minutes then closely follows the initial solution $G(t;\vec{\theta})$. This

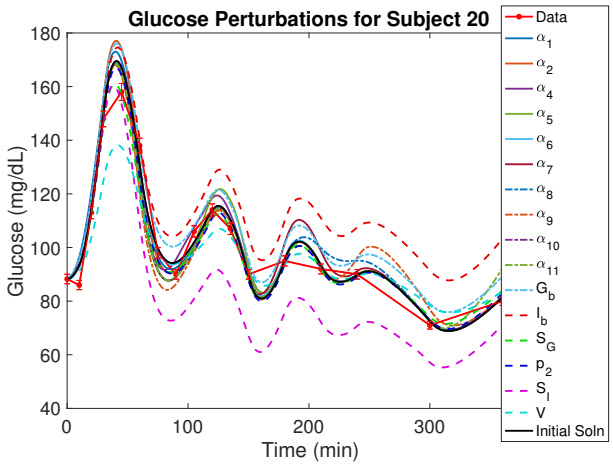

Figure 5.5: The perturbations of the Rescaled OMM simulated glucose profile for Subject 20 when the partial derivatives in the sensitivity measures s_{f_i/θ_j} were approximated with a large $\Delta\theta_j$ to highlight the changes to the glucose model output.

coincides with the decreased sensitivity of the model output to V for most of the protocol duration.

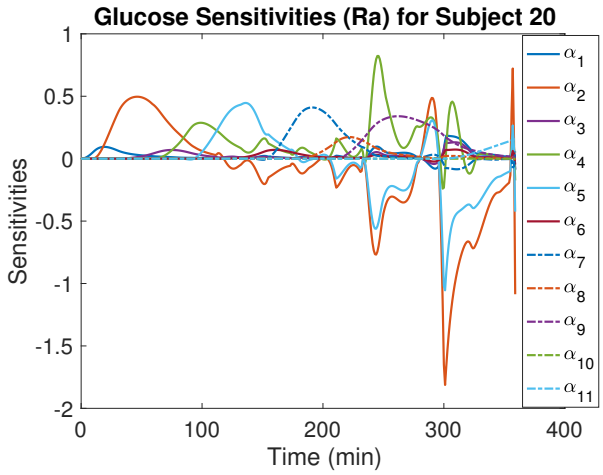

Figure 5.6: Local sensitivities of $\boldsymbol{\alpha}$ without the constraint on $Ra_{exo}(\boldsymbol{\alpha}, t)$ for Subject 20.

We also considered the $\boldsymbol{\alpha}$ sensitivities without the constraint on Ra_{exo}, which involves considering one more parameter in $\boldsymbol{\alpha}$. This did not have an effect on the sensitivities of the other model parameters so only the $Ra_{exo}(\boldsymbol{\alpha}, t)$ sensitivity measures are presented here (Figure 5.6). In contrast, the $\boldsymbol{\alpha}$ sensitivities where $Ra_{exo}(\boldsymbol{\alpha}, t)$ was unconstrained illustrate

that the OMM was largely sensitive to the α_i associated with each time breakpoint.

Table 5.2: The overall sensitivity of the OMM glucose output to each parameter as measured by sensitivity metric r_{f_i/θ_j} for all participants (n = 68).

Parameter	Median	Minimum	Max
α_1	23.85	0	615.89
α_2	41.69	7.33	469.54
α_4	34.66	5.44	563.92
α_5	45.17	0	596.23
α_6	32.12	0	659.54
α_7	38.80	0	430.95
α_8	15.73	0	405.15
α_9	10.57	0	292.32
α_{10}	9.22	0	271.99
α_{11}	3.95	0	123.81
G_b	200.91	48.91	650.44
I_b	40.1	0.003	325.24
S_G	75.77	30.63	268.22
p_2	93.27	0.03	591.8
p_3	129.93	0.03	392.97
V	138.23	101.02	272.95

The average sensitivity of the OMM and Rescaled OMM glucose model output to each parameter computed using r_{f_i/θ_j} is shown in Table 5.2 and Table 5.3. Overall, these calculations had a large variability across participants, within the order and in their magnitude, and for this reason the median and range are reported. There were several instances where the ordering of parameters differed from the typical ranking and the overall sensitivity to a parameter could range from 0 to 600 depending on the participant considered. Of the set of α_i, glucose output of was most sensitive to α_2, α_4, α_5, and α_7 for both OMM and the Rescaled OMM, corresponding to the amplitude of $Ra_{exo}(\boldsymbol{\alpha}, t)$ at 30, 90, 120, and 180 minutes. The OMM glucose model output was on average, most sensitive to changes in G_b and, of the non-$Ra_{exo}(\boldsymbol{\alpha}, t)$ parameters, least sensitive to changes in I_b then S_G (see Table 5.2 and Figure 5.7(a)). However, there are several instances where overall sensitivity to I_b was considerably larger than the sensitivity to S_G (Table 5.2). In slight contrast, the glucose

Table 5.3: The overall sensitivity of the Rescaled OMM glucose output to each parameter as measured by sensitivity metric r_{f_i/θ_j} for all participants (n = 68).

Parameter	Median	Minimum	Max
α_1	24.91	0	603.40
α_2	42.22	9.97	775.32
α_4	39.33	6.36	806.76
α_5	48.54	0	731.55
α_6	32.79	0	350.97
α_7	36.43	0	432.51
α_8	15.24	0	515.4
α_9	11.56	0	257.41
α_{10}	10.09	0	287.07
α_{11}	4.04	0	121.31
G_b	202.26	87.65	712.66
I_b	156.67	6.16	768.29
S_G	68.56	9.59	267.63
p_2	89.84	0.04	855.83
S_I	125.68	74.37	532.42
V	83.97	44.57	279.51

model output of the Rescaled OMM was least sensitive to changes in S_G and overall sensitivity to I_b was second only to G_b (Table 5.3 and Figure 5.7(b)). An additional difference between overall glucose sensitivities of the OMM and the Rescaled OMM is the significant reduction in sensitivity to V in the Rescaled OMM. This could be due to the appearance of the $\frac{p_2}{V}$ term in the equation for glucose (Eq. 5.8).

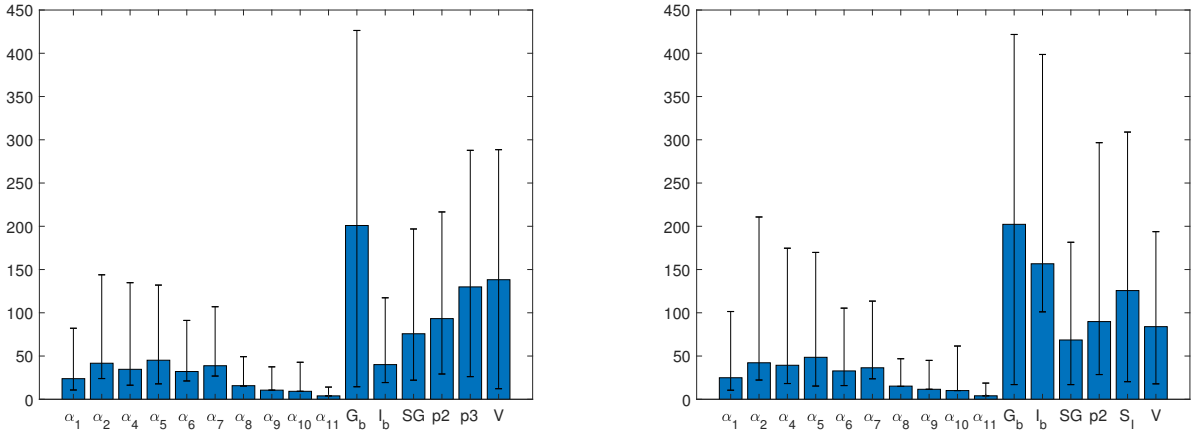

(a) OMM

(b) Rescaled OMM

Figure 5.7: Bar plot of the median overall sensitivity of the glucose outputs for the OMM and the Rescaled OMM to each parameter for all participants (n = 68). The errorbars represent the 75^{th} and 25^{th} percentiles.

5.4 Uncertainty Quantification

Table 5.4: List of the parameters considered in the uncertainty quantification of the rescaled OMM.

Parameter (units)	Description
$S_I\,(dl/kg/min$ per $\mu U/ml)$	insulin sensitivity index measuring insulin's ability to promote glucose disposal and inhibit endogenous glucose production
$S_G\,(1/min)$	glucose effectiveness (per unit distribution volume) to promote glucose disposal and inhibit endogenous glucose production
$p_2\,(1/min)$	rate constant governing insulin action

To quantify the uncertainty in the parameter estimates of the Rescaled OMM, MCMC was applied to determine the precision of parameters using the resultant probability distributions. The particular MCMC algorithm used here was the Metropolis-within-Gibbs sampling method. It is a component-wise algorithm whereby each parameter is updated individually during each iteration while all the other parameters are held fixed. Generally, the proposal is accepted if it is an improvement and rejected according to some probability [85].

Implementation

In this application, MCMC was used to obtain precision on the parameters of the Rescaled OMM so that we could directly produce distributions for S_I. First an optimal parameter set of the Rescaled OMM was obtained using MATLAB's constrained optimization function **fmincon**. The initial guesses for S_I, p_2, S_G and $\boldsymbol{\alpha}$ in $Ra_{meal}(\boldsymbol{\alpha}, t)$ were taken from the set of OMM solutions presented in Ch 4. Then this optimized set of parameters was used to initialize the MCMC chains. For each parameter, three chains were initialized at the optimal value then at $\pm$ 20% of this value. The α_i in $Ra_{exo}(\boldsymbol{\alpha}, t)$ and V are fixed and subsequently we obtain posterior distributions for S_I, p_2 and S_G. Uniform rather than normal priors were used so that assumptions on the parameters did not create a bias in the output posterior distributions.

$$
\begin{aligned}
p(S_I) &\sim U(2 \times 10^{-5}, 2 \times 10^{-3}) \\
p(p_2) &\sim U(3 \times 10^{-3}, 5\times^{-2}) \\
p(S_G) &\sim U(1 \times 10^{-3}, 5 \times 10^{2})
\end{aligned}
$$

The MCMC algorithm here is very similar to the one introduced in Ch 2. For each iteration, do the following:

1. Initialize the parameter chains with initial guess, θ^0.

2. Run OMM with the initial parameter set to get model output $\boldsymbol{y}^0 = OMM(\theta^0)$ where $\boldsymbol{y}^0$ is the model simulated total and meal glucose output given θ^0.

3. Compute the loglikelihood of θ^0 as

$$
L(\theta^0) = -\frac{1}{2\sigma^2} \sum_{i=1}^{n} [data_i - y_i^0]^2 = -\frac{1}{2} \left\| \frac{\boldsymbol{data} - \boldsymbol{y^0}}{\sigma} \right\|^2 \tag{5.9}
$$

   where σ is the measurement noise covariance and $\| \cdot \|$ is the l^2-norm. Since all of the prior distributions are uniform, $p(\theta) \propto 1$ and therefore does not affect $L(\theta)$.

4. Generate next proposal $\theta^* = \theta^0 + \varepsilon$ where random noise $\varepsilon = \beta \cdot \gamma$, $\gamma \sim N(0, \tau^2)$, $\tau^2 = [(a-b)/6]^2$ is the proposal covariance taken to be 1/6 the width of the uniform prior distribution $U(a,b)$ of θ_j, and β is a linear scaling factor between 0 and 1. β controls how much noise is added to the next proposal. If the newly generated proposal is out of bounds, a new one is created until it is within bounds.

5. Run OMM with new proposal set of parameters to get new output $\boldsymbol{y}^* = OMM(\theta^*)$

6. Compute $L(\theta^*) = -\frac{1}{2}\left\|\frac{\boldsymbol{data}-\boldsymbol{y^*}}{\sigma}\right\|^2$

7. Compare proposals

$$a = \min\left(1, \exp\left(L(\theta^0) - L(\theta^*)\right)\right). \tag{5.10}$$

8. Generate $u \sim U(0,1)$. If $a < u$, reject proposal and $\theta^1 = \theta^0$. If $a >= u$, accept θ^* and add it to the chain as $\theta^1 = \theta^*$.

9. Calculated the chain posterior as $\exp(-\theta^1)$.

10. Repeat from step 4 until the desired number of iterations is achieved.

Three chains were run for each parameter for 50,000 to 100,000 iterations. The first 20% of each chain was discarded as burnin and the remaining values were used to build the posterior density of each parameter. Chain convergence was analyzed by computing the potential scale reduction factor (PSRF) and the multivariate PSRF, which are functions of the within and between chain variability [33,35,86]. Also, the autocorrelation was used to assess convergence by identifying the correlation of the current draw to the k previous draws [87].

5.4.1 Results

The focus of this MCMC approach is as a means of uncertainty quantification and not parameter optimization. Thus, the OMM was directly applied to an individual's data first to identify an optimal parameter set. This allowed the chains to converge more quickly to the target distribution, therefore, requiring fewer iterations. The MCMC method for quantifying uncertainty was initially tested on a simulated individual's data where the key parameters were chosen and OMM was run to obtain the corresponding glucose profile. Once the MCMC method was validated on simulated data, data from 2 representative subjects with different sensitivities to insulin were used. After convergence for all parameter chains was achieved, the chain with the smallest $MSE = mean(\boldsymbol{data} - \boldsymbol{y})^2$ was used to determine the precision of the parameters.

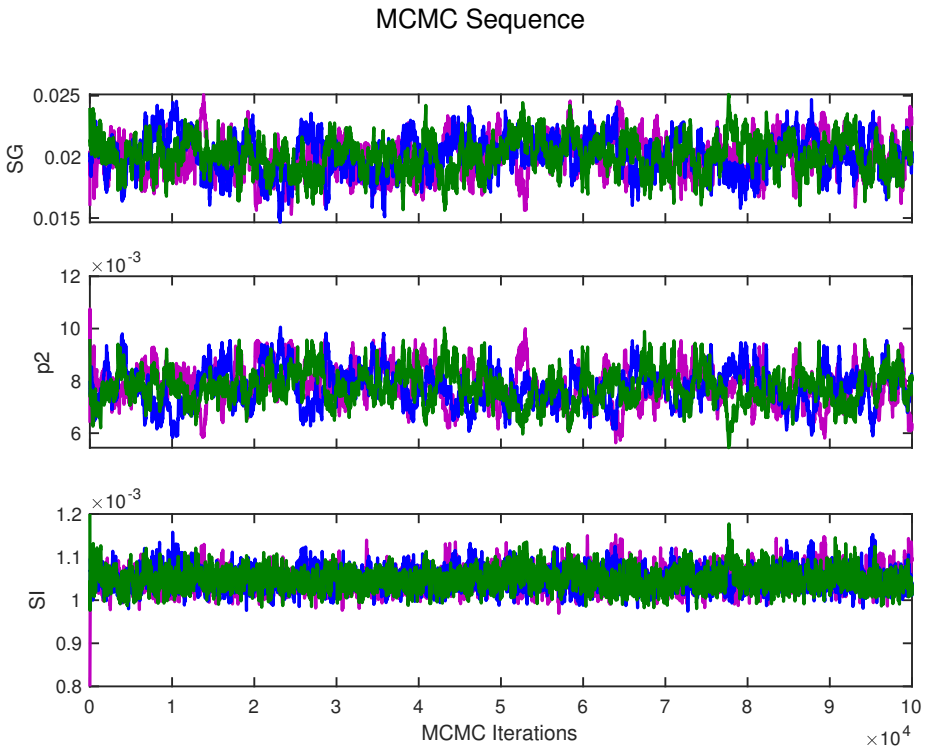

Figure 5.8: The sequence of MCMC chains S_G, p_2, and S_I for the fabricated dataset.

Simulated Subject

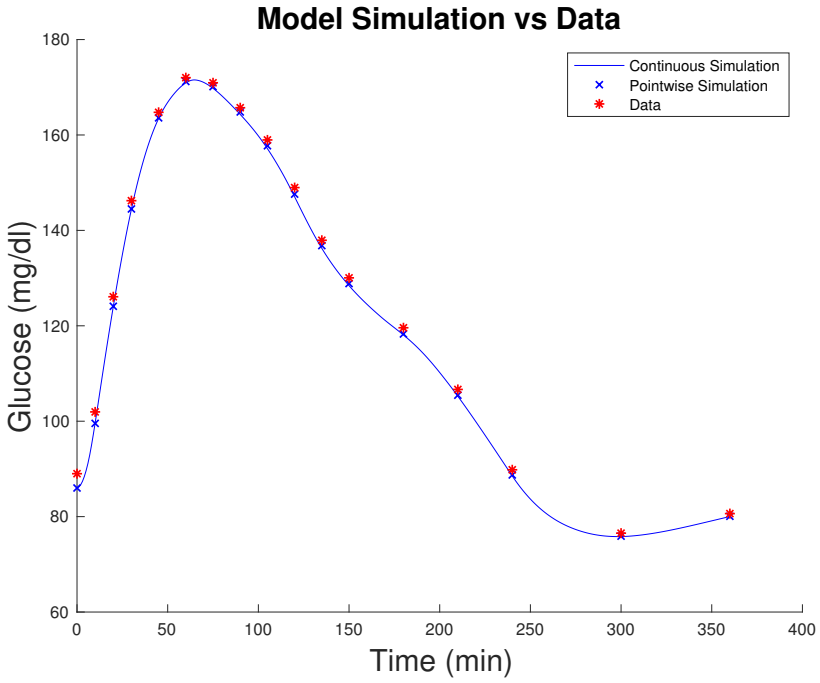

Figure 5.9: The MCMC simulated glucose and the data for the Simulated Subject.

To create the simulated data set, all the Rescaled OMM parameters were fixed to chosen values. Then the insulin concentrations, dose and body weight of a subject in the group were used to run the model. Then the simulated glucose concentrations were constructed as the glucose model output at the OGTT protocol blood sample schedule. The sequence of chains for parameters S_I, S_G and p_2 for this simulated individual are shown in Figure 5.8. This run had 100,000 iterations for each chain. The densities of the constructed posterior distributions for each parameter chain and their pooled density (black line) are shown in Figure 5.10. The known parameter values were $S_I = 1 \times 10^{-3}$, $p_2 = 8 \times 10^{-3}$ and $S_G = 2 \times 10^{-2}$. The MCMC estimates (mean) $\pm$ precision (standard deviation) for the key parameters were $S_I = 1.05 \pm 0.02 \times 10^{-3}$, $p_2 = 7.77 \pm 0.65 \times 10^{-3}$ and $S_G = 2.01 \pm 0.14 \times 10^{-2}$. These corresponded with small coefficient of variation (CV = 100·SD/mean%) at 1.9%, 8.3% and 7% for S_I, p_2 and S_G, respectively. The mean acceptance rates 15%, 10% and 14%. The simulated individual's glucose profile and MCMC estimate is shown in Figure 5.9; glucose

returned to baseline approximately 4 hours post drink ingestion, a common feature of this group of adolescent girls with obesity.

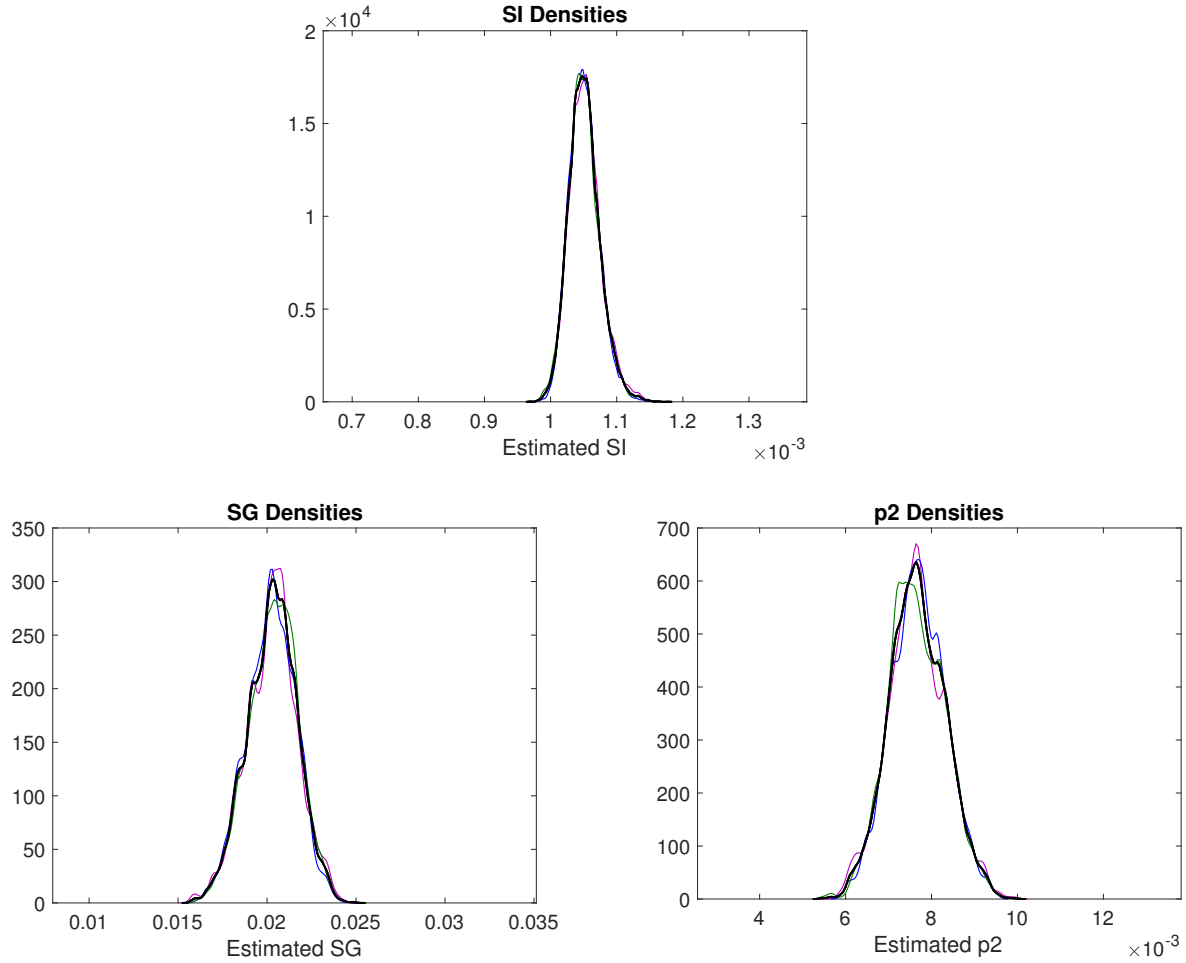

Figure 5.10: The posterior densities of S_I, S_G, and p_2 for the simulated individual.

Subject 60

The MCMC chain sequence of the key parameters for subject 60 are shown in Figure 5.11. There were 50,000 iterations performed. The densities of S_I, S_G, and p_2 are illustrated for each chain and the pooled densities are shown in Figure 5.12. The initial optimized parameter values were $S_I = 1.3 \times 10^{-4}$, $p_2 = 5 \times 10^{-3}$ and $S_G = 2 \times 10^{-2}$. The MCMC parameter estimates, precision and CV were $S_I = 1.3 \pm 0.05 \times 10^{-4}$ (3.8%), $p_2 = 5.95 \pm 0.42 \times 10^{-3}$

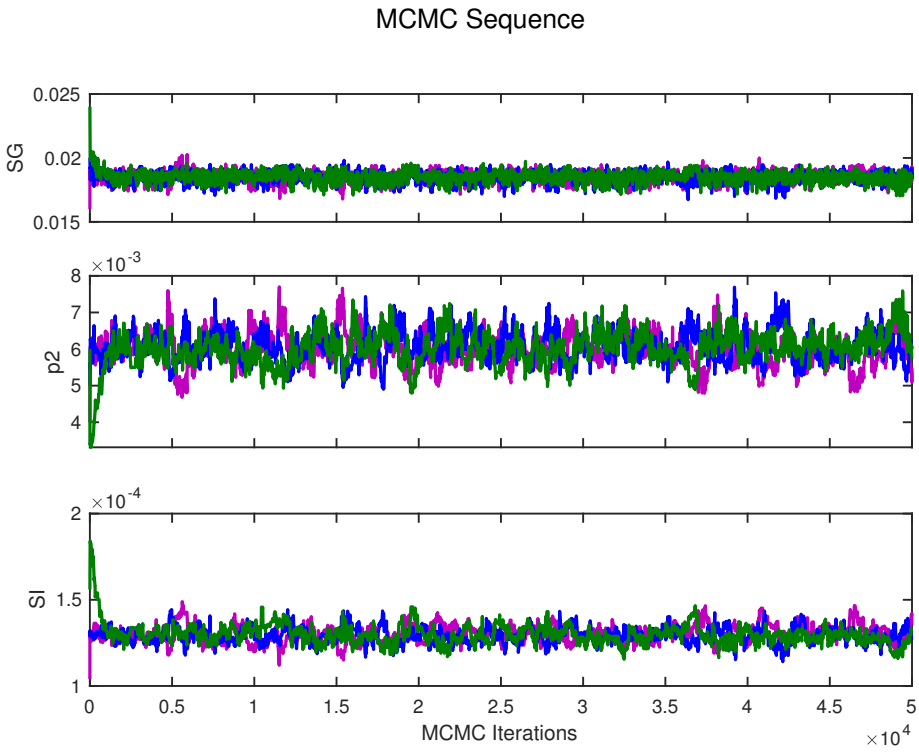

Figure 5.11: The sequence of MCMC chains S_G, p_2, and S_I for Subject 60.

(7%) and $S_G = 1.85 \pm 0.04 \times 10^{-2}$ (2.2%). The mean acceptance rates were 5%, 10% and 14% for S_I, p_2 and S_G, respectively. The glucose concentrations and the MCMC simulated glucose profile is shown in Figure 5.13(a).

Subject 20

Similarly, the MCMC sequences for each parameter are shown for Subject 20 in Figure 5.14. There were 100,000 iterations performed on this dataset. The estimated densities for each parameter for Subject 20 are shown in Figure 5.15. The optimized parameter estimates were $S_I = 1.5138 \times 10^{-3}$, $p_2 = 8.2133 \times 10^{-3}$ and $S_G = 2.6136 \times 10^{-2}$. The MCMC estimates, precision and CV of S_I and p_2 were $S_I = 1.516 \pm 0.0239 \times 10^{-3}$ (1.6%) and $p_2 = 8.6538 \pm 0.422 \times 10^{-3}$ (5%). The density for S_G was bimodal, giving a visualization that this parameter is not uniquely identifiable. Therefore, we report the median and in-

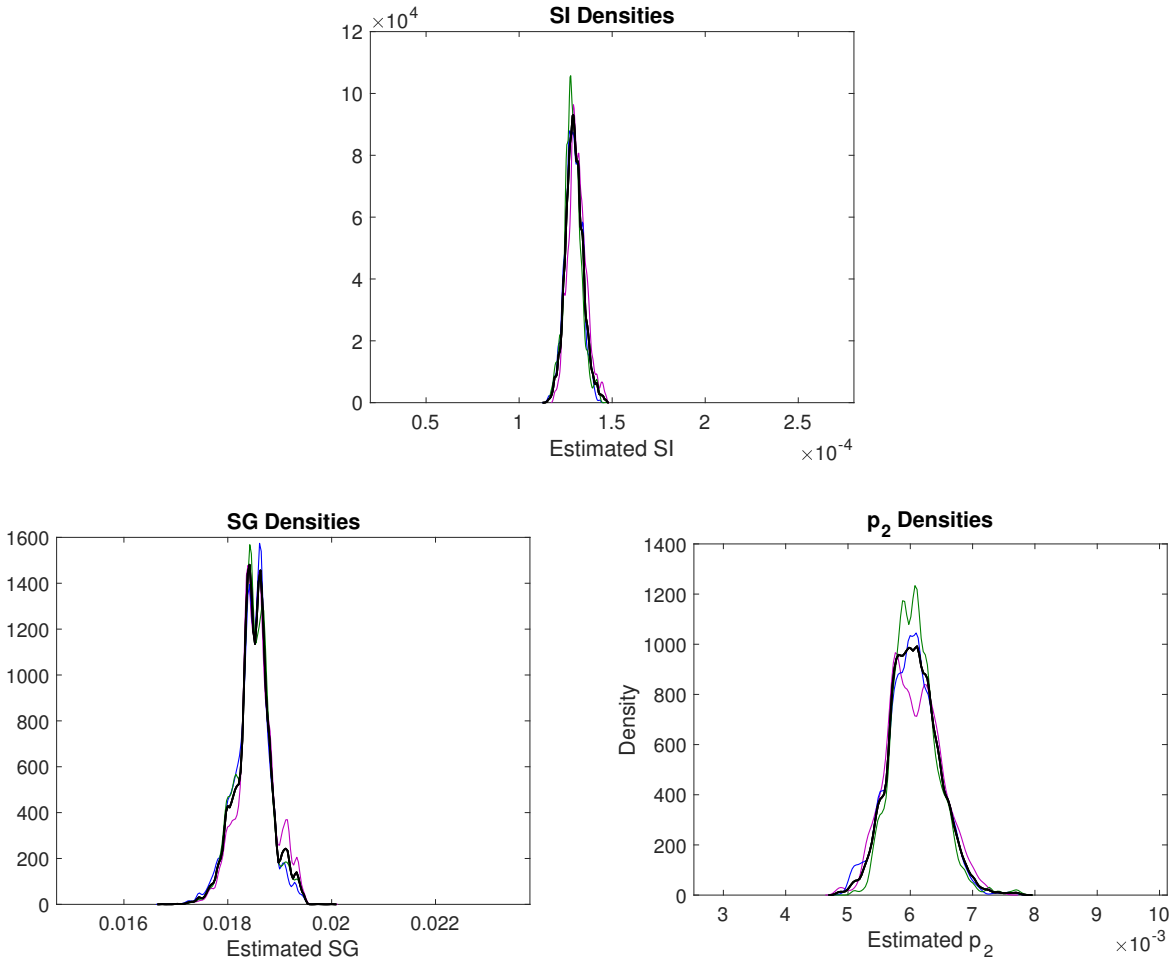

Figure 5.12: The posterior densities of S_I, S_G, and p_2 for Subject 60.

terquartile range, $2.54(2.39, 2.71)\times10^{-2}$. Additionally, the two modes for S_G corresponding to each peak in the densities were 2.36 and 2.76 $\times10^{-2}$. The mean acceptance rates were 27%, 11% and 16% for S_I, p_2 and S_G, respectively. The glucose concentrations and the MCMC simulated glucose profile are shown in Figure 5.13(b)

Convergence of the chains to the target distribution was achieved when the maximum PSRF was below 1.2, the within and between chain variance equaled each other, and the autocorrelation of the draws approached 0 [87]. For the simulated individual, the autocorrelation decreased towards 0 for all the parameter chains. However, the autocorrelation tended

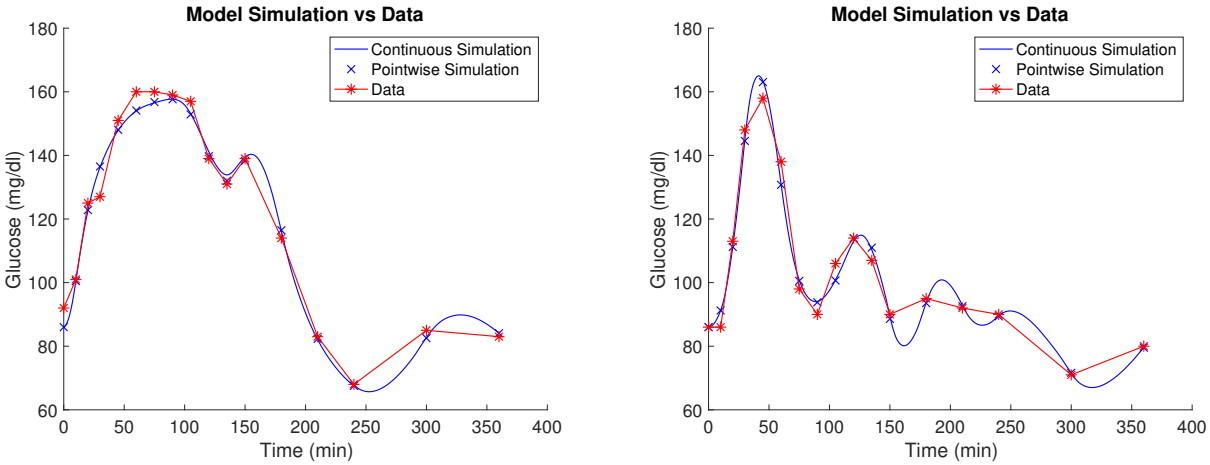

(a) Subject 60 (b) Subject 20

Figure 5.13: The MCMC simulated glucose and data for Subject 60 and Subject 20.

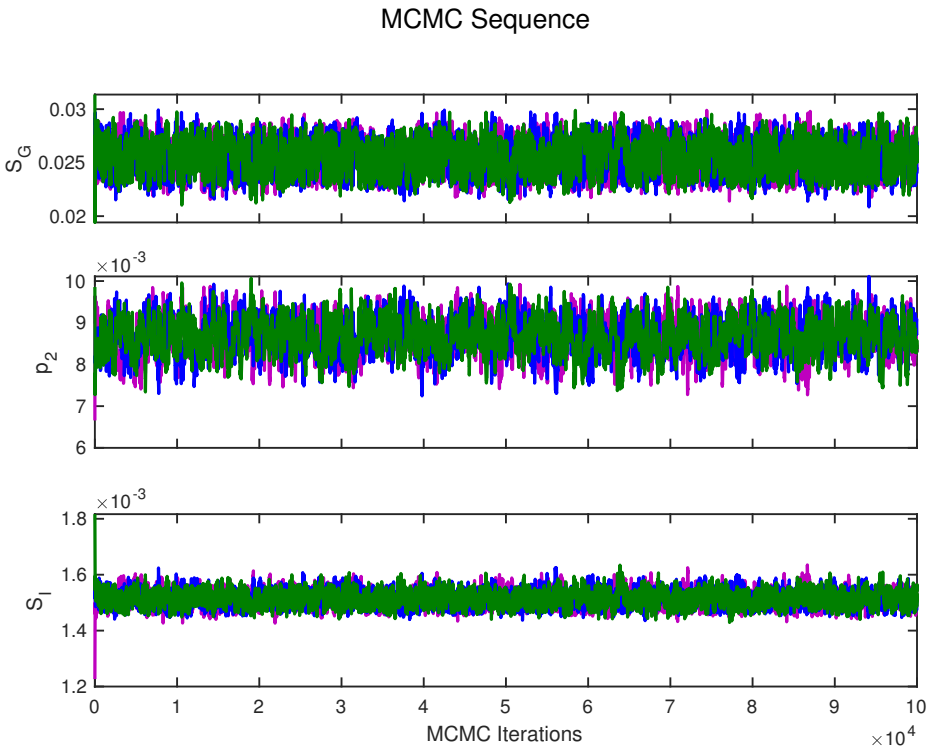

Figure 5.14: The sequence of MCMC chains S_G, p_2, and S_I for Subject 20.

to remain large for short lags for S_G and p_2 and decreased slowly. The autocorrelation for all parameter chains for Subject 60 and Subject 20 quickly decreased to 0. The within and

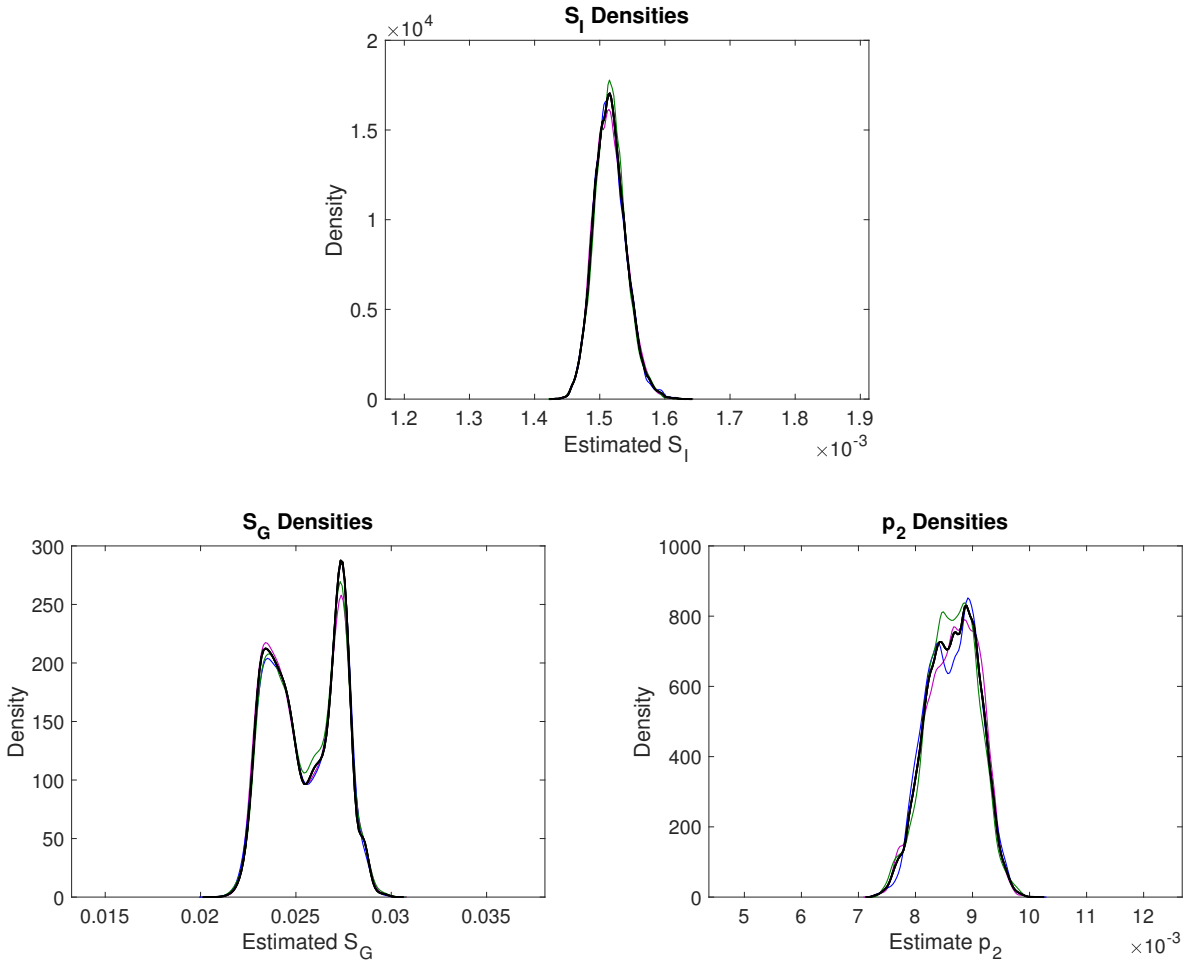

Figure 5.15: The posterior densities of S_I, S_G, and p_2 for Subject 20.

between chain variances converged to the same value for each individual. The maximum PSFR was 1, 1, and 1.1 for subjects 20, 60 and the simulated subject, respectively. These results led us to conclude that the chains had converged to the target posterior distributions for each individual's set of parameters.

5.5 Discussion

The local SA of OMM illustrated how perturbations to the parameters affected model output and how the sensitivity to these parameters changed throughout the duration of the

OGTT protocol. The main conclusions are that the Ra_{exo} constraint enforces a dependence of the α_i on the other α_i. Removing this constraint reduced this dependence but the sensitivity to α_i values larger than 5 did increase in magnitude towards the end of the protocol. In both OMM and Rescaled OMM, sensitivity to changes in S_G were low suggesting that this parameter may be difficult to identify or may be identified with high uncertainty [76]. This observations agrees with the known identifiability issues associated with S_G in OMM [19] that are further discussed in Ch 6. This SA of both OMM and the Rescaled OMM place the importance of the parameters, excluding the α_i, largely on the initial return to baseline phase. However, sensitivity to G_b and p_3 increased within the last hour of the protocol for the OMM. The Ra_{exo} constraint was proposed to help identify OMM and reduce the number of parameters [57] but we have shown that this constraint requires the full length of the protocol to identify the model. Appropriate assumptions about the end of the protocol would help to mitigate this dependence on the full duration of the protocol. In order to potentially reduce the length of data needed for application of OMM in this population, the return to baseline phase should be well studied. Then the model should be adapted to an appropriate formulation that can predict the return to basal glucose levels.

Assessing the average sensitivity of the glucose output to each parameter using the metric r_{f_i/θ_j} helped to confirm the conclusions drawn from the plots of $s_{f_i/\theta_j}(t)$. However, this metric is not able to fully quantify the time dependent nature of these sensitivity measures. For example, median overall sensitivity to I_b was minimal but the maximum magnitude achieved was much larger compared to S_G. Further development of sensitivity metrics could focus on the sensitivity of OMM during certain windows of the data such as the time to peak glucose. This could be done using the metric introduced here or with a variation of the infinity norm, $|x|_\infty = \max_i |x_i|$.

The inclusion of G_b and I_b in the local SA was meant to bring some understanding of how these assumptions of steady state and minimum glucose and insulin concentrations affect the model's ability to simulate the glucose profile and estimate S_I. The implication of sensitivity to G_b and I_b suggest that OMM may be more difficult to apply when the system does not start and end at steady state.

In this population of overweight and obese adolescent girls, RHG was common and caused glucose concentrations to go below G_b. This begs the question of whether the model is able to capture this feature of the data and represent it in the measures of S_I since the model assumes there is an equilibrium to return to. The OMM has been successfully validated in many populations including healthy adults populations [57], adults with pre-diabetes [62] and a small group adolescents [2]. A goal would be to apply the OMM in more diverse populations that are not able to maintain a fixed equilibrium such as populations with type 1 diabetes or cystic fibrosis where insulin is either being given externally or the pancreas struggles to release insulin.

A limitation of this local SA is that OMM is a nonlinear system and the dependence between parameters is not indicated as only one parameter was perturbed at a time. Additionally, the sensitivity functions computed here are not associated with a percent change in simulated glucose. Global SA methods are more suited for nonlinear models and allow for the identification of parameter compensations and the sensitivity of the model to subsets of parameters. Future directions involve performing a global SA on OMM and the Rescaled OMM to verify these results.

The MCMC approach to obtain the precision on key OMM parameter estimates was able to estimate most parameters with small CV indicating low uncertainty in those parameter estimate. For representative subjects, MCMC was able to estimate a better set of parame-

ters, as assessed by the MSE, as well as give the precision. This improved confidence in the estimates of S_I will allow for better comparison of S_I between groups.

The inability of MCMC to produce an approximately normal posterior distribution for S_G for Subject 20 highlighted the known identifiability issues with OMM initially presented in [19] and discussed in Ch 2. The application of MCMC discussed here focused on a small subset of the overall parameter set. This project highlights the need to determine either individual or population values of S_G and V, which will be addressed in Ch 6.

CHAPTER 6

RATE OF APPEARANCE OF EXOGENOUS GLUCOSE

6.1 Introduction

Insulin sensitivity (S_I) measures the body's ability to stop the production of glucose and take up glucose for utilization by tissues. This can differ depending on the tissues considered. Decreased S_I is highly prevalent in obese adolescent girls and is this decrease is more provide in adolescent girls with both obesity and polycystic ovary syndrome (PCOS). Current methods of estimating whole body and tissue specific S_I in this group involve multi-phase hyperinsulinemic euglycemic (HE) clamp protocols that are invasive, non-physiological and cost prohibitive for large population studies. The use of an OGTT with stable isotope glucose tracers would allow for a more physiological method for estimating total and tissue-specific S_I in this population. From an OGTT tracer protocol, the various glucose fluxes can be computed as well as the glucose coming from the liver separate from the meal glucose.

The dynamics describing the rate of appearance of exogenous glucose (Ra_{exo}) from a meal involves many processes that are hard to measure *in vivo* but is a key input to differential equation based models of glucose-insulin dynamics. The total Ra represents the rate of appearance of glucose due to both endogenous and exogenous glucose contributions. Investigators have developed various methods of computing Ra_{exo} utilizing data from glucose tolerance tests combined with glucose tracers. From these methods, the rate of appearance of endogenous glucose from the liver (Ra_{endo}) is defined to be the difference of total Ra and Ra_{exo}. This chapter focuses on comparing the implementation and results on estimates of insulin sensitivity (S_I) of four methods for calculating Ra_{exo}. Although Ra_{exo} is an important input in glucose-insulin models, the method-dependence of these implementations has not, to our knowledge, been systematically investigated. Each method will be thoroughly motivated

and derived. Following implementation, method-dependence of the simulated glucose-insulin dynamics and estimates of insulin sensitivity will be assessed.

6.2 Materials

A detailed description of the dual tracer oral glucose tolerance test protocol can be found in Ch. 3. In brief, a group of overweight and obese (BMI $\geq$ 90th percentile for age and sex) adolescent (Tanner Stage 5) girls underwent a frequently sampled 6-hour OGTT with constant intravenous infusion of $[6,6\text{-}^2H_2]$ glucose (tracer II). Blood was sampled at -30,-20,-10, 0, 10, 20, 30, 45, 60, 75, 90, 105, 120, 135, 150, 180, 210, 240, 300 and 360 minutes following ingestion of 75 g plus an additional 40 mg/kg of $[1\text{-}^{13}C]$ glucose (tracer I) for glucose, insulin and tracer concentrations (Figure 6.1). 9 participants of the cohort had their glucose samples analyzed for tracer amounts and these 9 participants were studied for this analysis. The corrected tracer amounts were used to calculate exogenous glucose as

$$G_{meal} = G * TTR_1 * \left(1 + \frac{1}{E_D}\right) \tag{6.1}$$

where G is total glucose concentrations and TTR_1 is the tracer-to-tracee ratio of tracer I.

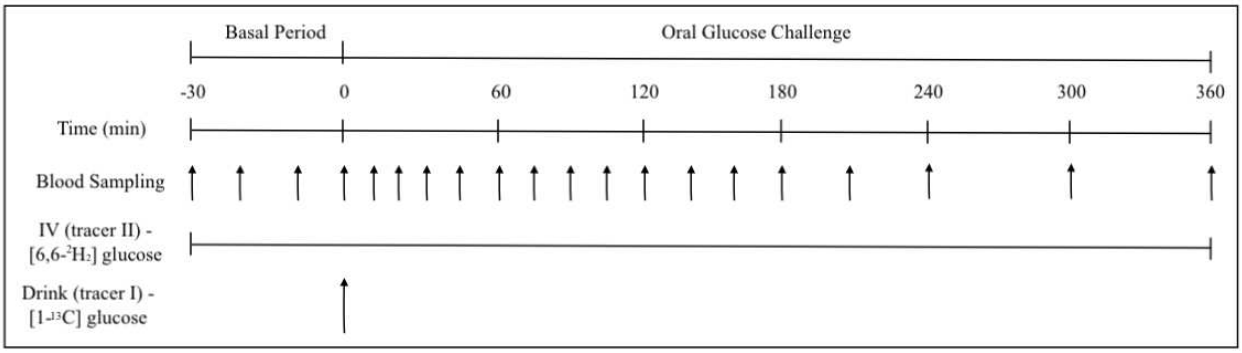

Figure 6.1: OGTT protocol with two stable isotope tracers showing blood sample times and protocol duration

In the following section, we take an in depth look into the derivations and implementation of each of the published methods for computing Ra_{exo}. To begin, we start by calculating

Steele's non-steady state model for total rate of appearance of glucose.

6.3 Methods

6.3.1 Steele's Non-Steady State Ra

Each of the following methods for calculating Ra_{exo} are based on Steele's non-steady state model for total Ra [88]. This model was developed to estimate the total Ra *in vivo* using glucose concentrations with intravenous infusion of at least one glucose isotope tracer. A glucose isotope is functionally identically to naturally occurring glucose, the tracee, but has a different mass. Measurement of the mass differences between the tracer and tracee allows us to better understand the movements of the tracee *in vivo* [89]. We use the mass balance equations for total glucose and tracer II from the OGTT protocol described above to determine the rate of appearance of total glucose, Ra:

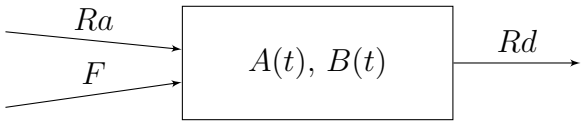

Figure 6.2: Schematic of glucose kinetics where Ra is the total rate of appearance of glucose, F is the infusion rate of glucose tracer, Rd is the rate of disappearance of glucose, $A(t)$ is the amount of tracer II and $B(t)$ is the amount of tracee.

In Figure 6.2, let Ra denote the rate of appearance of glucose, F be the infusion rate of the tracer II and Rd be the rate of disappearance of glucose. Define $A(t)$ and $B(t)$ as the amount of tracer II and tracee, respectively, at time t. Then $E(t)$, defined as $E(t) = \frac{A(t)}{B(t)}$, is the tracer-to-tracee ratio (TTR) of the plasma at time t. Then,

$$A(t) = B(t)E(t) \tag{6.2}$$

$$\frac{dA(t)}{dt} = B(t)\frac{dE(t)}{dt} + E(t)\frac{dB(t)}{dt} \tag{6.3}$$

The rate of change of tracee in the plasma is the rate in of tracee minus the rate out:

$$\frac{dB(t)}{dt} = Ra - Rd. \tag{6.4}$$

An analogous formula may be used to describe the rate of change of tracer II. However, since tracer II is constantly infused, $Ra_{2H} = F$ so the rate of change of tracer II is the infusion rate minus $E(t) \cdot Rd$,

$$\begin{aligned} \frac{dA(t)}{dt} &= Ra_{2H} - Rd_{2H} \\ &= F - \frac{A(t)}{B(t)} Rd \\ &= F - E(t)Rd \end{aligned} \tag{6.5}$$

Combining equations 6.3, 6.4 and 6.5 we obtain the following formula for total Ra:

$$Ra - Rd = \frac{\frac{dA(t)}{dt} - B(t)\frac{E(t)}{dt}}{E(t)} \tag{6.6}$$

$$\implies Ra = \frac{F - E(t)Rd - B(t)\frac{dE(t)}{dt}}{E(t)} + Rd \tag{6.7}$$

$$\implies Ra = \frac{F - B(t)\frac{dE(t)}{dt}}{E(t)} - \cancel{\frac{E(t)Rd}{E(t)} + Rd} \tag{6.8}$$

$$\implies Ra = \frac{F - B(t)\frac{dE(t)}{dt}}{E(t)} \tag{6.9}$$

Here, the entire glucose pool is regarded as a single compartment. To account for imperfect mixing of glucose throughout the pool, Steele introduces the pool fraction, p, to represent the fraction of the glucose pool that is rapidly mixing. Then we can rewrite $B(t)$ as $B(t) = pVC(t)$, where V is the total volume of the glucose pool and $C(t)$ is the concentration of glucose at time t. Hence, pV represents the rapidly mixing volume of distribution for glucose. Thus, Steele's equation for non-steady state Ra is written as

$$Ra = \frac{F - pV\,C(t)\,\frac{dE(t)}{dt}}{E(t)}. \tag{6.10}$$

In calculations, Ra is approximated using the following formula

$$Ra = \frac{F - pV[(C_2 + C_1)/2] \cdot [(E_2 - E_1)/(t_2 - t_1)]}{[(E_2 + E_1)/2]} \tag{6.11}$$

where the (t) notation has been suppressed; C_1 and C_2 are plasma glucose concentrations at times t_1 and t_2, respectively; and E_1 and E_2 are plasma TTR of tracer II to tracee at times t_1 and t_2, respectively [88, 90]. The rapid non-steady state changes following ingestion can lead to several errors in the calculation of the glucose fluxes. Mainly, this one compartment model has to assume rapid mixing of the glucose pool, which was known to be inaccurate. Therefore, the volume of distribution was fixed to be the rapidly equilibrating fraction, p, of the total glucose pool to account for the difference in TTR measured in the plasma and in other compartments of the body [88]. However, this fraction has been shown to vary with time [90, 91]. Additionally, the quick changes in TTR that occur within the first 90 min of the protocol make estimating the change in enrichments difficult and errors in this calculation propagate through to estimates of the desired glucose fluxes [92].

6.3.2 Exogenous Ra

Steele's equation represents the appearance of glucose in the blood from both endogenous and exogenous sources. Endogenous glucose is produced mainly by the liver, and exogenous glucose is ingested. The following sections outline the various methods for calculating the rate of appearance of ingested glucose.

Scaled Steele's Model

This method calculates Ra_{exo} by scaling total Ra by the normalized enrichment of tracer I. Total Ra is calculated using tracer II and Steele's formula. Then the total Ra is scaled by the ratio of the enrichment of tracer I in the plasma to the enrichment of tracer I in the test drink [90].

$$Ra_{exo} = Ra\left(\frac{E_P}{E_D}\right) \tag{6.12}$$

where E_D and E_P are the enrichments of [1-^{13}C] glucose from the test drink and plasma, respectively. The aim of scaling total Ra by this ratio is to calculate the proportion of glucose

appearance coming from an exogenous source.

One Pool Model

This method calculates Ra_{exo} by solving for the variable infusion rate of ingested glucose and then scaling this by the enrichment of tracer I in the drink. Known total Ra and Steele's non-steady state equation are used with tracer I to solve for the variable infusion rate, due to gut absorption dynamics, of tracer I, [93] Ra_{13C}. Theoretically, total Ra should be the same if computed with tracer I or tracer II. Tracer II is used in calculations of total Ra because the infusion rate of tracer II is known. Ra_{13C}, is scaled by the enrichment of tracer I in the drink to compute Ra_{exo}. To solve for Ra_{13C}, consider Steele's equation 6.10 in terms of tracer I where F is replaced with Ra_{13C} to represent the infusion rate of tracer I:

$$Ra = \frac{Ra_{13C} - pVC\frac{dE}{dt}}{E}.$$

Then solve for Ra_{13C}

$$Ra_{13C} = Ra \cdot E + pV \cdot C \cdot \frac{dE}{dt} \tag{6.13}$$

and scale by the enrichment of the drink to obtain

$$Ra_{exo} = \frac{Ra_{13C}}{E_D}. \tag{6.14}$$

One Compartment Model

Figure 6.3: Schematic showing change in tracers in one compartment where Ra_{13C} is the rate of appearance of tracer I, F_{2H} is the infusion rate of tracer II and G is the accessible compartment of each tracer.

This method computes Ra_{exo} by applying Steele's equation to estimated concentrations of [1-^{13}C] glucose. It assumes one accessible compartment from which Ra and Rd, the rates of appearance and disappearance, respectively, occur and where glucose tracers are measured (see Figure 6.3) [94]. The product pV represents the rapidly mixing compartment in which the mass balance equations for the [6, 6-$^2H_2$] glucose tracer imply

$$pV\frac{dG_{2H}}{dt} = F_{2H} - Rd_{2H} \tag{6.15}$$

where G_{2H} is the concentration of [6, 6-$^2H_2$] glucose tracer in plasma, F_{2H} is the rate of infusion and Rd_{2H} is the rate of disappearance in plasma.

Similarly, for the [1-^{13}C] glucose tracer

$$pV\frac{dG_{13C}}{dt} = Ra_{13C} - Rd_{13C} \tag{6.16}$$

where G_{13C} is the concentration of [1-^{13}C] glucose tracer in plasma, and Ra_{13C} and Rd_{13C} are the rate of appearance of [1-^{13}C] glucose tracer and disappearance in plasma, respectively.

The indistinguishability of the isotope tracers yields the following relationship that links the disappearance rate of the two glucose tracers

$$\frac{Rd_{13C}}{pVG_{13C}} = \frac{Rd_{2H}}{pVG_{2H}} = k_{01} \tag{6.17}$$

where k_{01} is the rate of glucose dissappearance, assumed to vary during the experiment. Using 6.17, rewrite 6.15 and 6.16 as

$$pV\frac{dG_{2H}}{dt} = F_{2H} - k_{01}\,pV\,G_{2H} \tag{6.18}$$

$$pV\frac{dG_{13C}}{dt} = Ra_{13_C} - k_{01}pVG_{13C}. \tag{6.19}$$

Then we have the mass balance equations for G_{2H} and G_{13C}. Solve 6.18 for k_{01} as

$$k_{01} = \frac{F_{2H}}{pVG_{2H}} - \frac{dG_{2H}/dt}{G_{2H}}. \tag{6.20}$$

Plugging 6.20 into 6.19 to arrive at an expression for Ra_{13C}:

$$\begin{aligned} Ra_{13C} &= pV\frac{dG_{13C}}{dt} + k_{01}pVG_{13C} \\ &= pV\frac{dG_{13C}}{dt} + \left(\frac{F_{2H}}{pVG_{2H}} - \frac{dG_{2H}/dt}{G_{2H}}\right)pVG_{13C} \\ &= \frac{F_{2H}}{G_{2H}/G_{13C}} + pV\frac{dG_{13_C}}{dt} - \frac{pV}{G_{2H}/G_{13C}}\frac{dG_{2H}/dt}{G_{2H}}. \end{aligned}$$

Using the relationship

$$\frac{d}{dt}\Big(\frac{G_{2H}}{G_{13\,C}}\Big) = \frac{G_{13\,C}\frac{dG_{2H}}{dt} - G_{2H}\frac{dG_{13\,C}}{dt}}{(G_{13\,C})^2} = \frac{1}{G_{13\,C}}\frac{dG_{2H}}{dt} - \frac{G_{2H}}{(G_{13\,C})^2}\frac{dG_{13\,C}}{dt},$$

the following expression for Ra_{13C} is found:

$$\begin{aligned} Ra_{13C} &= \frac{F_{2H}}{G_{2H}/G_{13C}} - pV\Big(\frac{1}{G_{2H}/G_{13C}}\frac{dG_{2H}}{dt} - \frac{dG_{13_C}}{dt}\Big) \\ &= \frac{F_{2H}}{G_{2H}/G_{13C}} - pV\Big(\frac{1}{G_{2H}/G_{13\,C}}\frac{dG_{2H}}{dt} - \frac{dG_{13_C}}{dt}\Big)\Big(\frac{G_{2H}}{G_{2H}}\Big)\Big(\frac{G_{13\,C}}{G_{13\,C}}\Big)^2 \\ &= \frac{F_{2H}}{G_{2H}/G_{13C}} - pV\Big(\frac{(G_{13C})^2}{G_{2H}}\Big)\Big(\frac{1}{G_{13C}}\frac{dG_{2H}}{dt} - \frac{G_{2H}}{(G_{13C})^2}\frac{dG_{13C}}{dt}\Big) \end{aligned}$$

$$Ra_{13C} = \frac{F_{2H}}{G_{2H}/G_{13C}} - \frac{pVG_{13C}}{G_{2H}/G_{13C}}\Big(\frac{d(G_{2H}/G_{13C})}{dt}\Big) \tag{6.21}$$

This formula for Ra_{13C} is then scaled by the enrichment of the drink to obtain Ra_{exo}:

$$Ra_{exo} = \frac{Ra_{13C}}{E_D}. \tag{6.22}$$

Two Compartment Model

This model computes Ra_{exo} by applying Steele's equation to estimated concentrations of [1-^{13}C] glucose and additionally considering exchange between a remote and an accessible compartment for the glucose pool. The assumed two-compartment system has a time-varying disappearance rate from the accessible compartment, k_{01}, and constant rate parameters between the accessible and peripheral compartments k_{21} and k_{12} [94, 95]. For glucose flow of the two tracers used in the protocol see Figure 6.4.

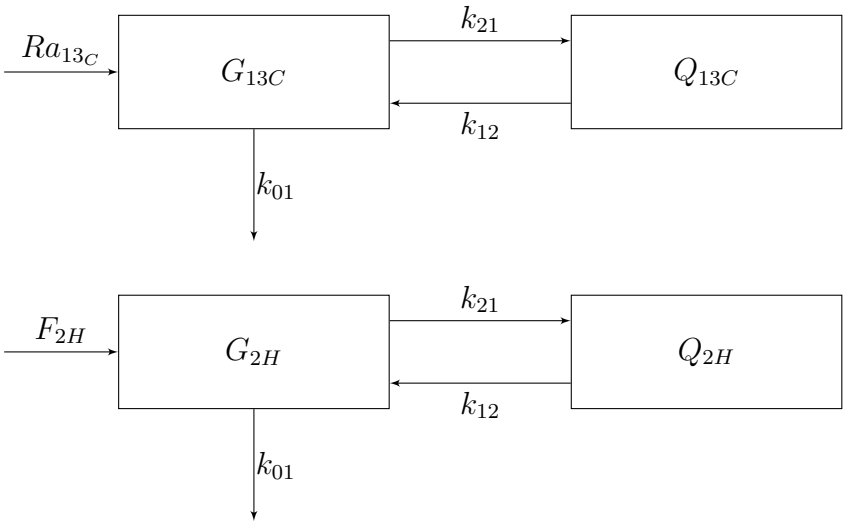

Figure 6.4: Schematic showing change in tracers in two compartments where Ra_{13C} is the rate of appearance of tracer I, F_{2H} is the infusion rate of tracer II, k_{12}, k_{21} and k_{01} are rate parameters, G and Q are the accessible and remote compartments, respectively, of each tracer.

From the mass balance equations for each isotope (see Figure 6.4) we have

$$V_1 \frac{dG_{2H}}{dt} = F_{2H} - (k_{01} + k_{21})V_1 G_{2H} + k_{12} Q_{2H} \tag{6.23}$$

$$V_1 \frac{dG_{13C}}{dt} = Ra_{13C} - (k_{01} + k_{21})V_1 G_{13C} + k_{12} Q_{13C}, \tag{6.24}$$

where V_1 is the volume of the accessible compartment, and Q_{2H} and Q_{13C} are the amounts of $[6,6\text{-}^2H_2]$ and $[1\text{-}^{13}C]$ glucose, respectively, in the peripheral compartments. We can derive a formula for k_{01} using 6.23 to yield

$$\begin{aligned} k_{01} &= \frac{V_1 \frac{dG_{2H}}{dt} - F_{2H} - k_{12} Q_{2H}}{-V_1 G_{2H}} - k_{21} \\ &= \frac{F_{2H}}{V_1 G_{2H}} + \frac{k_{12} Q_{2H}}{V_1 G_{2H}} - \frac{1}{G_{2H}} \frac{dG_{2H}}{dt} - k_{21}. \end{aligned} \tag{6.25}$$

Using 6.25 in 6.24 the following expression for Ra_{13C} is found.

$$V_1\frac{dG_{13C}}{dt} = Ra_{13_C} - \left(\frac{F_{2H}}{V_1G_{2H}} + \frac{k_{12}Q_{3H}}{V_1G_{2H}} - \frac{1}{G_{2H}}\frac{dG_{2H}}{dt}\right)V_1G_{13C} + k_{12}Q_{13_C}$$

$$\begin{aligned} Ra_{13_C} &= \frac{F_{2H}}{G_{2H}/G_{13C}} + V_1\frac{dG_{13C}}{dt} + \frac{V_1}{G_{2H}/G_{13C}}\frac{dG_{2H}}{dt} + k_{12}\left(\frac{Q_{2_H}}{G_{2H}/G_{13C}} - Q_{13_C}\right) \\ &= \frac{F_{2H}}{G_{2H}/G_{13C}} - \left(\frac{V_1G_{13\,C}^2}{G_{2H}}\right)\left(\frac{1}{G_{13\,C}}\frac{dG_{2H}}{dt} - \frac{G_{2H}}{{G_{13\,C}}^2}\frac{dG_{13\,C}}{dt}\right) + k_{12}\left(\frac{Q_{2_H}}{G_{2H}/G_{13C}} - Q_{13_C}\right) \end{aligned}$$

$$Ra_{13_C} = \frac{F_{2H}}{G_{2H}/G_{13C}} - \frac{V_1G_{13\,C}}{G_{2H}/G_{13\,C}}\left(\frac{d(G_{2H}/G_{13\,C})}{dt}\right) + k_{12}\left(\frac{Q_{2_H}}{G_{2H}/G_{13C}} - Q_{13C}\right) \tag{6.26}$$

Then Ra_{exo} is computed as

$$Ra_{exo} = \frac{Ra_{13C}}{E_D}. \tag{6.27}$$

The equations describing the amount of each tracer in the peripheral compartment were derived from the mass balance equations as

$$\frac{dQ_{2H}}{dt} = -k_{12}Q_{2H} + k_{21}V_1G_{2H} \tag{6.28}$$

$$\frac{dQ_{13C}}{dt} = -k_{12}Q_{13C} + k_{21}V_1G_{13C}. \tag{6.29}$$

The third term of 6.26 was computed iteratively using the calculation scheme below. This method required Ra_{exo} to be calculated over equally spaced time intervals. To utilize this approach, the OGTT data for each subject was interpolated with each time interval equal to 5 minutes. Let $R_2(t)$ denote the third term to be calculated using the following equations:

$$R_2(t_k) = V_2k_{12}\left[\frac{g^*(t_k)}{G_{2H}(t_k)/G_{13C}(t_k)} - g(t_k)\right] \tag{6.30a}$$

$$g(t_{k+1}) = b_1g(t_k) + b_2G_{2H}(t_k) + b_3G_{2H}(t_{k+1}) \tag{6.30b}$$

$$g^*(t_{k+1}) = b_1g^*(t_k) + b_2G_{13C}(t_k) + b_3G_{13C}(t_{k+1}) \tag{6.30c}$$

$$g(t_0) = G_{2H}(t_0) \qquad g^*(t_0) = G_{13C}(t_0) \tag{6.30d}$$

$$b_1 = e^{-k_{12}T} \tag{6.30e}$$

$$b_2 = \frac{1 - b_1}{k_{12}T} - b_1 \tag{6.30f}$$

$$b_3 = 1 - \frac{1 - b_1}{k_{12}T}. \tag{6.30g}$$

$R_2(t_k), g(t_k)$ and $g^*(t_k)$ are calculated at the discrete time points over the whole time interval of the OGTT protocol. Initially, $R_2(t_0) = 0$ and $g(t_k)$ and $g^*(t_k)$ are updated to calculate the next step of $R_2(t_k)$. The parameters b_1, b_2 and b_3 are constant, V_2 is the volume of the remote compartment and $T = 5$ minutes is the time interval between each time point [96].

6.3.3 Implementation into OMM/OMM*

Recall the equations of the Oral Minimal Model (OMM) and the Labeled-Oral Minimal Modem (OMM*) as

$$\begin{cases} \dot{G}(t) = -[S_G + X(t)] \cdot G(t) + S_G \cdot G_b + \frac{Ra_{exo}(\boldsymbol{\alpha},t)}{V} & G(0) = G_b \\ \dot{X}(t) = -p_2 \cdot X(t) + p_3 \cdot [I(t) - I_b] & X(0) = 0 \end{cases} \tag{6.31}$$

and

$$\begin{cases} \dot{G}_{meal}(t) = -[S_G^* + X^*(t)] \cdot G_{meal}(t) + \frac{Ra_{exo}(\boldsymbol{\alpha},t)}{V} & G_{meal}(0) = 0 \\ \dot{X}^*(t) = -p_2^* \cdot X^*(t) + p_3^* \cdot [I(t) - I_b] & X(0) = 0 \end{cases} \tag{6.32}$$

where

$$Ra_{exo}(\boldsymbol{\alpha}, t) = \begin{cases} \alpha_{i-1} + \frac{\alpha_i - \alpha_{i-1}}{t_i - t_{i-1}}(t - t_{i-1}) & \text{per } t_{i-1} \le t \le t_i \quad i = 1, \cdots, n \\ 0 & \text{otherwise} \end{cases} \tag{6.33}$$

Once the Ra_{exo} methods have been computed, sensitivity of S_I and S_I^* estimates to each method can be analyzed. As discussed in Ch 2, the OMM and OMM* are not structurally identifiable, so a two-step approach for parameter estimation is used. To begin, an estimate of Ra_{exo} from a chosen method was fixed in the Labeled Reference Model (RM*, 6.34) for

meal glucose [21, 62].

$$\begin{cases} \dot{G}_{meal}(t) = -[S_G^{*ref} + X(t)^*] \cdot G_{meal}(t) + \frac{Ra_{exo}^{ref}(t)}{V^{*ref}}, & G_{meal}(0) = 0 \\ \dot{X}^{*ref}(t) = -p_2^{*ref} \cdot X^{*ref}(t) + p_3^{*ref} \cdot [I(t) - I_b], & X^{*ref}(0) = 0 \end{cases} \tag{6.34}$$

Parameters S_G^{*ref}, p_2^{*ref}, p_3^{*ref} and V^{*ref} were estimated using constrained least squares optimization. Then the same Ra_{exo} approximation was fixed in the Reference Model (RM, [57,62]) and the parameters S_G^{ref}, p_2^{ref}, p_3^{ref} and V^{ref} were estimated. These parameters were initialized by the corresponding reference meal parameters.

$$\begin{cases} \dot{G}(t) = -[S_G^{ref} + X(t)^{ref}] \cdot G(t) + S_G^{ref} \cdot G_b + \frac{Ra_{exo}^{ref}(t)}{V^{ref}}, & G(0) = G_b \\ \dot{X}^{ref}(t) = -p_2^{ref} \cdot X^{ref}(t) + p_3^{ref} \cdot [I(t) - I_b], & X^{ref}(0) = 0 \end{cases} \tag{6.35}$$

The reference parameter estimates were used to fix S_G, S_G^*, V and V^* in the OMM and OMM* where total and meal glucose are solved simultaneously also by constrained least squares optimization. This allows unique estimation of the α_i, $i = 0, \ldots, n$ in $Ra_{exo}(\boldsymbol{\alpha}, t)$ as well as the parameters p_2, p_3, p_2^* and p_3^*. The time breakpoints for Ra_{exo} were 0, 10, 30, 60, 90, 120, 150, 180, 210, 240, 300, and 360 minutes. There was a constraint placed on $Ra_{exo}(\boldsymbol{\alpha}, t)$ such that

$$\int_0^{360} Ra_{exo}(\boldsymbol{\alpha}, t)\, dt = \frac{D \cdot f}{BW}. \tag{6.36}$$

where D is the dose of the drink, $f = 0.9$ is the fraction of glucose absorbed, and BW is the body weight of the participant. This constraint reduces the number of parameters in $\boldsymbol{\alpha}$ by one. Then for α_i, $i = 0, \cdots 11$

$$\int_0^{360} Ra_{exo}(\boldsymbol{\alpha}, t)\, dt = \frac{D \cdot f}{BW}$$
$$\frac{\alpha_1 \cdot (10-5)}{2} + \frac{\alpha_2 \cdot (30-10)}{2} + \frac{\alpha_3 \cdot (60-30)}{2} + \frac{\alpha_4 \cdot (90-60)}{2} + \frac{\alpha_5 \cdot (120-90)}{2}$$
$$+ \frac{\alpha_6 \cdot (150-120)}{2} + \frac{\alpha_7 \cdot (180-150)}{2} + \frac{\alpha_8 \cdot (210-180)}{2} + \frac{\alpha_9 \cdot (240-210)}{2}$$
$$+ \frac{\alpha_{10} \cdot (300-240)}{2} + \frac{\alpha_{11} \cdot (360-300)}{2} = \frac{D \cdot f}{BW}$$
$$12.5\alpha_1 + 25\alpha_2 + 30\alpha_3 + 30\alpha_4 + 30\alpha_5 + 30\alpha_6 + 30\alpha_7 + 30\alpha_8 + 45\alpha_9 + 60\alpha_{10} + 30\alpha_{11} = \frac{D \cdot f}{BW}$$

$$\alpha_3 = \frac{\frac{D \cdot f}{BW} - 12.5\alpha_1 - 25\alpha_2 - 30\alpha_3 - 30\alpha_4 - 30\alpha_5 - 30\alpha_6 - 30\alpha_7 - 30\alpha_8 - 45\alpha_9 - 60\alpha_{10} - 30\alpha_{11}}{30} \tag{6.37}$$

where we assume $Ra_{exo}(\boldsymbol{\alpha}, t) = 0$ for the first 5 minutes of the OGTT protocol [68]. This constraint on α_3 assumes glucose concentrations peak at 60 minutes. Then S_I, S_I^* and S_I^{Dyn} can be computed. All constrained optimization was performed using the **fmincon** command in MATLAB (Mathworks, Natick, MA).

To improve numerical identifiability, S_G, S_G^*, V and V^* are typically fixed to mean or median reference population values [21, 57, 62]. For this study, individual reference parameters were used to identify OMM and OMM* for each participant instead of using fixed population values. This allowed for a more individualized estimates of S_I and S_I^*. The OMM and OMM* were identified together. Since the Ra_{exo} parameters are estimated in OMM, the methods used to compute Ra_{exo} are an intermediate step in the process used to estimate all parameters and, therefore, the insulin sensitivity indices. This raises the issue of the sensitivity of the estimated values of S_I, S_I^* and S_I^{Dyn} as well as the fixed model parameters to the chosen method of estimating Ra_{exo}.

Statistical Analysis

Values were reported as mean ± standard deviation (SD) or median(min, max) where appropriate. Pearson's correlation test was used to compute correlations via the **corrcoef** function in MATLAB.

6.4 Results: Ra_{exo} Methods

For each subject (n = 9), we computed Ra_{exo} using each method and implemented these approximations of Ra_{exo} into RM/RM* and then OMM/OMM* to obtain the desired insulin sensitivity indices. We report glucose and insulin concentrations, Steele's total Ra, Ra_{exo} and Ra_{endo} for all the methods, and the results of the implementation of the Ra_{exo} methods into RM/RM* and OMM/OMM* for 3 subjects that illustrate the representative features of glucose and insulin dynamics in this population of obese adolescent girls. It is typical for this group to experience prolonged hyperglycemia which can be seen in Figure 6.5(a) and Figure 6.7(a). Also shown is Steele's total Ra estimate for each participant. This was used to compute Ra_{endo} as the difference of total Ra and Ra_{exo}.

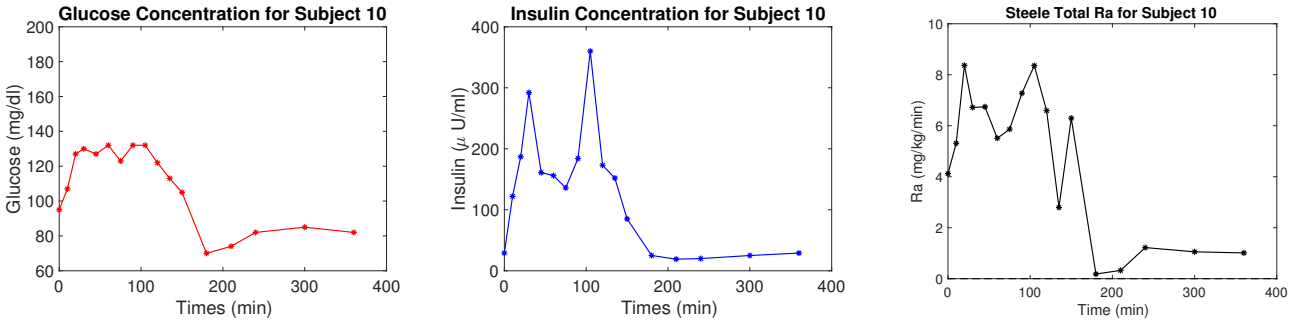

Figure 6.5: Glucose concentration, insulin concentration and Steele's total Ra for Subject 10.

The estimates of Ra_{exo} and corresponding Ra_{endo} estimates for each of the four exogenous Ra_{exo} methods are shown for the representative subjects in Figure 6.8, Figure 6.9, and Figure 6.10. Each method was computed at the blood sampling times mentioned in 6.2.

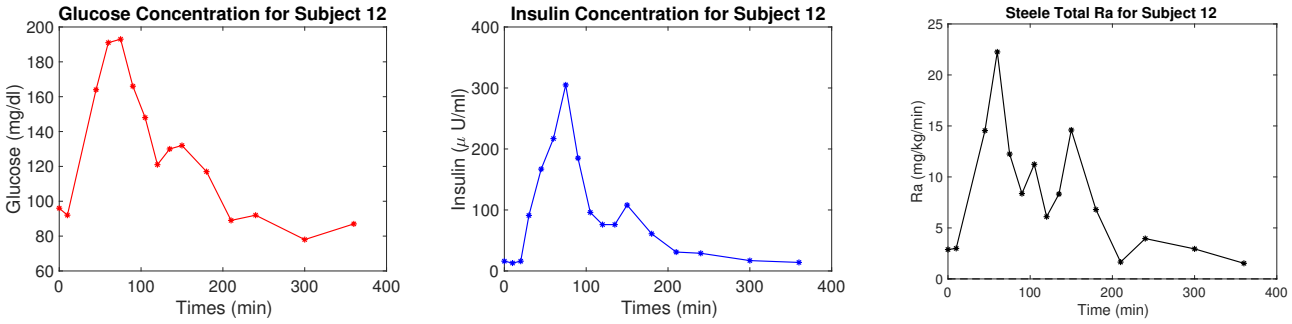

Figure 6.6: Glucose concentration, insulin concentration and Steele's total Ra for Subject 12.

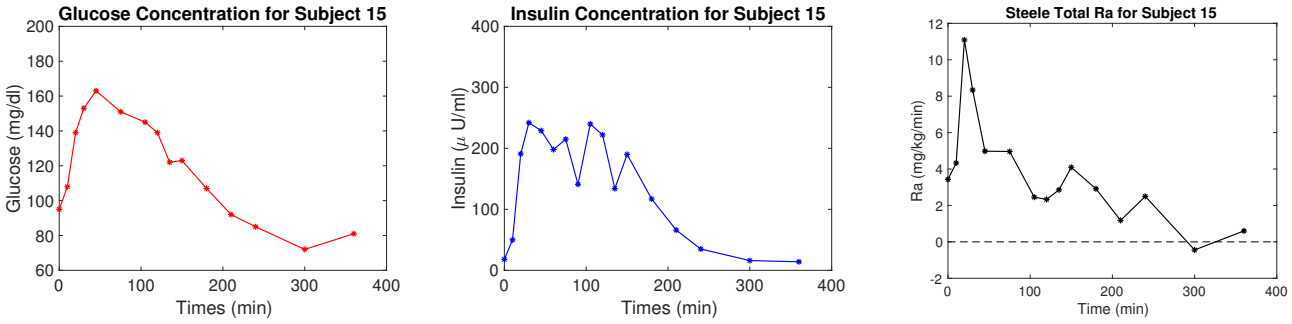

Figure 6.7: Glucose concentration, insulin concentration and Steele's total Ra for Subject 15.

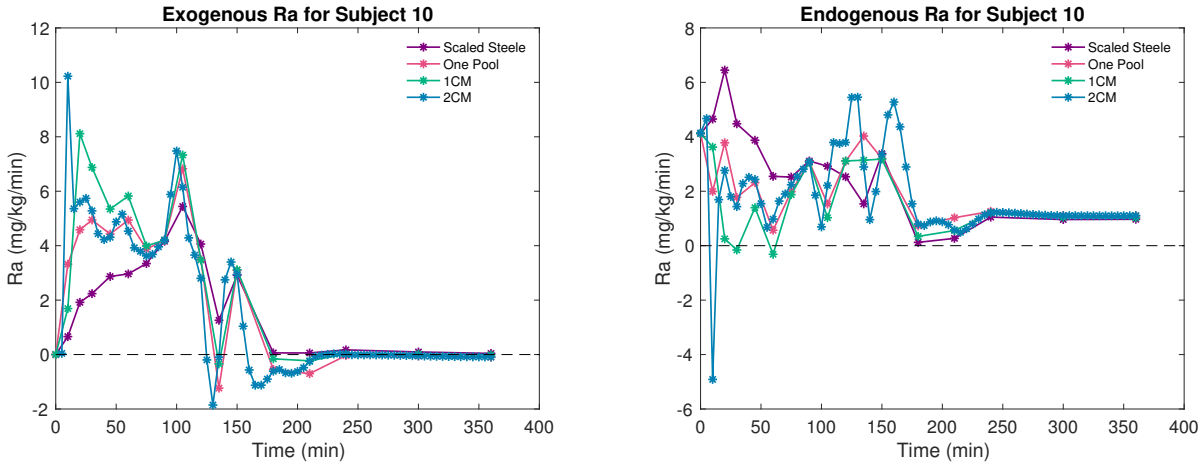

Figure 6.8: The calculated Ra_{exo} and the corresponding Ra_{endo} for each method for Subject 10.

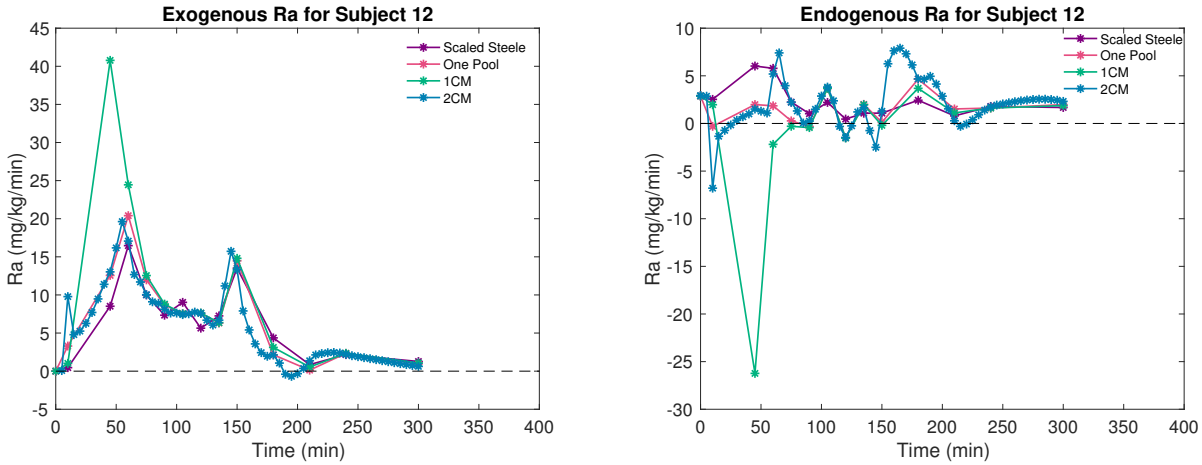

Figure 6.9: The calculated Ra_{exo} and the corresponding Ra_{endo} for each method for Subject 12.

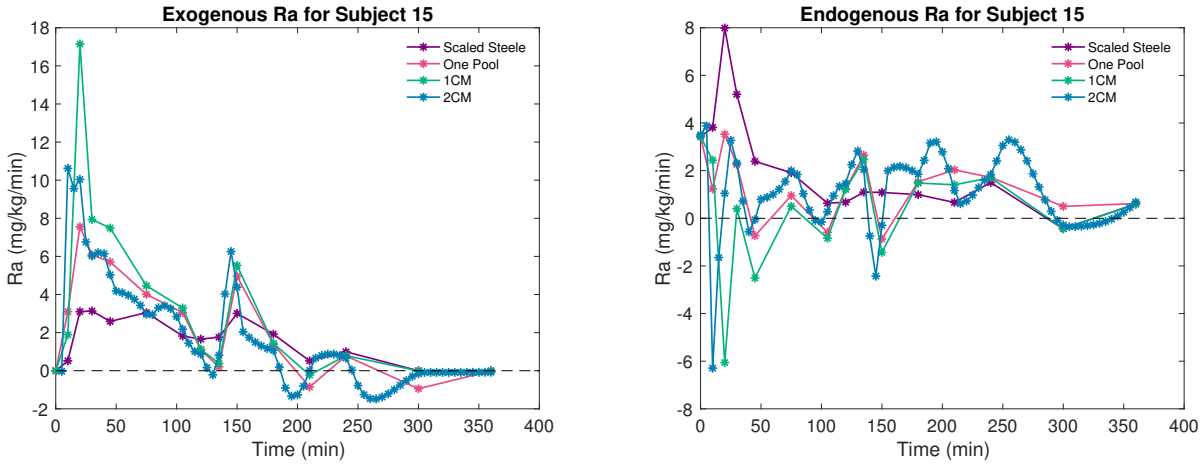

Figure 6.10: The calculated Ra_{exo} and the corresponding Ra_{endo} for each method for Subject 15.

The dotted line at 0 helps to visually identify when Ra_{exo} estimates were computed to be non-physiologically negative. Ra_{exo} is the rate of the amount of glucose entering the bloodstream and therefore should not be negative. The methods varied the most during the first approximately 90 minutes of the OGTT protocol.

In initial applications of OMM and OMM*, the model simulations of total and meal glucose would routinely produce poor fits to the data (see Figure 6.11 and Figure 6.12). The remaining implementations of OMM and OMM* were done with the addition of a constraint function in the optimization that enabled $\int_0^{360} Ra_{exo} dt = \frac{D \cdot f}{BW}$ but without assigning the dependence on a specific α_i as described in (Eq. 6.37).

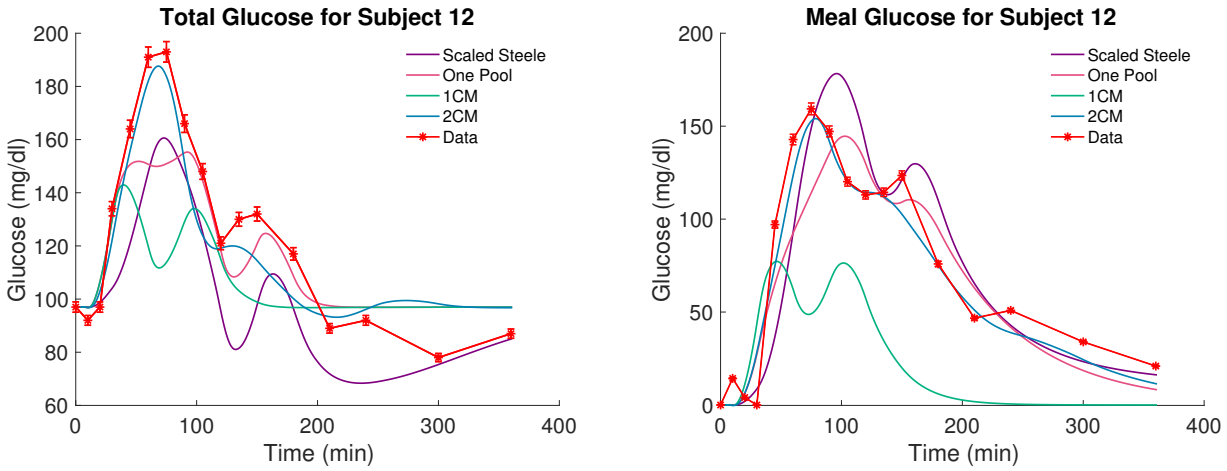

Figure 6.11: OMM/OMM* glucose simulations for total and meal glucose with the Ra_{exo} constraint on a select α_i for Subject 12.

The simulated total and meal glucose initialized with each reference Ra_{exo} method is shown in Figure 6.13, Figure 6.14 and Figure 6.15. Each implementation provided good fits to the data. The final $Ra_{exo}(\boldsymbol{\alpha}, t)$ estimates, shown in Figure 6.16, had some noticeable variations.

Estimates of the insulin sensitivity indices are reported for the 9 participants where OMM and OMM* was initialized with each Ra_{exo} method (Table 6.1, Table 6.2, Table 6.4) along with their mean ± SD in Table 6.3. There was high variability of S_I, S_I^* and S_I^{Dyn} estimates across methods as illustrated in the high coefficient of variations (CV = 100×SD/mean %). The CV was 104.38 ± 47.50% and 106.56 ± 48.56% for the S_I and S_I^* estimates, respectively. The variability in the estimates of S_I^{Dyn} was smaller in comparison as illustrated by

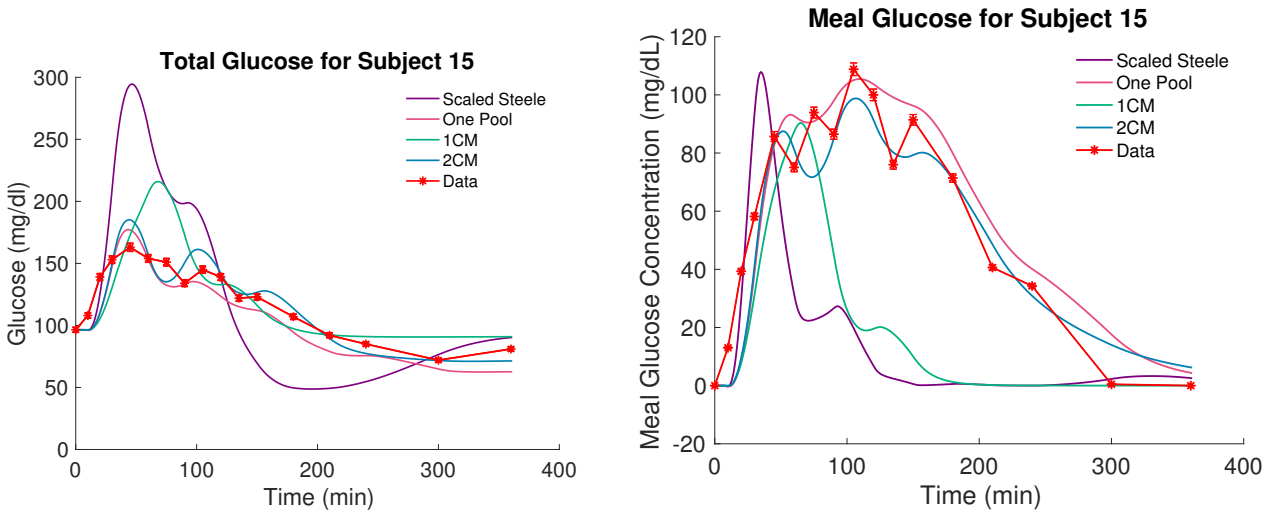

Figure 6.12: OMM/OMM* glucose simulations for total and meal glucose with the Ra_{exo} constraint on a select α_i for Subject 15.

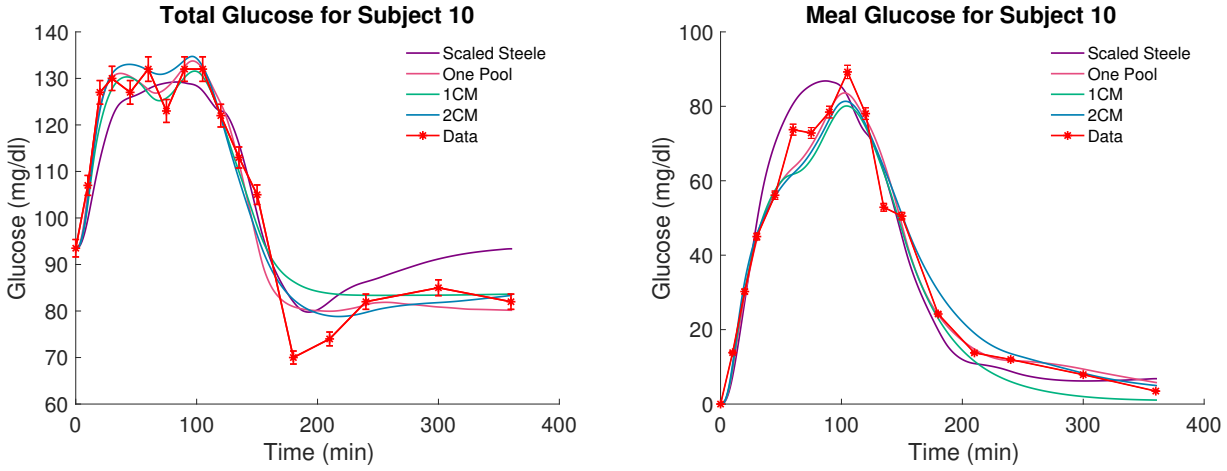

Figure 6.13: The simulated total and meal glucose for each of the 4 Ra_{exo} methods for Subject 10.

a CV of 69.17 ± 35.96%. The correlation of the Ra_{exo} methods on estimates of S_I, S_I^* and S_I^{Dyn} were either uncorrelated or moderately to strongly correlated (Table 6.5, Table 6.6, and Table 6.7). The Scaled Steele S_I, S_I^* and S_I^{Dyn} estimates did not correlate with any other method. The 1CM and 2CM estimates of S_I were moderately correlated (r = 0.65, p < 0.1). The One Pool S_I estimates correlated with both the 1CM (r = 0.71, p < 0.05) and

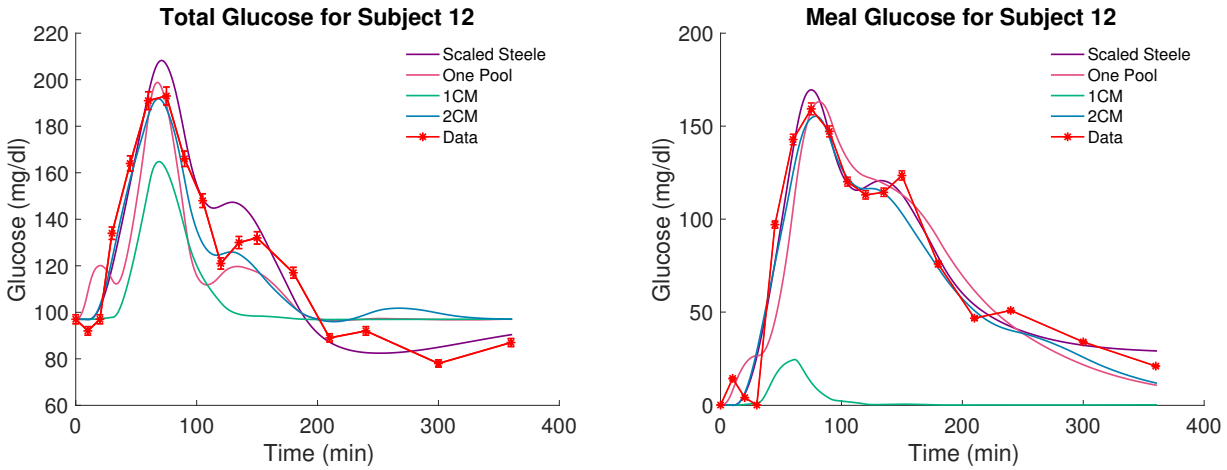

Figure 6.14: The simulated total and meal glucose for each of the 4 Ra_{exo} methods for Subject 12.

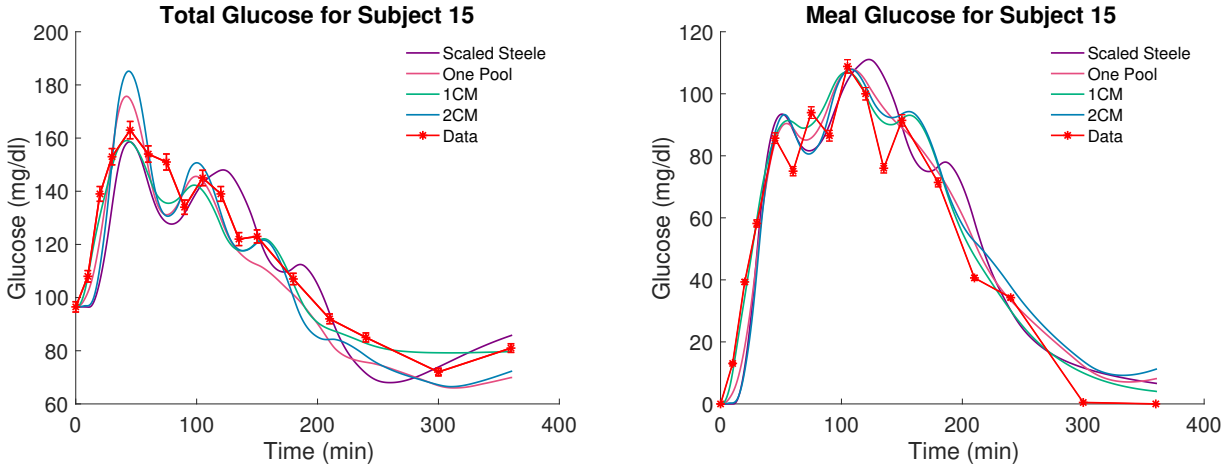

Figure 6.15: The simulated total and meal glucose for each of the 4 Ra_{exo} methods for Subject 15.

the 2CM (r = 0.83, p < 0.001). The only significant correlation among the S_I^* estimates was between the One Pool and the 2CM (r = 0.99, $p < 0.001$). Similarly, there was only one significant correlation among the estimates of S_I^{Dyn} between the One Pool method and the 1CM (r = 0.86, $p < 0.01$).

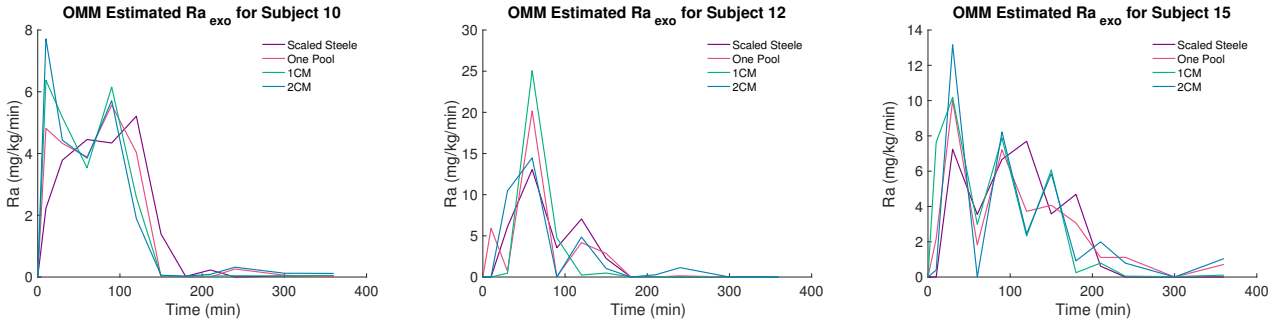

Figure 6.16: The OMM estimated Ra_{exo} resulting from the initialization with different Ra_{exo} methods for the representative participants.

Table 6.1: Estimates of S_I^{ref}, 10^{-4} and S_I, 10^{-4} for the 4 Ra_{exo} methods.

	Methods							
	Scaled Steele		One Pool		1CM		2CM	
Subject	S_I^{ref}	S_I	S_I^{ref}	S_I	S_I^{ref}	S_I	S_I^{ref}	S_I
10	2.41	1.67	8.28	71.93	6.91	20.24	2.68	3.27
12	6.07	2.31	43.82	0.15	0.10	0.11	4.36	0.97
15	1.69	2.37	33.76	115.04	0.13	3.48	30.53	11.08
29	3.85	2.54	3.23	3.15	3.44	1.86	2.56	5.24
33	98.71	0.23	3.71	5.364	98.90	0.19	2.51	1.74
43	24.97	14.40	23.57	0.342	16.75	25.20	8.37	3.05
44	51.75	36.64	47.50	1.10	22.99	0.074	30.99	0.817
66	16.39	57.96	77.47	33.25	0.34	0.11	0.11	8.72
67	1.88	0.056	2.26	0.072	34.24	0.11	2.03	0.098

The estimates of V, V^*, S_G and S_G^* in addition to their mean and SD for each method and participant are reported in Table 6.10, Table 6.11, Table 6.8 and Table 6.9. The CV was 27.27 $\pm$ 8.71% and 25.06 $\pm$ 10.28% for V and V^*, respectively. The variability among estimates of S_G and S_G^* was larger illustrated by the large standard deviations. This resulted in large CV values at 36.76% (15.67, 88.71 %) and 74.4% (23.55, 105.22%) for S_G and S_G^*, respectively.

Table 6.2: Estimates of S_I^{*ref}, 10^{-4} and S_I^*, 10^{-4} for the 4 Ra_{exo} methods.

	Methods							
	Scaled Steele		One Pool		1CM		2CM	
Subject	S_I^{*ref}	S_I^*	S_I^{*ref}	S_I^*	S_I^{*ref}	S_I^*	S_I^{*ref}	S_I^*
10	5.68	4.68	3.78	2.60	89	1.81	1.40	0.56
12	10.30	3.85	5.24	0.17	0.12	91.67	3.85	0.098
15	93.20	3.126	33.90	99.80	0.57	10.60	26.74	98.70
29	12.52	8.13	8.69	9.21	3.95	0.14	0.23	0.16
33	3.13	1.32	3.54	1.34	1.60	0.115	1.32	0.80
43	1256.8	23.18	421.40	0.055	1040	4.97	0.045	0.043
44	78.66	0.86	64.46	0.60	17.4	0.059	34	0.18
66	89.82	0.43	4.11	9.13	0.10	0.10	46.82	2.14
67	0.81	0.047	0.07	0.11	0.125	0.125	122	0.097

Table 6.3: The mean and standard deviation of S_I, S_I^{ref}, S_I^* and S_I^{*ref} (10^{-4}) for each participant (n = 9).

Subject	S_I	S_I^{ref}	S_I^*	S_I^{*ref}
10	24.30 ± 32.9	5.07 ± 2.97	2.41 ± 1.73	24.98 ± 42.80
12	0.88 ± 1.03	13.60 ± 20.30	23.95 ± 45.18	4.88 ± 4.21
15	64.70 ± 5.69	16.50 ± 1.81	53.30 ± 53.20	38.60 ± 39.10
29	3.20 ± 1.46	3.27 ± 0.54	4.41 ± 4.94	6.35 ± 5.38
33	1.88 ± 2.43e	51 ± 55.3	0.893 ± 0.58	2.40 ± 1.10
43	10.70 ± 11.40	18.4 ± 7.60	7.06e ± 11	679 ± 574
44	9.66± 18	38.30 ± 13.60	0.423 ± 0.37	48.60 ± 27.90
66	25 ± 26.10	23.60 ± 36.70	2.95 ± 4.22	35.20 ± 42.10
67	0.083 ± 0.023	2.40 ± 0.70	0.095 ± 0.034	30.90 ± 61

6.5 Discussion: Ra_{exo} Methods

The objective of this project was to identify potential method dependence on estimates of insulin sensitivity indices based on the Ra_{exo} approximation. The implementation and results of four published methods for computing Ra_{exo} were analyzed, and these estimates were used in the differential equations-based models OMM and OMM*. From these models of glucose-insulin dynamics, S_I, S_I^* and S_I^{Dyn} were calculated for each method and subject.

Table 6.4: Estimates of S_I^{Dyn}, 10^{-5} for the 4 Ra_{exo} methods for each participant (n = 9).

Subject	Scaled Steele	One Pool	1CM	2CM	Mean ± SD
10	9.1	2.87	2.43	4.14	4.63 ± 3.06
12	13.31	0.50	0.66	5.92	5.1 ± 6.03
15	13.5	4.64	0.97	4.422	5.88 ± 5.35
29	6.32	10.18	11.51	6.99	8.75 ± 2.49
33	1.15	2.42	1.15	10.77	3.87 ± 4.64
43	4.38	1.48	6.28	18.48	7.65 ± 7.49
44	1.46	0.92	0.46	1.04	9.69 ± 0.41
66	2.31	1.37	0.66	1.26	1.40 ± 0.68
67	0.34	0.45	0.63	0.61	5.07 ± 0.14

Table 6.5: The correlations of S_I estimates across Ra_{exo} methods.

Method	Scaled Steele	One Pool	1CM	2CM
Scaled Steele	1	-0.096	-0.26	-0.15
One Pool	-0.096	1	0.71*	0.83**
1CM	-0.26	0.71*	1	$0.65^{\dagger}$
2CM	-0.15	0.83**	$0.65^{\dagger}$	1

$^{\dagger}p < 0.1$, $*p < 0.05$, $**p < 0.01$

Table 6.6: The correlations of S_I^* estimates across Ra_{exo} methods.

Method	Scaled Steele	One Pool	1CM	2CM
Scaled Steele	1	-0.11	-0.03	-0.11
One Pool	-0.11	1	-0.04	0.99***
1CM	-0.03	-0.04	1	-0.01
2CM	-0.10785	0.99***	-0.01	1

*** $p < 0.001$

Table 6.7: The correlations of S_I^{Dyn} estimates for the Ra_{exo} methods.

Method	Scaled Steele	One Pool	1CM	2CM
Scaled Steele	1	0.24	0.145	0.04
One Pool	0.24	1	0.86**	0.11
1CM	0.15	0.86**	1	0.46
2CM	0.04	0.11	0.46	1

** $p < 0.01$

Reported here are the estimates of total, peripheral and dynamic insulin sensitivity computed using each Ra_{exo} method in the identification of OMM and OMM*. Both the reference

Table 6.8: Estimates of S_G, 10^{-2} for the 4 Ra_{exo} methods for all participants (n = 9).

Subject	Scaled Steele	One Pool	1CM	2CM	Mean ± SD
10	4.35	7.55	4.54	2.94	4.85 ± 1.94
12	1.63	9.57	9.61	3.11	5.99 ± 4.21
15	1.99	5.53	4.40	4.21	4.03 ± 1.48
29	9.08	5.78	5.06	4.65	6.14 ± 2.01
33	7.13	6.85	10.00	1.42	6.35 ± 3.58
43	9.99	9.98	9.99	3.84	8.46 ± 3.08
44	0.091	0.98	2.83	1.25	1.29 ± 1.14
66	7.09	10	9.99	10	9.27 ± 1.45
67	4.91	4.84	4.15	2.19	4.02 ± 1.27

Table 6.9: Estimates of S_G^*, 10^{-2} for the 4 Ra_{exo} methods for all participants (n = 9).

Subject	Scaled Steele	One Pool	1CM	2CM	Mean ± SD
10	0.038	.96	1.99	1.52	1.13 ± 0.84
12	0.025	1.21	4	1.29	1.63 ± 1.68
15	0.8	1.33	1.40	1.10	1.16 ± 0.27
29	0.011	0.93	3.40	3.73	2.02 ± 1.83
33	2.1	1.50	3.05	1.48	2.03 ± 0.74
43	2.68	10	4.55	9.31	6.64 ± 3.58
44	0.086	0.86	3.66	1.25	1.46 ± 1.54
66	3.34	0.26	4.50	0.67	2.19 ± 2.06
67	5.45	4	3.16	1.87	3.62 ± 1.50

Table 6.10: Estimates of V (dl/kg) for the 4 Ra_{exo} methods for all participants (n = 9).

Subject	Scaled Steele	One Pool	1CM	2CM	Mean ± SD
10	1.21	1.32	2.43	2.78	1.93 ± 0.79
12	2.23	1.560	3	2.99	2.46 ± 0.68
15	1.21	1.34	2.47	1.69	1.68 ± 0.57
29	1.24	1.21	1.52	1.47	1.36 ± 0.16
33	1.21	1.20	1.58	1.93	1.48 ± 0.35
43	1.59	2.07	1.21	2.15	1.76 ± 0.44
44	1.48	2.43	2.23	2.18	2.08 ± 0.41
66	1.88	1.74	2.99	2.99	2.40 ± 0.69
67	1.21	2.03	2.82	2.85	2.23 ± 0.77

Table 6.11: Estimates of V^* (dl/kg) for the 4 Ra_{exo} methods for all participants (n = 9).

Subject	Scaled Steele	One Pool	1CM	2CM	Mean ± SD
10	1.20	2.11	2.50	2.79	2.15 ± 0.69
12	2.11	3	2.99	2.95	2.76 ± 0.44
15	1.20	2.32	2.99	2.67	2.30 ± 0.78
29	1.73	2.77	2.99	3	2.62 ± 0.61
33	1.45	2.23	3	2.96	2.41 ± 0.73
43	1.2	1.2	1.2	1.30	1.23 ± 0.05
44	1.46	2.29	1.74	2.17	1.91 ± 0.39
66	1.44	2.84	3	2.19	2.37 ± 0.71
67	1.20	2.17	2.99	2.90	2.32 ± 0.83

insulin sensitivity measures S_I^{ref} and S_I^{*ref} and the final measures S_I, S_I^* and S_I^{Dyn} were highly sensitive to the chosen Ra_{exo} method. Estimates of S_I^{Dyn} were included in this comparison as they have been suggested to be more reliably estimated and a better marker of insulin's ability to regulate blood glucose in more insulin resistant populations [25, 26]. The large variability in estimates and generally low correlation of the insulin sensitivity measures across Ra_{exo} methods illustrate that this method dependence also affects the models' ability to rank uniformly the participants from least to most insulin sensitive.

The variations in the Ra_{exo} calculations used to obtain the reference parameters for OMM and OMM* caused high variability in estimates of V, V^*, S_G and S_G^* and may be a major cause of discrepancies in estimates of the insulin sensitivity indices. In an ideal setting, either one of these Ra_{exo} methods could be computed, within some predetermined margin of error, to gain insight into the physiology and reliably estimate measures of insulin sensitivity.

True Ra_{exo} cannot be directly measured without extremely invasive experiments that cannot be performed in humans [91]. However, this work has established that different methods for computing Ra_{exo} give rise to different estimates of insulin sensitivity (S_I, S_I^* and S_I^{Dyn}) when applied to OMM and OMM*. Clearly, this model-dependence represents a

major challenge for physicians wanting to quantify measures of insulin sensitivity.

All of the methods for computing Ra_{exo} peak at similar times, and the greatest variability among estimates of Ra_{exo} occurs in the first ≈ 90 minutes following ingestion of the test drink. This corresponds to the time period where the ratio of tracer I to tracer II changes rapidly. The 1CM and 2CM explicitly involve the ratio of tracer II to tracer I, so they are more sensitive to the changing ratios of the experiment compared to the Scaled Steele and One Pool methods. This may account for the increased peak height observed in the Ra_{exo} profiles produced by the 1CM and 2CM.

The total rate of appearance of glucose includes both exogenous and endogenous contributions so, physiologically, total Ra should always be greater than Ra_{exo}. Since total Ra is defined to be the sum of Ra_{exo} and Ra_{endo}, each method for computing Ra_{exo} predicts varying rates and degrees of suppression of Ra_{endo}. For some methods this leads to predictions of non-physiologic negative Ra_{endo} values. These non-physiologic Ra_{endo} values may be due to overestimates of Ra_{exo} associated with steady state assumptions that are not appropriate for the non-steady state conditions of the protocol [92].

There are limitations associated with each method. The Scaled Steele and One Pool model both use total Ra to calculate Ra_{exo}. This may introduce errors in Ra_{exo} due to known errors associated with computing Ra using Steele's non-steady state equation [92]. Specifically, the change in enrichment must be estimated and the fraction of the glucose pool that behaves as a rapidly mixing pool is assumed [90]. The latter limitation is common to all models of Ra_{exo} and is discussed in more detail below. Additionally, the Clamp model assumes the ratio of E_P to E_D is fixed for each time interval and computes Ra_{exo} as a proportion of total Ra based on this ratio. Since E_P actually changes over each time interval, this issue is most relevant soon after drink ingestion when E_P is changing quickly.

Although the 1CM and 2CM do not rely on explicitly computing total Ra, they apply Steele's non-steady state equation to labeled glucose. To minimize the non-steady state error, a third tracer with variable infusion may be used. This strategy seeks to keep the ratio of meal tracer to this additional tracer constant such that steady state conditions can be mimicked [92]. This is done by varying the infusion rate to mimic the anticipated pattern of appearance of the ingested glucose [94]. However, this method may introduce additional error because the patterns of endogenous glucose production and exogenous glucose appearance must be assumed and this approach may not be suitable for all participants. Although there have been tracer infusion profiles developed for some populations [92], tracer infusion profiles may be more variable in populations with IR such as obese adolescent females. Ideally, tracer infusion profiles should be individualized, but this is rarely feasible.

A common limitation among all of the methods is the assumption of a fixed volume of distribution for glucose. Studies suggest that the blood glucose pool where mixing occurs grows with time following an OGTT or a meal. A limitation of using Steele's equation for total Ra in calculations of glucose kinetics is the necessity of assuming a parameter p to account for imperfect mixing in the glucose pool. Different approaches have been applied to find the most accurate value of the volume of distribution to use in Steele's equation, but there is no one number that gives correct calculations of total Ra in all circumstances [90,91]. Proposed volumes of distribution range from 0.4 to 2 dl/kg in adults, but actual volumes of distribution could be higher in younger or more IR populations. In an adult cohort, Ra was more accurately computed in the early stages of an OGTT or IVGTT with 0.4 dl/kg. However, as the enrichment of plasma glucose reached a new equilibrium, changes in this enrichment reflected a much larger volume of distribution, closer to 2 dl/kg [90]. In a group of 11 adolescents in Tanner stages 4 and 5, V was estimated to be 2.4 dl/kg [2], suggesting that the volume of distribution in our cohort might be much larger than that estimated in

adults.

The practical and numerical identifiability of OMM and OMM* is a challenge for applying the OMM model framework to this dataset of a constant continuously infused dual tracer OGTT in highly IR adolescent girls with obesity. To properly use this set of models to estimate insulin sensitivity indices, S_G, S_G^*, V and V^* need to be fixed while the remaining parameters are estimated. By keeping S_G and S_G^* fixed while p_2, p_2^*, p_3, and p_3 are estimated forces insulin action to describe the dynamics of the body's response to the glucose challenge. Fixing V is necessary to estimate the α_i in $Ra_{exo}(\boldsymbol{\alpha}, t)$ as only the ratio $\boldsymbol{\alpha}/V$ is uniquely identifiable. The fixed parameters that enable identification of OMM and OMM* need to first be estimated with all model parameters simultaneously using a virtually known Ra_{exo}. This is a major problem for application in this data set where the Ra_{exo} has to be approximated. To this end, published methods were used to approximate reference Ra_{exo} and subsequently the parameters, S_G and V, needed for model identification. The method dependence in parameter estimates and final insulin sensitivity measures prompted the need to mitigate the differences in the Ra_{exo} methods and estimate S_G and V from a model independent estimate of Ra_{exo}.

The difference in the calculations of each Ra_{exo} method strongly contributed to the different estimates of the insulin sensitivity measures. We employed several methods to overcome this observed method dependence in S_I estimates. An initial approach was to potentially assist with the structural identifiability of OMM and OMM*, by independently estimating the volume of distribution V. Then, I tried to improve the calculations of each method so that they approximated a similar Ra_{exo} profile. This was done by implementing more sophisticated approximations of the necessary time derivatives compared to the suggested finite difference method. Next we developed an iterative scheme whereby after the two-step process used to identify OMM and OMM* was applied, then the estimated Ra_{exo} was used in

the RM and RM* to re-estimate better reference parameters and so forth until convergence of the parameters was achieved.

6.6 Methods: Strategies to Alleviate the Method Dependence of S_I Estimates

Estimate V Independently

Identification of OMM and OMM* requires fixing values for V and V^*. To assist with the identifiability of OMM and OMM* I sought to estimate the volume of distribution independent of the model. There are published methods to estimate V during a glucose tolerance test [97–99]. These methods utilize the data from an intravenous infusion of a glucose isotope tracer and use the time course by which the specific activity (radioactive) or the enrichment (stable) of the tracer reach steady state to estimate V. I attempted to apply several of these methods to our data set but the results were inconclusive. This was mostly due to not having enough data to identify the model equations. These studies had blood sampled at 20 or 30 min intervals starting at the beginning of the infusion through steady state. In this OGTT protocol, blood was only sampled 4 times in the 30 minutes before ingestion of the test drink. Therefore, I concluded there was not enough data to successfully implement these methods to obtain a model independent estimate of V.

Improved TTR Derivatives

A possible major factor in errors associated with computing Steele's total Ra and the Ra_{exo} methods may come in the approximations of the TTR derivatives. Our initial implementations involved approximating all of the derivatives using finite difference (see Eq. 6.11). This constrained us to the blood sample times, which are non-uniform and have larger time intervals towards the end of the protocol. To mitigate some of these errors in the calculations, I implemented two quick methods for approximating the necessary time derivatives: regularization methods and polynomial interpolation.

Regularization

The use of nonparametric methods based on regularization and Bayesian estimation helps to address measurement errors in the glucose and tracer data [100]. All the necessary data was smoothed and the 1st time derivative was computed for tracer I, II and the ratio (tracer II)/(tracer I). The WinSmoother package is a MATLAB compatible software that takes in the raw data with corresponding sample times, assumptions about the measurement error, the initial condition and the desired penalty corresponding to the regularization parameter. For glucose, measurement error was assumed to be CV = 2%. Regularization parameter penalty function of order 2 for smoothing and 1 for 1st time derivative. For both the tracers and their ratios, the measurement error is assumed to be constant but unknown. The chosen time step was set to 5 min for all. The outputs are the smoothed interpolated data or the approximated derivatives at every 5 min [101]. These were then used in the Ra_{exo} calculations.

Polynomial Interpolation

The derivatives of polynomial interpolates can be easily taken using the chain rule. To capitalize on this simplicity, piecewise cubic Hermite interpolating polynomials were used to interpolate the glucose concentrations, tracer I and tracer II amounts. The derivatives of tracer I and tracer II were computed as the derivative of their respective interpolating polynomials. These were then used in the calculations of total Ra and the Ra_{exo} methods. The polynomials were created using **pchip** in MATLAB.

Iterative Scheme

As shown and discussed in the previous sections, a poor estimate of Ra_{exo} can lead to unreliable estimates of key reference parameters needed to identify the OMM and the OMM*. The goal of this approach is to iteratively estimate a better Ra_{exo} that then is used to estimate better reference parameters, specifically S_G^{ref}, S_G^{*ref}, V^{ref} and V^{*ref}. The process

begins the same way we identify the OMM and OMM*. Once Ra_{exo} is estimated given the fixed reference parameters, it is then cycled back to be used in RM and RM* to re-estimate the desired reference parameters. This process of iteratively estimating each set of the model parameters is continued until convergence is achieved. Once convergence of the parameter set is achieved for each Ra_{exo} method, the converged parameter sets can be compared across Ra_{exo} methods.

This iterative approach creates a sequence of parameter estimates initialized with each Ra_{exo} method. This can be used to identify possible convergence of the parameter estimates. Define $\vec{\boldsymbol{\theta}}$ to be the parameter set of OMM and OMM* with length J and $\vec{\boldsymbol{\epsilon}} > \vec{\mathbf{0}}$ also length J. Then θ_n^j is the nth element in the sequence of parameter θ_j. Convergence of θ_n^j was defined as

$$|\theta_m^j - \theta_n^j| < \epsilon^j \tag{6.38}$$

for $\epsilon^j > 0$ and for some $m > M$ and $n > N$. To further assist with convergence and reduce the possible number of local minima, the set of time break points was reduced to 0, 30, 60, 90, 120, 180, and 360 minutes. Additionally, the upper and lower bounds for each parameter were narrowed to leverage published results in adolescents [2].

6.7 Results: Strategies to Alleviate the Method Dependence of S_I Estimates

Regularization

The approximations of Steele's total Ra, Ra_{exo} and corresponding Ra_{endo} estimates using the smoothed data and regularized TTR derivatives are presented here for 2 of the 3 participants previously discussed (Figure 6.17 and Figure 6.18). Figure 6.17(b) illustrates that the smoothed data did not make all of the approximations equal each other for Subject 10. This method worked better for Subject 12 (Figure 6.18(b)) as there was less variability across methods for this participant but initial calculations were similar to start with.

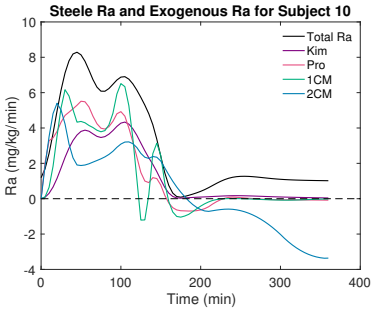

(a) Steele's Ra and Ra_{exo}

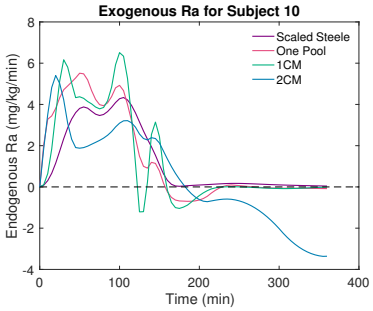

(b) Ra_{exo}

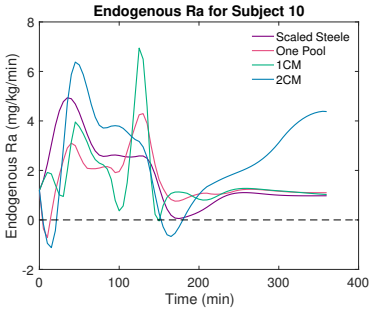

(c) Ra_{endo}

Figure 6.17: Steele's total, exogenous, and endogenous Ra for Subject 10 computed using regularization method.

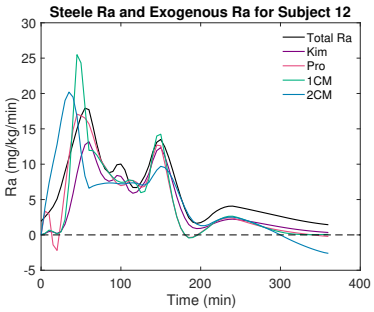

(a) Steele's Ra and Ra_{exo}

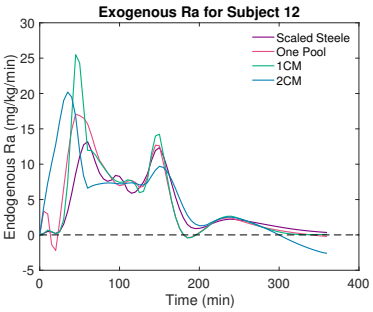

(b) Ra_{exo}

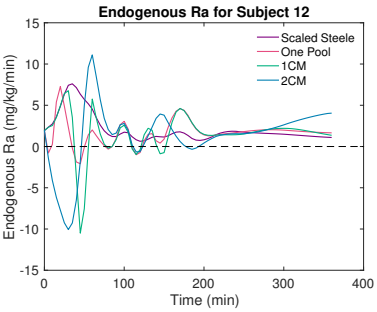

(c) Ra_{endo}

Figure 6.18: Steele's total, exogenous, and endogenous Ra for Subject 12 computed using regularization method.

Polynomial Interpolation

Calculations of total Ra and each Ra_{exo} method computed using interpolating polynomials evaluated at every 5 minutes for Subject 10 and Subject 12 are shown in Figure 6.19 and Figure 6.20. The One Pool, 1CM and 2CM Ra_{exo} methods predicted very similar approximations with the 1CM and the 2CM producing nearly identical estimates for both representative subjects. The Scaled Steele method was still distinctly different compared to the other approximations during the first 90 minutes for Subject 10 but was less so for Subject 12. Similarly, the Ra_{exo} approximations for Subject 12 had less variability but their

initial estimates were similar to begin with.

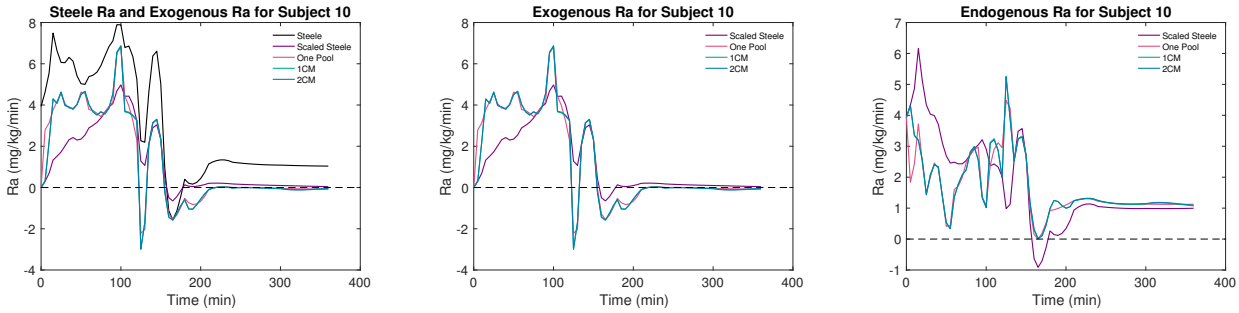

(a) Steele's Ra and Ra_{exo} (b) Ra_{exo} (c) Ra_{endo}

Figure 6.19: The total, exogenous, and endogenous Ra for Subject 10 computed using interpolating polynomials.

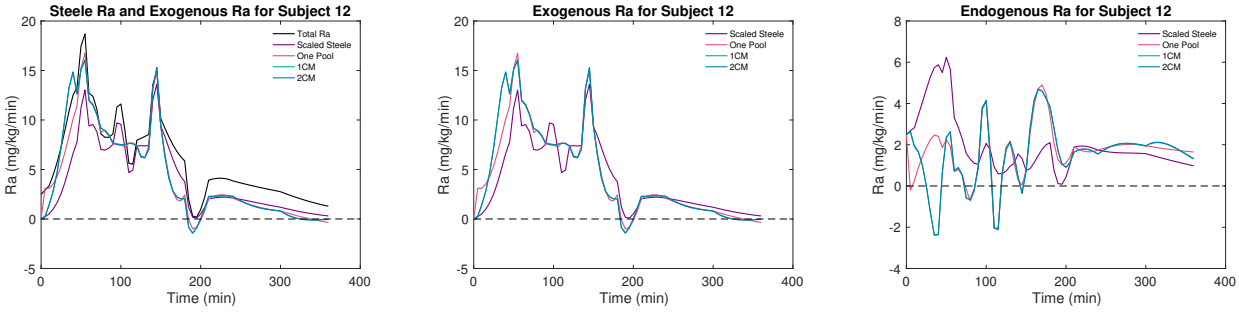

(a) Steele's Ra and Ra_{exo} (b) Ra_{exo} (c) Ra_{endo}

Figure 6.20: The total, exogenous, and endogenous Ra for Subject 12 computed using interpolating polynomials.

The reduction in the variation between Ra_{exo} approximations across methods suggested a potential reduction in the variance of the insulin sensitivity measures. Therefore, we ran RM/RM* and OMM/OMM* initialized with these polynomial Ra_{exo} approximations and report the resulting estimates of S_I, S_I^*, and S_I^{Dyn} for each Ra_{exo} method for all participants (Table 6.12, Table 6.13, Table 6.14). For implementation in to the reference models, Ra_{exo} estimated at the blood sample times were used instead of the estimate at every 5 minutes.

Table 6.12: The estimates of S_I, 10^{-4} for each Ra_{exo} method computed with interpolating polynomials for all participants (n = 9).

Participant	Scaled Steele	One Pool	1CM	2CM	Mean ± SD
10	2.76	3.46	3.45	2.64	3.08 ± 0.44
12	3.30	9.88	2.04	2.36	4.39 ± 3.70
15	7.97	2.08	8.80	4.68	5.88 ± 3.10
29	3.30	2.34	2.60	3.31	2.89 ± 0.50
33	2.90	2.36	2.29	2.64	2.55 ± 0.28
43	7.49	4.05	5.41	36.04	13.25 ± 15.26
44	26.52	21.07	14.88	6.77	17.31 ± 8.48
66	57.81	5.24	21.09	3.27	21.85± 25.27
67	1.11	0.98	0.64	1.10	0.96 ± 0.22

Table 6.13: The estimates of S_I^*, 10^{-4} for each Ra_{exo} method computed with interpolating polynomials for all participants (n = 9).

Participant	Scaled Steele	One Pool	1CM	2CM	Mean ± SD
10	9.11	3.52	4.49	1.58	4.67 ± 3.19
12	5.21	2.59	4.08	3.49	3.84 ± 1.10
15	219.43	9.26	146.06	143.54	129.58 ± 87.59
29	11.17	4.39	2.91	0.38	4.71 ± 4.61
33	5.70	3.05	3.12	3.64	3.88 ± 1.24
43	8.65	0.079	2.82	155.13	41.67 ± 75.72
44	50.11	42.26	32.61	22.88	36.97 ± 11.81
66	2.40	3.74	0.60	1.21	1.99 ± 1.39
67	1.71	0.046	0.048	0.046	0.5 ± 0.83

There was a reduction in the variability of S_I, S_I^*, and S_I^{Dyn} estimates across Ra_{exo} methods compared to their values computed with the initial Ra_{exo} calculations (Table 6.3 and Table 6.4). The CV was 53.51 ± 42.18%, 84.2 ± 59.28%, and 25.91 ± 10.9% for estimates of S_I, S_I^*, and S_I^{Dyn}, respectively. This decreased variability was significant for estimates of S_I (p = 0.029) and S_I^{Dyn} (p = 0.003) but not for S_I^* estimates (p = 0.39). The correlations of the insulin sensitivity indices for each Ra_{exo} method were computed and similarly resulted in low correlations between estimates of S_I and S_I^* (not shown). The correlation between the Scaled Steele and 1CM estimates of S_I and S_I^* were the only significant correlations at

Table 6.14: The estimates of S_I^{Dyn}, 10^{-5} for each Ra_{exo} method computed with interpolating polynomials for all participants(n = 9).

Participant	Scaled Steele	One Pool	1CM	2CM	Mean ± SD
10	6.18	3.91	3.96	4.79	4.71 ± 1.06
12	16.08	5.11	10.30	9.14	10.16 ± 4.53
15	5.97	8.36	5.12	6.13	6.40 ± 1.38
29	6.61	13.40	12.06	5.74	9.45 ± 3.84
33	7.35	11.52	11.67	10.17	10.18 ± 2
43	15.21	20.75	17.54	9.51	15.75 ± 4.74
44	1.07	0.84	0.94	0.85	0.92 ± 0.11
66	2.31	3.72	2.56	3.96	3.13 ± 0.82
67	5.73	5.08	3.87	4.58	4.81 ± 0.79

r = 0.95 (p < 0.001) and r = 0.99 (p < 0.001), respectively. There were more significant correlations among the estimates S_I^{Dyn} computed with each Ra_{exo} method (Table 6.15).

Table 6.15: The correlations of S_I^{Dyn} estimates across Ra_{exo} methods that were computed using interpolating polynomials.

Method	Scaled Steele	One Pool	1CM	2CM
Scaled Steele	1	0.58	0.79*	0.82**
One Pool	0.58	1	0.92**	0.69*
1CM	0.79*	0.92**	1	0.84**
2CM	0.82**	0.69	0.84	1

$*p < 0.05$, $**p < 0.01$

Iterative Scheme

We considered the iterative scheme with and without the specific α_3 constraint applied to $Ra_{exo}(\boldsymbol{\alpha}, t)$ and decided to focus on the constrained scheme because it often required fewer iterations to converge. In addition, the unconstrained scheme more consistently led to parameters converging to different values and S_I^* was estimated to be larger than S_I more often (not shown). Presented here are the results for the iterative scheme applied to Subject 10.

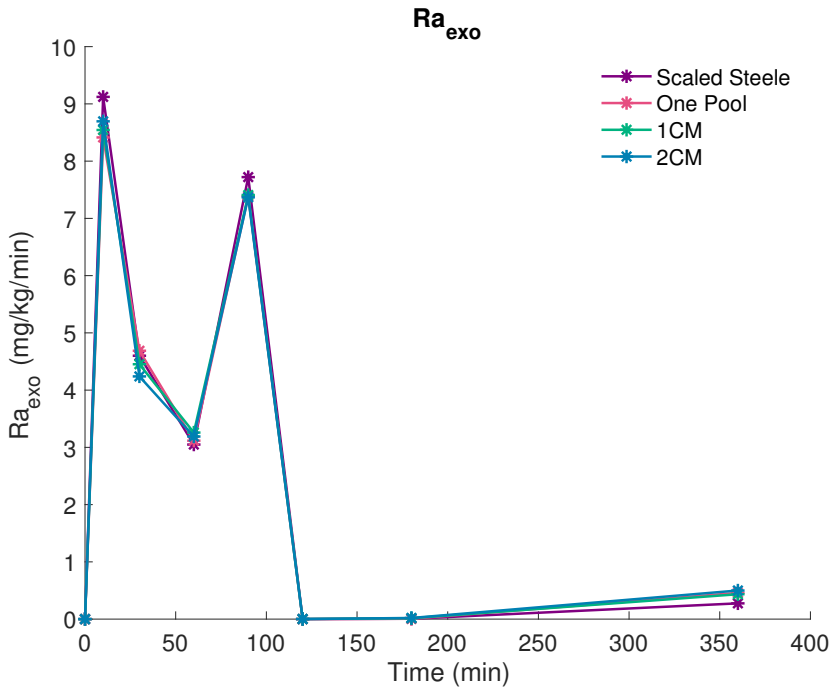

Figure 6.21: The estimated OMM/OMM* $Ra_{exo}(\boldsymbol{\alpha}, t)$ initialized with each Ra_{exo} method after 200 iterations for Subject 10.

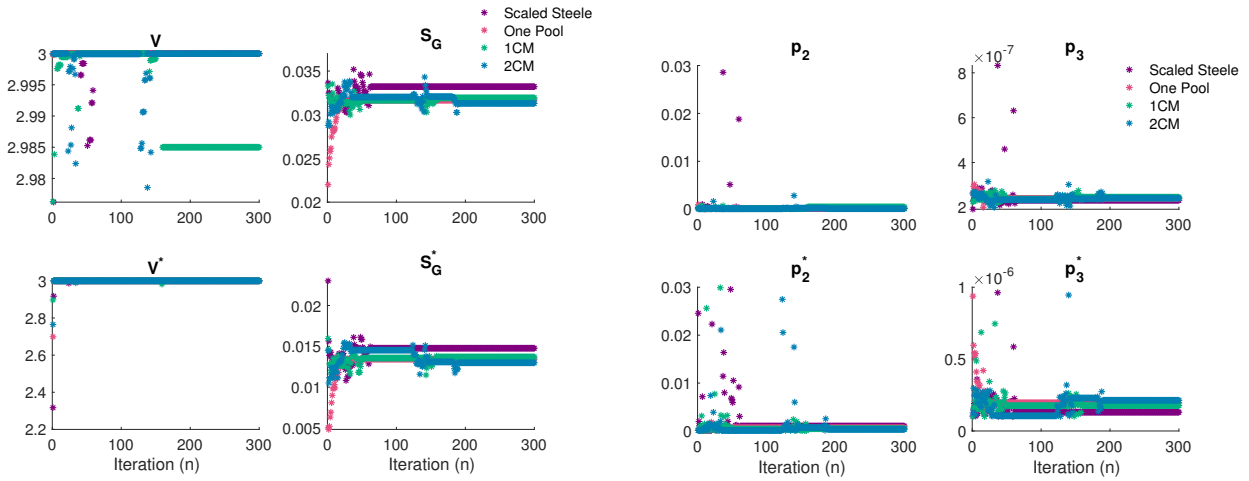

(a) V, V^*, S_G, and S_G^*

(b) p_2, p_2^*, p_3 and p_3^*

Figure 6.22: The estimates of the OMM and OMM* parameters at each iteration for Subject 10.

The iterative scheme initialized with each Ra_{exo} method converged to virtually the same OMM estimated $Ra_{exo}(\boldsymbol{\alpha}, t)$ after 300 iterations (Figure 6.21). This allowed for estimates of

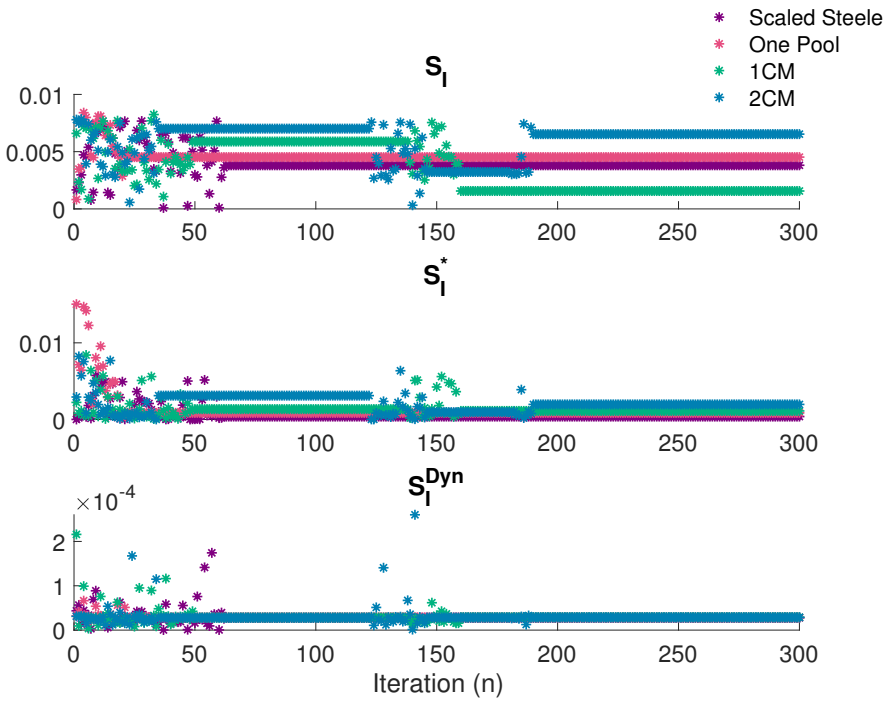

Figure 6.23: The estimates of S_I , S_I^* and S_I^{Dyn} initialized with each Ra_{exo} method after 200 iterations for Subject 10.

S_G, S_G^*, V, and V^* to converge to similar values with minimal variance across methods. The CV was just 2.60% and 5.53% for S_G and S_G^*, respectively, highlighting the low variability of estimates between Ra_{exo} methods (Table 6.16). The iterative method converged to 3 dl/kg for both V and V^*. The converged S_I^{Dyn} estimates were very similar for each Ra_{exo} with a CV = 1.98%. In contrast,, the converged estimates of S_I and S_I^* had high variability across Ra_{exo} methods. The CV of converged estimates was 49.89% and 61.22% for S_I and S_I^*, respectively (Table 6.17).

6.8 Discussion: Strategies to Alleviate the Method Dependence of S_I Estimates

After identifying method dependence in estimates of insulin sensitivity measures, several efforts were implemented to correct for this dependence, specifically, better approximations of the necessary time derivatives in the Ra_{exo} calculations and an iterative scheme approach.

Table 6.16: Final iterative scheme estimates of S_G, S_G^*, V and V^* for each Ra_{exo} method for Subject 10.

Method	S_G, 10^{-2}	S_G^*, 10^{-2}	V	V^*
Scaled Steele	3.32	1.48	3	3
One Pool	3.17	1.34	3	3
1CM	3.19	1.37	2.99	3
2CM	3.13	1.30	3	3
Mean ± SD	3.20 ± 0.083	1.37 ± 0.08	2.996 ± 0.0075	3 ± 0.004

Table 6.17: Final iterative scheme estimates of S_I, S_I^*, and S_I^{Dyn} for each Ra_{exo} method for Subject 10.

Method	S_I, 10^{-3}	S_I^*, 10^{-4}	S_I^{Dyn}, 10^{-5}
Scaled Steele	3.81	3.85	2.767
One Pool	4.52	8.64	2.86
1CM	1.56	11.17	2.89
2CM	6.53	19.69	2.88
Mean ± SD	4.11 ± 2.05	10.84 ± 6.64	2.85 ± 0.056

The iterative scheme proved to be the best method for mitigating the observed method dependence of S_I estimates as the methods converged to virtually the same OMM estimated $Ra_{exo}(\boldsymbol{\alpha}, t)$ independent of the initial reference Ra_{exo} method chosen. Convergence to virtually the same $Ra_{exo}(\boldsymbol{\alpha}, t)$ approximation meant the estimates of the parameters necessary to identify OMM and OMM* (V, V^*, S_G and S_G^*) were reliably estimated and properly fixed for each participant. Both S_I and S_I^* were estimated with high variability but this is likely a result of the difficulty of estimating these parameters in an IR population. As discussed in [25, 26, 80], there are known non-identifiable regions in the parameter space associated with the models of this framework where different combinations of S_I and p_2 elicit the same insulin response on some finite time interval and, therefore, these parameters may not always be estimated with high precision, especially in IR groups. The combination of the information present in S_I and p_2 give S_I^{Dyn}, which has proven to be estimated more robustly in comparison [26]. Estimates of S_I^{Dyn} may be more suitable for comparing the sensitivity

to insulin in this group of adolescent girls with obesity.

The regularization approach produced smoother approximations of the time derivatives needed to compute Steele's total Ra and each Ra_{exo} method. This resulted in approximations that were slightly more similar, however, there was still large variability in the Ra_{exo} profiles within the first approximate 90 minutes post drink ingestion. Therefore, these reference Ra_{exo} approximations were not used to identify OMM and OMM*. The smoothness of the interpolating polynomials allowed for the mitigation of the non-steady state errors inherent in approximations of the time derivatives. They were able to reduce the variability between Ra_{exo} calculations and this translated into a reduction of the variability of the insulin sensitivity measures. Unfortunately, the Ra_{exo} methods calculated with interpolating polynomials frequently produced estimates of S_I^* that were larger than S_I, which results in non-physiologically negative estimates of hepatic S_I. Additionally, there was still a high degree of variability among S_I and S_I^* estimates indicating dependence on the Ra_{exo} methods. The significant reduction in the variance of the S_I^{Dyn} estimates further illustrate that this measure can be estimated more robustly in this IR population, and, therefore, potentially a more reliable measure of metabolic health.

Researchers have developed alternate methods for estimation of Ra_{exo} that utilized techniques from a statistical framework. These methods incorporate maximum likelihood, regularization and Bayes modeling via an application of MCMC to the two compartment model discussed here [102, 103]. This study concluded that a dual tracer OGTT protocol was sufficient and that the addition of a third tracer was not necessary for reconstruction of the glucose fluxes [102]. Thus, the the dual tracer OGTT protocol done in this group of IR adolescent girls is adequate for reliable estimation of glucose fluxes and utilization in computing OMM-based estimates of insulin sensitivities.

Future work will involve estimating the volume of distribution independently of the model. The ideal data set for separate estimation of V would be to sample blood during the intravenous infusion phase before ingestion of the test drink. This way the time course to steady state in known. Additionally, S_I and S_I^* can be estimated with their precision using the Markov chain Monte Carlo (MCMC) approach described in Ch 5 applied to OMM and OMM*. The key parameters S_G, S_G^*, V, and V^* necessary to identify the models would be fixed to values determined from the iterative scheme.

The method dependence of the reference Ra_{exo} calculations was analyzed and a solution to the observed dependence on the estimates of the desired insulin sensitivity measures was proposed. The iterative scheme enabled estimation of the appropriate set of parameters necessary to identify OMM and OMM* and, thus, can be used to estimate whole body and hepatic measures of insulin sensitivity.

CHAPTER 7

QUANTIFYING HEPATIC S_I IN OBESE ADOLESCENT GIRLS

7.1 Introduction

Polycystic ovary syndrome (PCOS) is a metabolic disorder that affects roughly 12% of reproductive-aged women [56]. Insulin resistance (IR) is highly prevalent in women with PCOS and they have increased risk of developing type 2 diabetes, cardiovascular disease and nonalcoholic fatty liver disease (NAFLD) [43, 56, 104, 105]. This endocrine disorder begins at the onset of puberty. Thus, PCOS status is associated with decreased measures of total and tissue-specific insulin sensitivity (S_I) in girls [56], consistent with findings in women [105–107]. The PCOS phenotype in adult women has been characterized, however, there is recognition that the disorder may be different in adolescents partly due to a pubertal increase in IR [43,56]. In addition, improved understanding of PCOS in youth will provide insight into the pathogenesis and help to develop more targeted therapies for use in adolescents.

S_I measures how sensitive the body is to the insulin it produces and is an indicator of the metabolic state of an individual. There are multiple factors that play a role in how insulin helps to regulate blood glucose. Insulin simultaneously signals the liver to stop glucose production and switch to storing glucose for later use, suppresses lipolysis, the process whereby fat cells are broken down, and facilitates glucose disposal into other peripheral tissues such as muscle. When tissues begin to lose their sensitivity to insulin, more and more insulin is required to attain the same physiologic effect. This reduction in sensitivity to insulin can vary across tissues. The multi-phase hyperinsulinemic euglycemic (HE) clamp is non-physiological and labor intensive but it is the gold standard for quantifying both whole body and tissue specific S_I. The procedure involves maintaining elevated insulin concentrations with a multi-phase infusion of insulin to quantify adipose, hepatic and muscle S_I as

different insulin infusion rates signal different tissues. Glucose is infused at a variable rate to maintain blood glucose levels at baseline and the glucose infusion rate (GIR) is computed based on steady-state measurements during the final 20 to 30 minutes of each high-dose insulin phase [43, 108]. To quantify hepatic S_I under a more physiological setting, oral glucose tolerance test (OGTT)-based measures have been applied in a similar group of adolescent girls with obesity but they were not successfully validated against the HE clamp [64].

We seek to obtain alternate measures of tissue-specific S_I using data from an OGTT with stable isotope glucose tracers. The addition of the glucose tracers will allow us to track the various sources of glucose during the OGTT. The Production and Disposal Oral Minimal Model (OMM^{PD}), previously introduced in Ch 2, utilizes such data and enables simultaneous quantification of both hepatic and peripheral sensitivity indices. It combines a model of endogenous glucose production with the classical Oral Minimal Model framework [24].

During an OGTT with two stable isotope tracers, fast changes in relative enrichments of the isotopes due to non-steady state behavior may introduce error into the model. This can be corrected by using a third tracer with the infusion rate varied to mimic the expected rate of appearance of exogenous glucose while another tracer is intravenously infused to mimic endogenous glucose suppression dynamics [94]. However, appropriate application of the triple tracer method requires assumptions about endogenous glucose suppression dynamics that, if inaccurate, may introduce unknown error into the protocol. We discussed methods for overcoming non-steady state errors to enable reliable quantification of insulin sensitivity measures using a dual tracer protocol in an IR cohort of obese adolescent girls in Ch 6. Here, we implement the results of the iterative scheme for the application of OMM^{PD} in the same cohort.

7.2 Materials and Methods

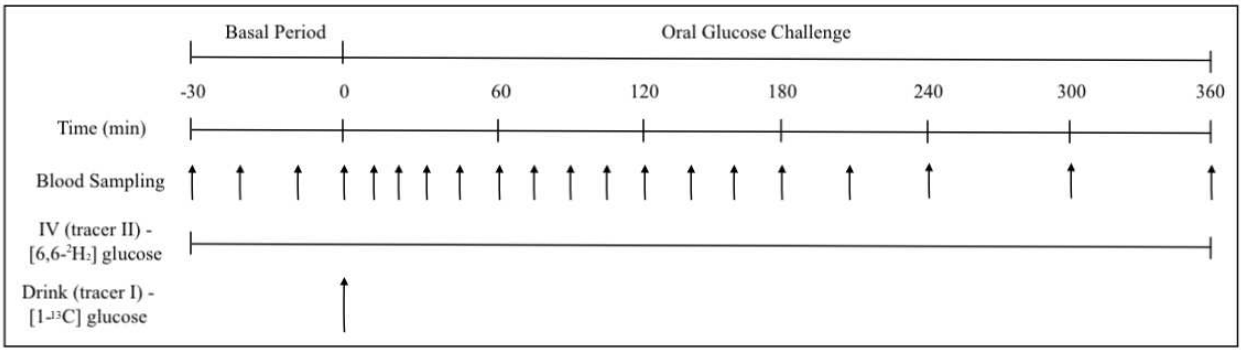

Figure 7.1: OGTT protocol with two stable isotope tracers showing blood sampling times and duration

Participants and Protocol

This is a continued analysis of the 9 participants described in the Ch 6. In brief, a group of overweight and obese adolescent girls (BMI $\geq$ 90th percentile for age and sex) adolescent (Tanner Stage 5) girls underwent a frequently sampled 6-hour OGTT with two stable isotope glucose tracers protocol. The detailed description of this dual tracer OGTT protocol can be found in Chapter 3. In summary, the protocol began by collecting baseline blood samples then a bolus of 4.5 mg/kg [6, 6-$^2H_2$] glucose (tracer II) was administered intravenously. Then [6, 6-$^2H_2$] glucose was infused at a constant rate of 0.04 mg/kg/min throughout the protocol. At time 0, participants consumed a drink containing 75 g of glucose plus an additional 40 mg/kg of [1-^{13}C] glucose (tracer I). Blood was sampled at -30,-20,-10, 0, 10, 20, 30, 45, 60, 75, 90, 105, 120, 135, 150, 180, 210, 240, 300 and 360 minutes following ingestion of the drink (Figure 7.1) for glucose (G) and insulin concentrations and tracer amounts. One representative participant is included in the following analysis.

The tracer data was corrected for background enrichments and glucose recycling. Details for specific tracer correction methods are in Ch 3. Exogenous glucose (G_{exo}) was computed using total glucose as

$$G_{exo} = G^* \cdot \left[1 + \frac{1}{z_{meal}}\right] \tag{7.1}$$

where G^* is the [1-^{13}C] labeled glucose from the test drink computed as

$$G^* = G \cdot \text{tracer I TTR in plasma}$$

where G is total glucose and z_{meal} is the TTR of the test drink. Endogenous glucose (G_{end}) is computed as

$$G_{end} = G - G_{exo} - G_2 \tag{7.2}$$

where G_2 is the amount of [6, 6-$^2H_2$] computed as

$$G_2 = G \cdot \text{tracer II TTR in plasma}$$

The Production and Disposal Oral Minimal Model

The Production and Disposal Oral Minimal Model (OMM^{PD}), previously described in Chapter 2, combines a model of endogenous glucose production (EGP) and the OMM to reliably estimate hepatic and peripheral insulin sensitivity, S_I^P and S_I^D, respectively, simultaneously from an oral or meal protocol. This model was shown to outperform the labeled oral minimal model where the disposal insulin sensitivity (S_I^D) was estimated to be higher than total whole body S_I in 19 % of the adult participants [21]. This model was validated in healthy adults and adults with prediabetes against the original EGP model, introduced in Ch 2 [22] and the triple-tracer protocol where the EGP is virtually known. The system of differential equations representing OMM^{PD} is below.

$$\begin{cases} \dot{G}(t) = \frac{\text{EGP}(t)+F+Ra_{exo}(\boldsymbol{\alpha},t)-R_d(t)}{V}, & G(0) = G_b \\ \dot{G}_{exo}(t) = \frac{Ra_{exo}(\boldsymbol{\alpha},t)-R_{d\,exo}(t)}{V}, & G_{exo}(0) = 0 \\ \dot{G}_{end}(t) = \frac{\text{EGP}(t)-R_{d\,end}(t)}{V}, & G_{end}(0) = G_{end\,b} \end{cases} \tag{7.3}$$

where G, G_{exo} and G_{end} are total, exogenous and endogenous glucose concentrations, $EGP(t)$ is endogenous glucose production (Eq. 7.6), F is the rate of infusion of tracer II, $Ra_{exo}(\boldsymbol{\alpha}, t)$ is the rate of appearance of exogenous glucose (Eq. 7.4) and R_d is the rate of disappearance of glucose (Eq. 7.5).

$$Ra_{exo}(\boldsymbol{\alpha}, t) = \begin{cases} \alpha_{i-1} + \frac{\alpha_i - \alpha_{i-1}}{t_i - t_{i-1}}(t - t_{i-1}) & \text{per } t_{i-1} \le t \le t_i \, i = 1, \cdots, n \\ 0 & \text{otherwise} \end{cases} \tag{7.4}$$

have unknown amplitudes $\boldsymbol{\alpha} = [\alpha_0, \cdots, \alpha_n]^T$ and known time breakpoints t_i.

$$\begin{cases} R_d(t) = V \cdot [S_G^D + X^D(t)] \cdot G(t) \\ R_{d\,exo}(t) = V \cdot [S_G^D + X^D(t)] \cdot G_{exo}(t) \\ R_{d\,end}(t) = V \cdot [S_G^D + X^D(t)] \cdot G_{end}(t) \\ \dot{X}^D(t) = -k_1^D \cdot [X^D(t) - k_2^D \cdot (I(t) - I_b)], \quad X^D(0) = 0 \end{cases} \tag{7.5}$$

where D refers to glucose disposal and X^D is the insulin action on glucose disposal.

$$\begin{cases} \mathrm{EGP}(t) = \mathrm{EGP}_b - k_G \cdot [G(t) - G_b] - X^P(t) - X^{Der}(t), & \mathrm{EGP}(0) = \mathrm{EGP}_b \\ \dot{X}^P(t) = -k_1^P \cdot [X^P(t) - X_1(t)], & X^P(0) = 0 \\ \dot{X}_1(t) = -k_1^P \cdot [X_1(t) - k_2^P \cdot (I(t) - I_b)], & X_1(0) = 0 \end{cases} \tag{7.6}$$

where P refers to glucose production, X^P is hepatic insulin action, X^1 is the additional delay in hepatic insulin action, k_G, k_1^P and k_2^P are rate parameters,

$$X^{Der}(t) = \begin{cases} k_{GR} \cdot \frac{dG(t)}{dt} & \frac{dG(t)}{dt} \ge 0 \\ 0 & \frac{dG(t)}{dt} < 0 \end{cases} \tag{7.7}$$

which is a surrogate for portal insulin and

$$\mathrm{EGP}_b = V \cdot S_G^D \cdot G_b - F \tag{7.8}$$

This model is identified on total, exogenous, and endogenous glucose data from an OGTT or MMT protocol with glucose tracers. The exogenous and endogenous glucose is computed using the tracer data and the following formulas:

$$G_{exo} = G^* \cdot \left[1 + \frac{1}{z_{meal}}\right] \tag{7.9}$$

$$G_{end} = G - G_{exo} - G_2 \tag{7.10}$$

where G_2 is the amount of tracer II during the protocol and G^* is the amount of tracer I glucose coming from the drink or meal and z_{meal} is the TTR of the drink or meal. The WinSmoother software was used to estimate the glucose derivative present in the $X^{Der}(t)$ term [101]. It is estimated remotely prior to identification of OMM^{PD}.

The production (hepatic) and disposal (peripheral) insulin sensitivity indices, S_I^P and S_I^D and glucose effectiveness indices, GE^D and GE^D, are derived from steady state model equations (derivations in Appendix B).

$$S_I^P = \left.\frac{\partial EGP}{\partial I}\right|_{SS} \cdot \frac{1}{G_b} = \frac{k_2^P}{G_b} \tag{7.11}$$

$$S_I^D = \left.\frac{\partial^2 R_d}{\partial G\, \partial I}\right|_{SS} = k_2^D \cdot V \tag{7.12}$$

$$GE^P = \left.\frac{\partial EGP}{\partial G}\right|_{SS} = k_G + k_{GR} \cdot \frac{G_{max} - G_b}{AUC_G} \tag{7.13}$$

$$GE^D = \left.\frac{\partial R_d}{\partial G}\right|_{SS} = S_G^D \cdot V \tag{7.14}$$

Additional constraints for parameter estimation help with model identification.

$$\int_0^\infty Ra_{exo}(\boldsymbol{\alpha}, t)dt = \frac{D \cdot f}{BW} \tag{7.15}$$

where D is the dose, f is the fraction of glucose absorbed and BW is the body weight (kg). To individualize EGP_b estimation in a given subject, GE^D and S_G^D were decomposed into insulin-independent and insulin-dependent components:

$$GE^D = GEZI^D + S_I^D \cdot I_b \cdot V \tag{7.16}$$

$$S_G^D = \frac{GEZI^D}{V} + S_I^D \cdot I_b \tag{7.17}$$

where $GEZI^D$ is the disposal value of glucose effectiveness at zero insulin. $GEZI^D = 0.021 \pm 0.001$ and $GEZI^D = 0.017 \pm 0.001$ dl/kg/min in the healthy adult and prediabetes group, respectively [24].

Implementation

Similar to the OMM and OMM* previously described in Ch 2 and Ch 6, the OMM^{PD} is also structurally unidentifiable so a 2-step process is used to identify the model against the total, exogenous and endogenous glucose concentrations. First, the converged OMM Ra_{exo} estimate found in Ch 6 was used as a reference $Ra_{exo}(\boldsymbol{\alpha}, t)$ to estimate reference parameters. Then V was fixed and the remaining parameters were estimated. A constraint (Eq. 7.17) was applied to S_G^D to assist with model identifiability where $GEZI^D = 0.017$ was fixed to the value reported for the prediabetes group [24] as they displayed increased IR common in this population of adolescent girls with obesity. The full details of how the $Ra_{exo}(\boldsymbol{\alpha}, t)$ constraint (Eq. 7.15) is implemented can be found in Ch 6. The time breakpoints chosen here were 0, 10, 30, 60, 90, 120, 180, and 360 min.

7.3 Results

The total, exogenous and endogenous glucose and insulin concentrations for Subject 10 are shown in Figure 7.2. This individual's glucose remained elevated around 132 mg/dl for a prolonged duration until total glucose concentrations returned to baseline between 150 and 180 min. There was a biphasic insulin response as the initial insulin response was not sufficient to cause glucose to return to basal values. The higher second insulin peak pushed this person's glucose levels far below their baseline resulting in mild reactive hypoglycemia.

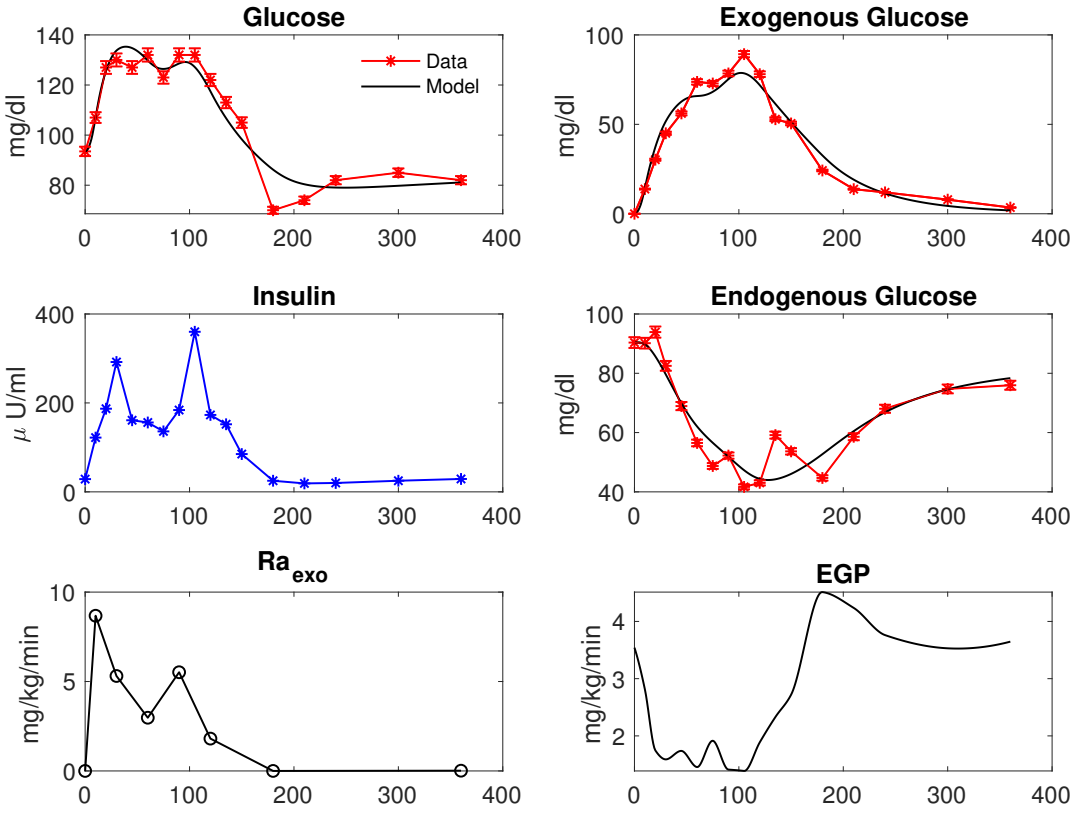

Figure 7.2: Total, exogenous and endogenous glucose with OMM^{PD} simulations, insulin concentrations, OMM^{PD} estimated $Ra_{exo}(\boldsymbol{\alpha}, t)$ and endogenous glucose production profile for Subject 10.

OMM^{PD} provided good fits to the data (Figure 7.2). Hepatic insulin sensitivity for this subject was estimated as $S_I^P = 2.84 \times 10^{-4}$ dl/kg/min per μU/ml. This accounted for approximately 53 % of total S_I. Peripheral S_I was $S_I^D = 2.49 \times 10^{-4}$ and total S_I, computed as the sum, was $S_I = 5.33 \times 10^{-4}$. The estimated endogenous glucose production profile reflects glucose suppression beginning immediately follow drink ingestion and returning to near baseline after approximately 3 hours.

7.4 Discussion

The method dependence of estimates of insulin sensitivity indices due to differences in the reference Ra_{exo} approximations have been addressed in Ch 6. This enabled us to move forward with the application of OMM^{PD} in this group of obese adolescent girls with and without PCOS. We were able to obtain plausible estimates of whole body and tissue-specific insulin sensitivity for this individual. Hepatic S_I, S_I^P, represented 53 % of total S_I which coincides with published results of OMM^{PD} applied in a prediabetes group [24].

The mass spectrometer analysis of the glucose tracer data is in progress for the full cohort discussed throughout this dissertation. Once the full data set is processed, this method to compute hepatic S_I from an OGTT is ready to be applied. This model-based method to quantify hepatic S_I during an OGTT allows the natural physiological dynamics to play a role in glucose disposal and insulin action. The suppression of endogenous glucose production is captured by the model and produces a measurable quantity of hepatic S_I.

Furthermore, studies that used multi-phase HE clamp to measure hepatic and peripheral S_I can be extended to include gut dynamics using these OGTT-based methods. This will yield a more complete picture of the metabolic phenotype of obese adolescent girls with and without PCOS. These measures can then be used to potentially investigate etiology of metabolic disorders and diseases in youth and evaluate the efficacy of specific therapies.

CHAPTER 8

CONCLUSIONS

The models of the Oral Minimal Model (OMM) framework have been successfully applied and validated in adults and adolescents with varying glucose tolerance [2, 20, 21, 24, 57, 62]. Not only are these models able to capture the dynamics of glucose and insulin after a meal, these model-based measures of S_I are also sensitive to group differences [58, 59]. Therefore, we sought to utilize this model-based approach to quantify whole body and tissue-specific insulin sensitivity (S_I). The glucose and insulin dynamics of adolescent girls differ greatly compared to their adult counterparts. Methods to evaluate measures of insulin sensitivity were developed in adult populations and cannot be directly applied to highly insulin resistant (IR) populations where the dynamics are different. Specifically, it is typical for this population to experience prolonged elevated glucose levels followed by a large decrease in glucose concentrations well below baseline, typically referred to as reactive hypoglycemia (RHG). Additionally, adolescents tend to produce considerably more insulin compared to adults [3, 4] and that has certain implications within this model framework. These differences coupled with the numerical identifiability issues associated with the OMM make application of this model framework more challenging for use in highly IR adolescent girls with obesity. Furthermore, our results show that the full glucose and insulin dynamics of a study population need to be considered when applying the OMM framework in youth and other populations with diverse metabolic phenotypes.

In our application of OMM to quantify S_I from shorter OGTT protocols, we compared the implementation of OMM identified on shorter OGTT durations of data to the full 6 hour protocol to determine protocol dependence on estimates of S_I. We found that in our IR cohort, the assumption of exponential decay in the $Ra_{exo}(\boldsymbol{\alpha}, t)$ was not an appropriate

assumption to account for the time course of glucose return to baseline. There was more variability in how participants returned to their baseline glucose concentrations in this group compared to published OGTT data in adults. There were frequent instances of RHG and second peaks in glucose and insulin concentrations before returning to basal values. This application of OMM in obese and overweight adolescent girls with and without polycystic ovary syndrome (PCOS) highlighted the challenges of applying simple minimal models in highly IR populations and provided insight into optimal protocol design for reliable estimation of S_I in this cohort.

The local sensitivity analysis (SA) of the OMM highlighted known structural and numerical indentifiablility issues associated with S_G and V as OMM was least sensitive to perturbations of these parameters. This suggested and then resulted in low precision of S_G estimates in one of the representative subjects when an uncertainty quantification of parameter estimates was performed. To overcome the problem of structural unidentifiability, OMM developers suggested the utilization of a reference model to estimate S_G and V given a reliable approximation of the rate of meal glucose appearance, Ra_{exo}. With S_G and V fixed to individual or population values, OMM can be identified on glucose and insulin concentrations during an OGTT. The sensitivity metric r_{f_i/θ_j} presented in Ch 5 was able to rank the parameters by their overall effect on the OMM glucose output but more work can be done here by focusing on the different phases of the OGTT protocol. For example, determine the ranking of parameters during phase after peak glucose concentration can detect which parameters are more important for model identification during the return to baseline phase of an OGTT. A global SA of the models of the OMM framework would be better equipped to manage this nonlinear system and rank the model parameters based off importance. Potentially, a global could identify important parameter subsets such as the set of α_i in $Ra_{exo}(\boldsymbol{\alpha}, t)$ the model is most sensitive to.

In order to estimate the parameters needed to apply OMM in this population, an appropriate approximation of Ra_{exo} is key. There have been multiple methods for computing Ra_{exo} using data from a dual tracer protocol. We compared the implementation of 4 published methods for computing Ra_{exo} and the dependence of estimates of S_I and peripheral S_I on these Ra_{exo} methods. We found that the methods had the most variability in approximately the first 90 minutes of the OGTT protocol, a result of the rapid change in tracer enrichments and the different ways the methods handle these non-steady state changes. We also found strong method dependence on the estimates of the desired insulin sensitivity indices. This is likely a result of errors in the tracer data that can propagate through the calculations of each method. When a poor approximation of Ra_{exo} is fed into OMM and OMM*, the model outputs and estimates of total and peripheral S_I are not reliable. Techniques to mitigate these types of errors included independent estimation of the volume of distribution, smoothing and more sophisticated computation of TTR derivatives via regularization methods and interpolating polynomials, and an iterative scheme. The iterative scheme was the most successful method in mitigating the established Ra_{exo} method dependence of S_I estimates. This process was able to converge to virtually the same OMM estimated $Ra_{exo}(\boldsymbol{\alpha}, t)$ from each initial reference model and thus enabled convergence of the key parameters necessary to use OMM in this cohort of adolescent girls with obesity.

After the iterative scheme was developed to cope with Ra_{exo} method dependence of S_I estimates, we were able to move forward with quantification of hepatic S_I in this group. This was done using the OMM^{PD} which enables simultaneous quantification of both hepatic and peripheral insulin sensitivities. OGTT or other meal tolerance tests provide a more physiologically sound method of computing insulin sensitivity measures compare to the HE clamp as they encapsulate the glucose and insulin dynamics undergone during ingestion. The application of OMM^{PD} to the full data set will help to further characterize the metabolic phenotype of obese adolescent girls with and without PCOS. Additionally, validation of

OMM^{PD} will enable replication of studies where a multi-phase HE clamp was used to assess tissue-specific S_I.

The application of the OMM framework in populations with dysglycemia would help with assessment of total and tissue-specific insulin sensitivity measures where the hyperinsuinemic euglycemic (HE) clamp protocol may be ill-advised or difficult to implement. However, as shown in this analysis, certain features of of dysglycemia such as RHG or very high insulin secretion rates can make application of OMM difficult due to model identifiability concerns. In the RHG phase, glucose concentrations may fall much as 40 mg/dl below baseline, but an assumed glucose baseline value, G_b, is built into the model equations. Similarly, I_b is a fixed parameter that assumes an equilibrium to return to. This is a potential limitation of applying OMM in populations were glucose and insulin steady states are not well maintained, such as individuals with type 1 diabetes and cystic fibrosis. This model framework may need further adaptions to be able to quantify S_I in people with these metabolic diseases.

A major motivating factor of this research is to help pediatric endocrinologists learn how the development of PCOS during adolescence affects the metabolism. It has been established that PCOS increases risk and prevalence of hepatic steatosis (HS), the build up of fat in the liver, in adolescent girls with obesity and is associated with decreased hepatic S_I as assessed by a multi-stage HE clamp [43]. Meal-based measures of hepatic S_I are more physiological and can be indicative of the presence of HS. Validation of the OMM^{PD} could lead to a less invasive method of assessing and diagnosis HS. Future work will focus on application of OMM^{PD} to a larger cohort of obese adolescent girls with and without obesity to assess HS and gain insight into the etiology of HS in this population.

The mathematical techniques and analysis performed here have enabled the adaptation of this model framework to a different population. The qualitative exploration of the model

structure helped to identify areas of difficulty for application in a population with dysglycemia.

REFERENCES CITED

[1] V. Marks. Metabolism and maintenance of blood glucose level. In Benjamin Caballero, editor, *Encyclopedia of Human Nutrition*, volume 2, pages 1–14. Elsevier Ltd, Radarweg 29, PO Box 211, 1000 AE Amsterdam, The Netherlands, 3 edition, 2013.

[2] Agneta L. Sunehag, Chiara Dalla Man, Gianna Toffolo, Morey W. Haymond, Dennis M. Bier, and Claudio Cobelli. β-cell function and insulin sensitivity in adolescents from an ogtt. *Obesity*, 17(2):233–239, 2009.

[3] RISE Consortium. Metabolic contrasts between youth and adults with impaired glucose tolerance or recently diagnosed type 2 diabetes: Ii. observations using the oral glucose tolerance test. *Diabetes Care*, 41(8):1707–1716, 2018.

[4] RISE Consortium. Metabolic contrasts between youth and adults with impaired glucose tolerance or recently diagnosed type 2 diabetes: I. observations using the hyperglycemic clamp. *Diabetes Care*, 41(8):1696, 2018.

[5] Lindsey George, Fida Bacha, SoJung Lee, Hala Tfayli, Elisa Andreatta, and Silva Arslanian. Surrogate estimates of insulin sensitivity in obese youth along the spectrum of glucose tolerance from normal to prediabetes to diabetes. *The Journal of Clinical Endocrinology & Metabolism*, 96(7):2136–2145, 07 2011.

[6] Antoinette Moran, Jr. David R. Jacobs, Julia Steinberger, Ching-Ping Hong, Ronald Prineas, Russel Luepker, and Alan R. Sinaiko. Insulin resistance during puberty: results from clamp studies in 357 children. *Diabetes*, 48(10):2039–2044, 1999.

[7] Ricardo Azziz. Evaluation for insulin resistance and comorbidities related to insulin resistance in polycystic ovary syndrome. In Evanthia Diamanti-Kandarakis, John E. Nestler, Dimitrios Panidis, and Renato Pasquali, editors, *Insulin Resistance and Polycystic Ovarian Syndrome: Pathogenesis, Evaluation and Treatment*, pages 1–14. Humana Press, 99 Riverview Drive, Suite 208, Totowa, New Jersey 07512, 2007.

[8] R A DeFronzo, J D Tobin, and R Andres. Glucose clamp technique: a method for quantifying insulin secretion and resistance. *American Journal of Physiology-Endocrinology and Metabolism*, 237(3):E214, 1979.

[9] DR Matthews, JP Hosker, A Rudenski, and RC Turner. Homeostatic model assessment (homa). measurement of insulin resistance and beta-cell deficit in man. *Diabetologia*, 28:412–419, 1985.

[10] M Matsuda and R A DeFronzo. Insulin sensitivity indices obtained from oral glucose tolerance testing: comparison with the euglycemic insulin clamp. *Diabetes Care*, 22(9):1462–1470, 1999.

[11] O. Vahidi, K. E. Kwok, R. B. Gopaluni, and F. K. Knop. A comprehensive compartmental model of blood glucose regulation for healthy and type 2 diabetic subjects. *Medical & Biological Engineering & Computing*, 54:1383 – 1398, 2016.

[12] Joon Ha, Leslie S. Satin, and Arthur S. Sherman. A mathematical model of the pathogenesis, prevention, and reversal of type 2 diabetes. *Endocrinology*, 157:625 – 635, 2015.

[13] Richard N Bergman, Ziya Y Ider, Charles R. Bowden, and Claudio Cobelli. Quantitative estimation of insulin sensitivity. *American Journal of Physiology-Endocrinology and Metabolism*, 236(6):E667–E677, 1979.

[14] Richard N. Bergman, Lawrence S. Phillips, and Claudio Cobelli. Physiologic evaluation of factors controlling glucose tolerance in man: Measurement of insulin sensitivity and β-cell glucose sensitivity from the response to intravenous glucose. *Journal of Clinical Investigation*, 68:1456– 1467, 1981.

[15] Richard N. Bergman, Diane T. Finegood, and Marilyn Ader. Assessment of insulin sensitivity *in vivo*. *Endocrine Reviews*, 6(1):45–86, 1985.

[16] C. Cobelli, G. Pacini, G. Toffolo, and L. Sacca. Estimation of insulin sensitivity and glucose clearance from minimal model: new insights from labeled ivgtt. *American Journal of Physiology-Endocrinology and Metabolism*, 250(5):E591–E598, 1986. PMID: 3518490.

[17] James C Beard, Richard N Bergman, W Kenneth Ward, and Daniel Porte. The insulin sensitivity index in nondiabetic man: correlation between clamp-derived and ivgtt-derived values. *Diabetes*, 35(3):362–369, 1986.

[18] Andrea Caumo, Richard N Bergman, and Claudio Cobelli. Insulin sensitivity from meal tolerance tests in normal subjects: a minimal model index. *The Journal of Clinical Endocrinology & Metabolism*, 85(11):4396–4402, 2000.

[19] Chiara Dalla Man, Andrea Caumo, and Claudio Cobelli. The oral glucose minimal model: Estimation of insulin sensitivity from a meal test. *IEEE Transactions on Biomedical Engineering*, 49.5:419–429, 2002.

[20] Chiara Dalla Man, Marco Campioni, Kenneth S. Polonsky, Rita Basu, Robert A. Rizza, Gianna Toffolo, and Claudio Cobelli. Two-hour seven-sample oral glucose tolerance test and meal protocol. *Diabetes*, 54(11):3265–3273, 2005.

[21] Chiara Dalla Man, Andrea Caumo, Rita Basu, Robert Rizza, Gianna Toffolo, and Claudio Cobelli. Measurement of selective effect of insulin on glucose disposal from labeled glucose oral test minimal model. *American Journal of Physiology - Endocrinology and Metabolism*, 289(5):E909–E914, 2005.

[22] Chiara Dalla Man, Gianna Toffolo, Rita Basu, Robert A. Rizza, and Claudio Cobelli. Use of labeled oral minimal model to measure hepatic insulin sensitivity. *American Journal of Physiology-Endocrinology and Metabolism*, 295(5):E1152–E1159, 2008.

[23] Chiara Dalla Man, Francesca Piccinini, Rita Basu, Ananda Basu, Robert A. Rizza, and Claudio Cobelli. Modeling hepatic insulin sensitivity during a meal: validation against the euglycemic hyperinsulinemic clamp. *American Journal of Physiology-Endocrinology and Metabolism*, 304(8):E819–E825, 2013.

[24] Roberto Visentin, Chiara Dalla Man, Rita Basu, Ananda Basu, Robert A. Rizza, and Claudio Cobelli. Hepatic insulin sensitivity in healthy and prediabetic subjects: from a dual- to a single-tracer oral minimal model. *American Journal of Physiology-Endocrinology and Metabolism*, 309(2):E161–E167, 2015.

[25] Gianluigi Pillonetto, Andrea Caumo, Giovanni Sparacino, and Claudio Cobelli. A new dynamic index of insulin sensitivity. *IEEE transactions on biomedical engineering*, 53(3):369–379, 2006.

[26] Gianluigi Pillonetto, Andrea Caumo, and Claudio Cobelli. Dynamic insulin sensitivity index: importance in diabetes. *American Journal of Physiology-Endocrinology and Metabolism*, 298(3):E440–E448, 2010.

[27] Andrea Saltelli, Ksenia Aleksankina, William Becker, Pamela Fennell, Federico Ferretti, Niels Holst, Sushan Li, and Qiongli Wu. Why so many published sensitivity analyses are false: A systematic review of sensitivity analysis practices. *Environmental Modeling & Software*, 114:29 – 39, 2019.

[28] Andrea Saltelli and Paola Annoni. How to avoid a perfunctory sensitivity analysis. *Environmental Modelling & Software*, 25(12):1508–1517, 2010.

[29] Roger Ghanem, David Higdon, and Houman Owhadi. Introduction to uncertainty quantification. In Roger Ghanem, David Higdon, and Houman Owhadi, editors, *Handbook of Uncertainty Quantification*, pages 3–6. Springer International Publishing, Cham, 2017.

[30] Ralph C Smith. *Uncertainty quantification: theory, implementation, and applications*, volume 12. Siam, 2013.

[31] Samuel A Schmitt. *Measuring uncertainty: An elementary introduction to Bayesian statistics*. Addison-Wesley, 1969.

[32] Vincent A. Mousseau and Brian J. Williams. Uncertainty quantification in a regulatory environment. In Roger Ghanem, David Higdon, and Houman Owhadi, editors, *Handbook of Uncertainty Quantification*, pages 1613–1648. Springer International Publishing, Cham, 2017.

[33] Andrew Gelman, John B Carlin, Hal S Stern, David B Dunson, Aki Vehtari, and Donald B Rubin. *Bayesian Data Analysis*. CRC press, 3 edition, 2014.

[34] Jeff Gill. *Bayesian methods: A social and behavioral sciences approach*, volume 20. CRC press, 2014.

[35] Antti Solonen, Heikki Haario, and Marko Laine. Statistical analysis in modeling.

[36] Don Van Ravenzwaaij, Pete Cassey, and Scott D Brown. A simple introduction to markov chain monte–carlo sampling. *Psychonomic bulletin & review*, 25(1):143–154, 2018.

[37] C. D. Gilker, G. R. Pesola, and DE Matthews. A mass spectrometric method for measuring glycerol levels and enrichments in plasma using 13c and 2h stable isotopic tracers. *Anal Biochem*, 205:172–178, 1992.

[38] B. C. Bergman, D. Howard, I. E. Schauer, D. M. Maahs, J. K. Snell-Bergeon, R. H. Eckel, L. Perreault, and M. Rewers. Features of hepatic and skeletal muscle insulin resistance unique to type 1 diabetes. *J Clin Endocrinol Metab*, 97:1663–1672, 2012.

[39] BC Bergman, D Howard, IE Schauer, DM Maahs, JK Snell-Bergeon, TW Clement, RH Eckel, L Perreault, and M Rewers. The importance of palmitoleic acid to adipocyte insulin resistance and whole-body insulin sensitivity in type 1 diabetes. *J Clin Endocrinol Metab*, 98:E40–50, 2013.

[40] Robert R. Wolfe and D.L. Chinkes. *Isotope tracers in metabolic research: principles and practice of kinetic analysis*. John Wiley & Sons, 2005.

[41] K. A. Lindquist, K Chow, A West, L Pyle, TS Isbell, M Cree-Green, and KJ Nadeau. The statstrip glucose monitor is suitable for use during hyperinsulinemic euglycemic clamps in a pediatric population. *Diabetes Technology & Therapeutics*, 2014.

[42] Claire Levy-Marchal, Silva Arslanian, Wayne Cutfield, Alan Sinaiko, Celine Druet, M Loredana Marcovecchio, and Francesco Chiarelli. Insulin resistance in children: consensus, perspective, and future directions. *The Journal of Clinical Endocrinology & Metabolism*, 95(12):5189–5198, 2010.

[43] Melanie Cree-Green, Bryan C Bergman, Gregory V Coe, Lindsey Newnes, Amy D Baumgartner, Samantha Bacon, Ann Sherzinger, Laura Pyle, and Kristen J Nadeau. Hepatic steatosis is common in adolescents with obesity and pcos and relates to de novo lipogenesis but not insulin resistance. *Obesity*, 24(11):2399–2406, 2016.

[44] Melanie Cree-Green, Abhinav Gupta, Gregory V Coe, Amy D Baumgartner, Laura Pyle, Jane EB Reusch, Mark S Brown, Bradley R Newcomer, and Kristen J Nadeau. Insulin resistance in type 2 diabetes youth relates to serum free fatty acids and muscle mitochondrial dysfunction. *Journal of diabetes and its complications*, 31(1):141–148, 2017.

[45] Melanie Cree-Green, Pattara Wiromrat, Jacob J Stuppy, Jessica Thurston, Bryan C Bergman, Amy D Baumgartner, Samantha Bacon, Ann Scherzinger, Laura Pyle, and Kristen J Nadeau. Youth with type 2 diabetes have hepatic, peripheral, and adipose insulin resistance. *American Journal of Physiology-Endocrinology and Metabolism*, 316(2):E186–E195, 2019.

[46] Kenneth C Copeland, Philip Zeitler, Mitchell Geffner, Cindy Guandalini, Janine Higgins, Kathryn Hirst, Francine R Kaufman, Barbara Linder, Santica Marcovina, Paul McGuigan, et al. Characteristics of adolescents and youth with recent-onset type 2 diabetes: the today cohort at baseline. *The Journal of Clinical Endocrinology & Metabolism*, 96(1):159–167, 2011.

[47] TODAY Study Group. A clinical trial to maintain glycemic control in youth with type 2 diabetes. *New England Journal of Medicine*, 366(24):2247–2256, 2012.

[48] Kara Mizokami-Stout, Melanie Cree-Green, and Kristen J. Nadeau. Insulin resistance in type 2 diabetic youth. *Current opinion in endocrinology, diabetes, and obesity*, 19(4):255–262, 2012.

[49] Robert P. Hoffman, Paolo Vicini, William I. Sivitz, and Claudio Cobelli. Pubertal adolescent male-female differences in insulin sensitivity and glucose effectiveness determined by the one compartment minimal model. *Pediatric Research*, 48(3):384–388, 2000.

[50] Robert P. Hoffman, Palo Vicini, and Claudio Cobelli. Comparison of insulin sensitivity and glucose effectiveness determined by the one- and two-compartment-labeled minimal model in late prepubertal children and early adolescents. *Metabolism - Clinical and Experimental*, 51(12):1582–1586, 2002.

[51] Kristen J. Nadeau, Phillip S. Zeitler, Timothy A. Bauer, Mark S. Brown, Jennifer L. Dorosz, Boris Draznin, Jane E. B. Reusch, and Judith G. Regensteiner. Insulin resistance in adolescents with type 2 diabetes is associated with impaired exercise capacity. *The Journal of Clinical Endocrinology & Metabolism*, 94(10):3687–3695, 2009.

[52] Kristen J. Nadeau, Judith G. Regensteiner, Timothy A. Bauer, Mark S. Brown, Jennifer L. Dorosz, Amber Hull, Phil Zeitler, Boris Draznin, and Jane E. B. Reusch. Insulin resistance in adolescents with type 1 diabetes and its relationship to cardiovascular function. *The Journal of Clinical Endocrinology & Metabolism*, 95(2):513–521, 2010.

[53] Tara M. Wallace, Jonathan C. Levy, and David R. Matthews. Use and abuse of homa modeling. *Diabetes Care*, 27(6):1487–1495, 2004.

[54] Arie Katz, Sridhar S. Nambi, Kieren Mather, Alain D. Baron, Dean A. Follmann, Gail Sullivan, and Michael J. Quon. Quantitative insulin sensitivity check index: A simple, accurate method for assessing insulin sensitivity in humans. *The Journal of Clinical Endocrinology & Metabolism*, 85(7):2402–2410, 2000.

[55] Muhammad A. Abdul-Ghani, Masafumi Matsuda, Bogdan Balas, and Ralph A. DeFronzo. Muscle and liver insulin resistance indexes derived from the oral glucose tolerance test. *Diabetes Care*, 30(1):89–94, 2007.

[56] Melanie Cree-Green, Ninghe Cai, Jessica E. Thurston, Gregory V. Coe, Lindsay Newnes, Yesenia Garcia-Reyes, Amy D. Baumgartner, Laura Pyle, and Kristen J. Nadeau. Using simple clinical measures to predict insulin resistance or hyperglycemia in girls with polycystic ovarian syndrome. *Pediatric Diabetes*, 19(8):1370–1378, 2018.

[57] Chiara Dalla Man, Andrea Caumo, Rita Basu, Robert Rizza, Gianna Toffolo, and Claudio Cobelli. Minimal model estimation of glucose absorption and insulin sensitivity from oral test: validation with a tracer method. *Endocrinology and Metabolism - American Journal of Physiology*, 287:637–643, 2004.

[58] Corey Rynders, Ju Weltman, Steven Malin, Boyi Jiang, Marc Breton, Eugene Barrett, and Arthur Weltman. Comparing simple insulin sensitivity indices to the oral minimal model postexercise. *Medicine and science in sports and exercise*, 48:66–72, 07 2015.

[59] S. Bordenave, F. Brandou, J. Manetta, C. Fdou, J. Mercier, and J.-F. Brun. Effects of acute exercise on insulin sensitivity, glucose effectiveness and disposition index in type 2 diabetic patients. *Diabetes & Metabolism*, 34(3):250 – 257, 2008.

[60] Catrina Cropano, Nicola Santoro, Leif Groop, Chiara Dalla Man, Claudio Cobelli, Alfonso Galderisi, Romy Kursawe, Bridget Pierpont, Martina Goffredo, and Sonia Caprio. The rs7903146 variant in the tcf7l2 gene increases the risk of prediabetes/-type 2 diabetes in obese adolescents by impairing β-cell function and hepatic insulin sensitivity. *Diabetes Care*, 40(8):1082–1089, 2017.

[61] Anna MG Cali, Chiara Dalla Man, Claudio Cobelli, James Dziura, Aisha Seyal, Melissa Shaw, Karin Allen, Shu Chen, and Sonia Caprio. Primary defects in β-cell function further exacerbated by worsening of insulin resistance mark the development of impaired glucose tolerance in obese adolescents. *Diabetes care*, 32(3):456–461, 2009.

[62] Chiara Dalla Man, Kevin E. Yarasheski, Andrea Caumo, Heather Robertson, Gianna Toffolo, Kenneth S. Polonsky, and Claudio Cobelli. Insulin sensitivity by oral glucose minimal models: validation against clamp. *American Journal of Physiology-Endocrinology and Metabolism*, 289(6):E954–E959, 2005.

[63] Claudio Cobelli, Chiara Dalla Man, Gianna Mariatoffolo, Rita Basu, Adrian Vella, and Robert Rizza. The oral minimal model method. *Diabetes*, 63:1203–13, 2014.

[64] Danielle Xie, Anne-Marie Carreau, Yesenia Garcia Reyes, Haseeb Rahat, Kai Bartlette, Cecilia Diniz Behn, Laura Pyle, Kristen Nadeau, and Melanie Cree-Green. Or07-3 validation of surrogate models to assess tissue and whole-body insulin resistance among high-risk adolescent girls. *Journal of the Endocrine Society*, 3(Supplement_1), 2019.

[65] Anne-Marie Carreau, Danielle Xie, Yesenia Garcia-Reyes, Haseeb Rahat, Kai Bartlette, Cecilia Diniz Behn, Laura Pyle, Kristen J Nadeau, and Melanie Cree-Green. Good agreement between hyperinsulinemic-euglycemic clamp and 2 hours oral minimal model assessed insulin sensitivity in adolescents. *Pediatric Diabetes*, 2020.

[66] Jean-Frédéric Brun, Edouard Ghanassia, Christine Fédou, Sylvain Bordenave, Eric Raynaud de Mauverger, and Jacques Mercier. Assessment of insulin sensitivity (S_I) and glucose effectiveness (S_G) from a standardized hyperglucidic breakfast test in type 2 diabetics exhibiting various levels of insulin resistance. *Acta Diabetologica*, 50(2):143–153, 2013.

[67] Melanie Cree-Green, Danielle Xie, Haseeb Rahat, Yesenia Garcia-Reyes, Bryan C Bergman, Ann Scherzinger, Cecilia Diniz Behn, Christine L Chan, Megan M Kelsey, Laura Pyle, et al. Oral glucose tolerance test glucose peak time is most predictive of prediabetes and hepatic steatosis in obese girls. *Journal of the Endocrine Society*, 2(6):547–562, 2018.

[68] Group TE. SAAM II manual.

[69] Douglas G Altman and J Martin Bland. Measurement in medicine: the analysis of method comparison studies. *Journal of the Royal Statistical Society: Series D (The Statistician)*, 32(3):307–317, 1983.

[70] David Groppe. r_test_paired.

[71] Melinda E. Chen, Aaditya G. Chandramouli, Robert V. Considine, Tamara S. Hannon, and Kieren J. Mather. Comparison of β-cell function between overweight/obese adults and adolescents across the spectrum of glycemia. *Diabetes Care*, 41(2):318–325, 2018.

[72] Gianna Toffolo, Chiara Dalla Man, Claudio Cobelli, and Agneta L Sunehag. Glucose fluxes during ogtt in adolescents assessed by a stable isotope triple tracer method. *Journal of Pediatric Endocrinology and Metabolism*, 21(1):31–46, 2008.

[73] Elena Breda, Melissa K. Cavaghan, Gianna Toffolo, Kenneth S. Polonsky, and Claudio Cobelli. Oral glucose tolerance test minimal model indexes of β-cell function and insulin sensitivity. *Diabetes*, 50(1):150–158, 2001.

[74] Ananda Basu, Chiara Dalla Man, Rita Basu, Gianna Toffolo, Claudio Cobelli, and Robert A Rizza. Effects of type 2 diabetes on insulin secretion, insulin action, glucose effectiveness, and postprandial glucose metabolism. *Diabetes care*, 32(5):866–872, 2009.

[75] Stefania Audoly, Giuseppina Bellu, Leontina D'Angio, Maria Pia Saccomani, and Claudio Cobelli. Global identifiability of nonlinear models of biological systems. *IEEE Transactions on biomedical engineering*, 48(1):55–65, 2001.

[76] Marisa C. Eisenberg, Suzanne L. Robertson, and Joseph H. Tien. Identifiability and estimation of multiple transmission pathways in cholera and waterborne disease. *Journal of Theoretical Biology*, 324:84 – 102, 2013.

[77] Marisa Eisenberg. Generalizing the differential algebra approach to input-output equations in structural identifiability. *arXiv preprint arXiv:1302.5484*, 2013.

[78] John A Jacquez and Peter Greif. Numerical parameter identifiability and estimability: Integrating identifiability, estimability, and optimal sampling design. *Mathematical Biosciences*, 77(1-2):201–227, 1985.

[79] Jacqueline L Simens, Melanie Cree-Green, Bryan C Bergman, Kristen J Nadeau, and Cecilia Diniz Behn. Structural identifiability analysis of a labeled oral minimal model for quantifying hepatic insulin resistance. In *Association for Women in Mathematics Research Symposium*, pages 145–160. Springer, 2017.

[80] Gianluigi Pillonetto, Giovanni Sparacino, and Claudio Cobelli. Numerical non-identifiability regions of the minimal model of glucose kinetics: superiority of bayesian estimation. *Mathematical biosciences*, 184(1):53–67, 2003.

[81] Andrea Saltelli, Marco Ratto, Terry Andres, Francesca Campolongo, Jessica Cariboni, Debora Gatelli, Michaela Saisana, and Stefano Tarantola. *Global sensitivity analysis: the primer*. John Wiley & Sons, 2008.

[82] W. Becker, J. Rowson, J.E. Oakley, A. Yoxall, G. Manson, and K. Worden. Bayesian sensitivity analysis of a model of the aortic valve. *Journal of Biomechanics*, 44(8):1499 – 1506, 2011.

[83] Mohammad Munir. Generalized sensitivity analysis of the minimal model of the intravenous glucose tolerance test. *Mathematical Biosciences*, 300:14–26, 2018.

[84] Daniel P. Loucks and Eelco van Beek. *System Sensitivity and Uncertainty Analysis*, pages 331–374. Springer International Publishing, Cham, 2017.

[85] Byran Hall and Statisticat LLC. Mcmc algorithms.

[86] Stephen P Brooks and Andrew Gelman. General methods for monitoring convergence of iterative simulations. *Journal of computational and graphical statistics*, 7(4):434–455, 1998.

[87] Marco Taboga. Markov chain monte carlo (mcmc) diagnostics. *Lectures on probability theory and mathematical statistics*, 2017.

[88] Robert Steele. Influences of glucose loading and of injected insulin on hepatic glucose output. *Annals of the New York Academy of Sciences*, 1959.

[89] Il-Young Kim, Sang-Hoon Suh, In-Kyu Lee, and Robert R Wolfe. Applications of stable, nonradioactive isotope tracers in in vivo human metabolic research. *Experimental & molecular medicine*, 48(1):e203–e203, 2016.

[90] Il-Young Kim, Rick H. Williams, Scott E. Schutzler, Cosby J. Lasley, Donald L. Bodenner, Robert R. Wolfe, and Robert H. Coker. Acute lysine supplementation does not improve hepatic or peripheral insulin sensitivity in older, overweight individuals. *Nutrition & Metabolism*, 11.1:1–8, 2014.

[91] John R. Allsop, Robert R. Wolfe, and John F. Burke. The reliability of rates of glucose appearance in vivo calculated from constant tracer infusions. *Biochemical Journal*, 172(3):407–416, 1978.

[92] Robert Rizza, Gianna Toffolo, and Claudio Cobelli. Accurate measurement of postprandial glucose turnover: Why is it difficult and how can it be done (relatively) simply? *Diabetes*, 65:1133–1145, 2016.

[93] J. Proietto. Estimation of glucose kinetics following an oral glucose load. *Hormone and Metabolic Research Supplement Series*, pages 25 – 30, 1990.

[94] Rita Basu, Barbara DI Camillo, Gianna Toffolo, Ananda Basu, Pankaj Shah, Adrian Vella, Robert Rizza, and Claudio Cobelli. Use of a novel triple-tracer approach to assess postprandial glucose metabolism. *Endocrinology and Metabolism - American Journal of Physiology*, 284:55–69, 2003.

[95] J Radziuk, KH Norwich, and M Vranic. Experimental validation of measurements of glucose turnover in nonsteady state. *American Journal of Physiology-Endocrinology And Metabolism*, 234(1):E84, 1978.

[96] Andrea Mari. Estimation of the rate of appearance in the non-steady state with a two-compartment model. *American Journal of Physiology-Endocrinology and Metabolism*, 263(2):400–415, 1992.

[97] Geoff Livesey, PDG Wilson, Jack R Dainty, JC Brown, RM Faulks, MA Roe, TA Newman, John Eagles, FA Mellon, and RH Greenwood. Simultaneous time-varying systemic appearance of oral and hepatic glucose in adults monitored with stable isotopes. *American Journal of Physiology-Endocrinology And Metabolism*, 275(4):E717–E728, 1998.

[98] J Radziuk and S Pye. Production and metabolic clearance of glucose under basal conditions in type ii (non-insulin-dependent) diabetes mellitus. *Diabetologia*, 44(8):983–991, 2001.

[99] J Radziuk and S Pye. Quantitation of basal endogenous glucose production in type ii diabetes: importance of the volume of distribution. *Diabetologia*, 45(8):1053–1084, 2002.

[100] Giuseppe De Nicolao, Giovanni Sparacino, and Claudio Cobelli. Nonparametric input estimation in physiological systems: problems, methods, and case studies. *Automatica*, 33(5):851–870, 1997.

[101] Michele Schiavon and Giovanni Sparacino. WinSmoother.

[102] Ahmad Haidar, Daniela Elleri, JM Allen, Julie Harris, Kavita Kumareswaran, Marianna Nodale, CL Acerini, ME Wilinska, Nicola Jackson, AM Umpleby, et al. Validity of triple-and dual-tracer techniques to estimate glucose appearance. *American Journal of Physiology-Endocrinology and Metabolism*, 302(12):E1493–E1501, 2012.

[103] Ahmad Haidar, Elizabeth Potocka, Benoit Boulet, A Margot Umpleby, and Roman Hovorka. Estimating postprandial glucose fluxes using hierarchical bayes modelling. *Computer methods and programs in biomedicine*, 108(1):102–112, 2012.

[104] Michael L Traub. Assessing and treating insulin resistance in women with polycystic ovarian syndrome. *World Journal of Diabetes*, 2(3):33, 2011.

[105] Enrique Reyes-Muñoz, Carlos Ortega-González, Nayeli Martínez-Cruz, Lidia Arce-Sánchez, Guadalupe Estrada-Gutierrez, Carlos Moran, Ana Paola Sánchez-Serrano, Rodolfo Higareda-Sánchez, and Julio Francisco de la Jara-Díaz. Association of obesity and overweight with the prevalence of insulin resistance, pre-diabetes and clinical–biochemical characteristics among infertile mexican women with polycystic ovary syndrome: a cross-sectional study. *BMJ open*, 6(7), 2016.

[106] Theodore P Ciaraldi, Vanita Aroda, Sunder Mudaliar, R Jeffrey Chang, and Robert R Henry. Polycystic ovary syndrome is associated with tissue-specific differences in insulin resistance. *The Journal of Clinical Endocrinology & Metabolism*, 94(1):157–163, 2009.

[107] Andrea Dunaif, Magaret Graf, John Mandeli, Vimla Laumas, and Areta Dobrjansky. Characterization of groups of hyperaiidrogenic women with acanthosis nigricans, impaired glucose tolerance, and/or hyperinsulinemia. *The Journal of Clinical Endocrinology & Metabolism*, 65(3):499–507, 1987.

[108] Kristen J Nadeau, Phillip S Zeitler, Timothy A Bauer, Mark S Brown, Jennifer L Dorosz, Boris Draznin, Jane EB Reusch, and Judith G Regensteiner. Insulin resistance in adolescents with type 2 diabetes is associated with impaired exercise capacity. *The Journal of Clinical Endocrinology & Metabolism*, 94(10):3687–3695, 2009.

APPENDIX A

RESCALED OMM

The Oral Minimal Model (OMM) and the Labeled-Oral Minimal Model (OMM*) were rescaled in the following way to enable direct estimation of S_I and S_I^*.

$$\begin{cases} \dot{G} &= -[S_G + X] \cdot G + S_G \cdot G_b + \frac{Ra_{meal}}{V} \\ \dot{X} &= -p_2 \cdot X + p_3[I(t) - I_b] \end{cases}$$

$$\begin{aligned} & \frac{V}{p_2}\dot{X} = -p_2\frac{V}{p_2} \cdot X + p_3\frac{V}{p_2}[I(t) - I_b] \\ \implies & \frac{V}{p_2}\dot{X} = -V \cdot X + S_I[I(t) - I_b] \end{aligned}$$

Let $Y = \frac{V}{p_2}X$ then $\dot{Y} = \frac{V}{p_2}\dot{X}$

$\implies X = \frac{p_2}{V}Y, \quad \dot{X} = \frac{p_2}{V}\dot{Y}$ and $Y(0) = 0$

Rescaled OMM

$$\begin{cases} \dot{G} &= -[S_G + \frac{p_2}{V}Y] \cdot G + S_G \cdot G_b + \frac{Ra_{meal}}{V} \\ \dot{Y} &= -p_2 \cdot Y + S_I[I(t) - I_b] \end{cases}$$

Dimensional analysis of OMM and Rescaled OMM

Let $[\cdot]$ denote the units of the quantity contained within.

$$[G] = [G_b] = \frac{mg}{dl}, \quad [V] = \frac{dl}{kg}, \quad [Ra] = \frac{mg}{kg\,min}, \quad [S_G] = \frac{1}{min}$$

$$[X] = \frac{1}{min}, \quad [I] = [I_b] = \frac{\mu U}{ml}, \quad [p_2] = \frac{1}{min}, \quad [p_3] = \frac{ml}{\mu U min^2}$$

The total glucose ODE

$$
\begin{aligned}
[\dot{G}] &= \left[-[S_G + X] \cdot G + S_G \cdot G_b + \frac{Ra_{meal}(\boldsymbol{\alpha}, t)}{V}\right] \\
\frac{mg}{dl\,min} &= \left[\frac{1}{min} + \frac{1}{min}\right] \cdot \frac{mg}{dl} + \frac{1}{min} \cdot \frac{mg}{dl} + \frac{mg}{\cancel{kg}\,min} \cdot \frac{\cancel{kg}}{dl} \\
\frac{mg}{dl\,min} &= \frac{mg}{dl\,min} + \frac{mg}{dl\,min} + \frac{mg}{dl\,min}
\end{aligned}
$$

The total insulin action ODE

$$
\begin{aligned}
[\dot{X}(t)] &= -p_2 \cdot X(t) + p_3 \cdot [I(t) - I_b]] \\
\frac{1}{min^2} &= \frac{1}{min} \cdot \frac{1}{min} + \frac{\cancel{mL}}{\cancel{\mu U}\,min^2}\left[\frac{\cancel{\mu U}}{\cancel{mL}}\right] \\
\frac{1}{min^2} &= \frac{1}{min^2} + \frac{1}{min^2}
\end{aligned}
$$

Insulin sensitivity, S_I

$$
\begin{aligned}
[S_I] &= \frac{[p_3]}{[p_2]}[V] \\
&= \frac{ml}{\mu U \cancel{min^2}} \cdot \cancel{min} \cdot \frac{dl}{kg} \\
\implies [S_I] &= \frac{dl}{kg\,min} \cdot \frac{ml}{\mu U}
\end{aligned}
$$

The Rescaled OMM Y variable

$$
\begin{aligned}
[Y] &= \frac{[V]}{[p_2]}[X] \\
&= \frac{dl}{kg} \cdot \cancel{min} \cdot \frac{1}{\cancel{min}} \\
\implies [Y] &= \frac{dl}{kg}
\end{aligned}
$$

$$[\dot{G}] = \left[-[S_G + \frac{p_2}{V} Y] \cdot G + S_G \cdot G_b + \frac{Ra_{meal}(\boldsymbol{\alpha}, t)}{V} \right]$$

$$\frac{mg}{dl\,min} = \left[\frac{1}{min} + \frac{1}{min} \cdot \frac{\cancel{kg}}{\cancel{dl}} \cdot \frac{\cancel{dl}}{\cancel{kg}} \right] \cdot \frac{mg}{dl} + \frac{1}{min} \cdot \frac{mg}{dl} + \frac{mg}{\cancel{kg}\,min} \cdot \frac{\cancel{kg}}{dl}$$

$$\frac{mg}{dl\,min} = \frac{mg}{dl\,min} + \frac{mg}{dl\,min} + \frac{mg}{dl\,min}$$

Similarly, OMM* rescaled

$$\begin{cases} \dot{G}_{meal} &= -[S_G^* + \frac{p_2^*}{V} Y^*] \cdot G_{meal} + \frac{Ra_{meal}}{V^*} \\ \dot{Y}^* &= -p_2^* \cdot Y^* + S_I^* [I(t) - I_b] \end{cases}$$

APPENDIX B

OMM^{PD} SENSITIVITY INDICES DERIVATION

The indices for production and disposal insulin sensitivity and glucose effectiveness are derived from steady state equations.

$$S_I^D = \left.\frac{\partial^2 R_d}{\partial G\, \partial I}\right|_{SS} = k_2^D \cdot V \tag{B.1}$$

Recall

$$\begin{cases} R_d(t) = V \cdot [S_G^D + X^D(t)] \cdot G(t) \\ \dot{X}^D(t) = -k_1^D \cdot [X^D(t) - k_2^D \cdot (I(t) - I_b)] \quad X^D(0) = 0 \end{cases}$$

At steady state and suppressing the (t) notation,

$$\begin{aligned} & - k_1^D \cdot [X^D - k_2^D \cdot (I - I_b)] = 0 \\ & X^D = k_2^D \cdot (I - I_b) \\ \Longrightarrow\ & R_d = V \cdot [S_G^D + k_2^D \cdot (I - I_b)] \cdot G \\ \Longrightarrow\ & \frac{\partial R_d}{\partial G} = V \cdot [S_G^D + k_2^D \cdot (I - I_b)] \\ \Longrightarrow\ & \frac{\partial R_d}{\partial G \partial I} = k_2^D \cdot V \end{aligned}$$

$$S_I^P = \left.\frac{\partial EGP}{\partial I}\right|_{SS} \cdot \frac{1}{G_b} = \frac{k_2^P}{G_b} \tag{B.2}$$

Recall

$$\begin{cases} \mathrm{EGP}(t) = \mathrm{EGP}_b - k_G \cdot [G(t) - G_b] - X^P(t) - X^{Der}(t) & \mathrm{EGP}(0) = \mathrm{EGP}_b \\ \dot{X}^P(t) = -k_1^P \cdot [X^P(t) - X_1(t)] & X^P(0) = 0 \\ \dot{X}_1(t) = -k_1^P \cdot [X_1(t) - k_2^P \cdot (I(t) - I_b)] & X_1(0) = 0 \end{cases}$$

where

$$X^{Der}(t) = \begin{cases} k_{GR} \cdot \frac{dG(t)}{dt} & \frac{dG(t)}{dt} \geq 0 \\ 0 & \frac{dG(t)}{dt} < 0 \end{cases}$$

At steady state,

$$\begin{aligned} & - k_1^P \cdot [X^P - X_1] = 0 \\ \implies & X^P = X_1 \\ & - k_1^P \cdot [X_1 - k_2^P \cdot (I - I_b)] = 0 \\ \implies & X_1 = k_2^P \cdot (I - I_b) \\ \implies & EGP = EGP_b - k_G \cdot [G - G_b] - k_2^P \cdot (I - I_b) \\ \implies & \frac{\partial EGP}{\partial I} = k_2^P \end{aligned}$$